Summer 8-13-2021

Utilizing Proteolysis-Targeting Chimeras to Target the Transcriptional Cyclin-Dependent Kinases 9 and 12

Hannah King
University of Nebraska Medical Center

UTILIZING PROTEOLYSIS-TARGETING CHIMERAs TO TARGET THE TRANSCRIPTIONAL CYCLIN-DEPENDENT KINASES 9 AND 12

by

Hannah M. King

A DISSERTATION

Presented to the Faculty of

the University of Nebraska Graduate College

in Partial Fulfillment of the Requirements

for the Degree of Doctor of Philosophy

Cancer Research Graduate Program

Under the Supervision of Professor Amarnath Natarajan

University of Nebraska Medical Center
Omaha, NE

June, 2021

Supervisory Committee Members:

Justin Mott, M.D., Ph.D. Angie Rizzino, Ph.D. Nicholas Woods, Ph.D.

Dedicated to my parents Lisa, and Dana King, who has always believed in me and pushed me to be the best version of myself. Without their continual support, I would not have gotten this far.

ACKNOWLEDGEMENT

First, I would like to thank my advisor Dr. Amarnath Natarajan. You have an incredible mind for science, and you have truly taught me how to think outside of the box. Thank you for believing in me when I did not. Graduate school started and ended very rocky, but you could keep me on track to graduate.

Next, I would like to thank my supervisory committee members for their critical inputs towards my project and continuous support throughout my graduate career. Dr. Nick Woods for giving me my first experience working in a lab as a SURP student and supporting it since then. Dr. Angie Rizzino, for your critical analysis of my work and for always making me think way outside my comfort zone as a scientist. Dr. Justin Mott for always being an open set of ears when I was struggling. I would also like to thank Dr. Joyce Solheim for always putting us students first. And Misty, for keeping me on track with enrollment and other critical due dates.

I would also like to thank all the members of the Natarajan lab, past and present. Thank you, Smit and Caroline, for providing me with a wonderful and supportive start to my graduate education. To Dr. Sandeep Rana for synthesizing the compounds, I got the privilege of working with. To Sydney, who has been my rock through the last year, pandemic and all. You have always been so eager to help with anything I need, and I have appreciated your friendship through it all. Special thanks to Smitha, without whom the lab would cease to function. Thank you to Jayapal and Sarabjit for always answering my chemistry-based questions; you both are a wealth of knowledge.

Lastly, I want to thank my family, who have always supported me and my dreams. My parents who have always pushed me to be the best version of myself I can be. And for

always telling me I could do anything I set my mind to. This is, honestly, the best advice they have ever given me.

UTILIZING PROTEOLYSIS-TARGETING CHIMERAs TO TARGET THE TRANSCRIPTIONAL CYCLIN-DEPENDENT KINASES 9 AND 12

Hannah M. King, Ph.D.

University of Nebraska, 2021

Advisor: Amarnath Natarajan, Ph.D.

Cyclin-dependent kinases (CDKs) are a family of serine-threonine kinases involved in various cellular functions, such as regulating the cell cycle and gene transcription. CDK9, a transcriptional CDK, regulates highly expressed enhancer-associated oncogenic transcription factors, including the oncogene Myc. CDK9 is responsible for the transcription and stabilization of Myc; consequently, it was a validated target for pancreatic cancer treatment.

As such, we developed a panel of aminopyrazole based proteolysis targeting chimera where we identified PROTAC **2** as a selective degrader of CDK9 (DC_{50} = 158 ± 6 nM). PROTAC **2** was capable of cereblon mediated proteasomal degradation of CDK9 while sparing other CDK family members. However, PROTAC **2** binds to CDK2 and CDK5, inhibiting their kinase activity, but did not induce their degradation, likely due to differentially exposed lysine residues. In MiaPaCa2 and Suit-2, we observed reduced PROTAC **2** mediated degradation of CDK9. Mass spectrometry-based kinome profiling further validated PROTAC **2** selective degradation of CDK9 in HEK293 and MiaPaCa2 cells. PROTAC **2** sensitized MiaPaCa2 cells to Venetoclax mediated growth inhibition, likely due to concurrent inhibition of Mcl-1 and Bcl2.

Furthermore, this panel of PROTACs also included PROTAC **4,** which we identified as a selective CDK12 degrader (DC_{50} = 1.1 ± 0.3 μM). CDK12 plays a significant role in transcriptional elongation/termination, mRNA splicing, and DNA damage response. CDK12 is upregulated in several cancers, including breast, ovarian, stomach, and

colorectal. We observed colorectal cancer-specific cereblon mediated proteasomal degradation of CDK12. PROTAC **4** selective degradation of CDK12 in HCT116 sensitized them to Gemcitabine mediated growth inhibition.

Since PROTAC **2** and PROTAC **4** only vary in linker length and composition, our studies demonstrate the importance of chemical characteristics in developing selective degraders utilizing the PROTAC strategy. Moreover, PROTACs offer a new therapeutic approach.

TABLE OF CONTENTS

LIST OF FIGURES

LIST OF TABLES

LIST OF ABBREVIATIONS

^{13}C NMR	Carbon-13 (C13) Nuclear Magnetic Resonance
^{1}H NMR	Proton Nuclear Magnetic Resonance
AML	Acute Myeloid Leukemia
ATP	Adenosine Triphosphate
AR	Androgen Receptor
BCA	Bicinchoninic Acid
c-FOS	Cellular FBJ Osteosarcoma Virus
Cacld	Calculated
CAK	Cyclin-Dependent Activating Kinase
$CDCl_3$	Deuterated Chloroform
CDK(s)	Cyclin-Dependent Kinases
CDK1	Cyclin-Dependent Kinase 1
CDK2	Cyclin-Dependent Kinase 2
CDK4	Cyclin-Dependent Kinase 4
CDK5	Cyclin-Dependent Kinase 5
CDK6	Cyclin-Dependent Kinase 6
CDK7	Cyclin-Dependent Kinase 7
CDK8	Cyclin-Dependent Kinase 8
CDK9	Cyclin-Dependent Kinase 9
CDK12	Cyclin-Dependent Kinase 12
CH_3CN	Acetonitrile
CI	Combination Index
CPSF	Cleavage and Polyadenylation Specificity Factor
CTD	C-Terminal Domain

CRBN	Cereblon
CstF	Cleavage Stimulatory Factor
DDR	DNA Damage Response
DIPEA	N,N-Diisopropylethylamine
DMA	Dimethylacetamide
DMEM	Dulbecco's Modified Eagle Medium
DMF	Dimethylformamide
DMSO	Dimethyl Sulfoxide
DSIF	DRB Sensitivity-Inducing Factor
ECL	Enhanced Chemiluminescence
EDC	1-ethyl-3-(3-dimethylaminopropyl)carbodiimide
FBJ	Finkel-Biskis-Jinkins (FBJ)
FBS	Fetal Bovine Serum
GTF	General Transcription Factor
JPEG	Joint Photographic Experts Group
HOBT	Hydroxybenzotriazole
HPLC	High Performance Liquid Chromatography
HRMS	High-Resolution Liquid Chromatography
HRP	Horseradish Peroxidase
Mcl-1	Myeloid Cell Leukemia-1
NELF	Negative Elongation Factor
NEt_3	Triethylamine
PAGE	Polyacrylamide Gel
PBS	Phosphate Buffered Saline
Penstrep	Penicillin-Streptomycin

Pd/C	Palladium on Carbon
PDAC	Pancreatic Ductal Adenocarcinoma
PIC	Pre-Initiation Complex
PMSF	Phenylmethylsulfonyl Flouride
poly(A)	Polyadenylation
POI	Protein of Interest
PRM	Proline-Rich Motifs
p-TEFb	Positive Transcription Elongation Factor b
PVDF	Polyvinylidene Fluoride
RPB	RNA polymerase II subunit B
RIPA	Radioimmunoprecitation
RNA Pol	RNA Polymerase
RPMI-1640	Roswell Park Memorial Institute – 1640 Medium
RS	Arginine/Serine-Rich
SDS	Sodium Dodecyl Sulphate
T3P	Propanephosphonic Acid Anhydride
TBST	Tris-Buffered Saline (TBS) and Tween 20
TFII	Transcription factor II
TLC	Thin Layer Chromatography
UPS	Ubiquitin/Proteasome System
VHL	Von-Hippel-Lindau
XRN2	5′–3′ Exoribonuclease 2

CHAPTER 1: INTRODUCTION

CYCLIN-DEPENDENT KINASES

Cyclin-dependent kinases (CDK) are a family of 20 serine-threonine kinases that regulate a plethora of cellular processes. CDKs are members of the evolutionarily conserved CMGC group of kinases, along with mitogen-activated protein kinases (MAPK), glycogen synthase kinase-3 beta (GSK3), and CDK-like kinases (CLK) [1, 2]. Members of the CDK family are subdivided into three subfamilies: CDKs that regulate cell-cycle progression (CDKs 1-7), CDKs that regulate gene transcription (CDKs 7-13, 19), and TAIRE CDKs named for their common sequence motif (CDKs 14-18) [3, 4]. The cellular localization of CDKs is correlated to their specific subfamily. Cell-cycle and transcriptional CDKs are present in the nucleus, while the TAIRE CDKs are mainly found in the cytoplasm [4, 5].

As with typical protein kinase domains, the CDK kinase domains are bilobal in nature. The smaller amino-terminal lobe contains several beta-sheets and a major Cα-helix, and the larger carboxyl-terminal lobe is predominately composed of alpha-helices [4]. In between the N- and C-terminal lobes resides the hinge region, which contains the ATP (adenosine triphosphate) binding pocket. The hinge region is a single peptide strand that operates like a swivel allowing the two lobes to rotate in relation to each other, which allows the secondary protein structure to be undisturbed [6, 7]. The C-lobe also contains the activation domain, which spans from the DFG motif (Asp-Phe-Gly) to the APE motif (Ala-Pro-Glu). This domain includes the flexible loop, called the T-loop or activation loop, which contains a phosphorylation-sensitive residue [4]. Due to CDKs regulatory role in several cellular processes, these proteins undergo several layers of regulation. Initially, CDKs are inactive monomers; the first step in CDK activation is the association with cyclins

or activators that mimic cyclins, forming heterodimer complexes. Cyclin binding to the CDK causes a Cα-helix conformational change, making the catalytic ATP pocket accessible [8-10]. Some CDKs require further activation through a threonine residue's phosphorylation in the T-loop; this phosphorylation stabilizes the kinase's activated form, allowing for activator binding [4, 11, 12]. The DFG motif also undergoes conformational changes to regulate kinase activation. In the “DFG in” confirmation, this motif resides in a hydrophobic pocket deep within the kinase fold, allowing it to be catalytically active. In the “DFG out” confirmation, this motif is flipped out of its hydrophobic pocket, transforming it into catalytically inactive kinase [13, 14]. Besides regulation by CDK activation, CDKs can also be regulated through inhibition. CDKs are primarily negatively regulated by two families of proteins, the INK4 family of proteins and the Cip/Kip family [1, 15]. CDKs are regulatory enzymes that facilitate signaling by transferring the gamma-phosphate from ATP to a hydroxyl group on a serine or threonine residue of a downstream substrate. Like other CMGC kinases, CDKs are proline-directed, recognizing a particular consensus sequence (S/T-P-X-K/R) in downstream substrates that facilitate their identification and phosphorylation of their specific targets [4, 16].

CDKs, as stated above, play a crucial regulatory role in several biological processes. These include cell-cycle control, transcriptional regulation, RNA-splicing, cell proliferation, DNA damage response, cell death, and cell migration [4, 17-19]. CDKs are frequently dysregulated in a broad spectrum of cancers due to their influential role in several of these biological processes. For example, cancer cells can utilize CDKs for sustained proliferation by deregulation of cell cycle controls and fuel transcription addiction [20]. Therefore, CDK family members are considered attractive therapeutic targets.

TRANSCRIPTION AND CYCLIN-DEPENDENT KINASES

The task of transcribing the eukaryotic genome is carried out by nuclear enzymatic RNA polymerase I (Pol I), RNA polymerase II (Pol II), and RNA polymerase III (Pol III). RNA pol I transcribes only ribosomal (r)RNAs, RNA poll II is responsible for messenger (m)RNA, and RNA pol III transcribes transfer (t)RNAs and other untranslated RNAs. In short, RNA pol II is primarily responsible for transcribing all protein-encoding genes, and RNA pol I & III only transcribe non-coding RNAs [21, 22]. RNA pol II transcriptional regulation is essential for cellular maintenance, including cellular differentiation, adaptation, and identity [21]. RNA pol II-mediated transcription is divided into four phases based on the mechanisms that regulate it and the components involved; these phases are initiation, pausing, elongation, and termination [23, 24]. Each of these phases undergoes regulation by a multitude of proteins. These include members of the cyclin-dependent kinase family (**Figure 1**).

The first step in RNA pol II-mediated transcription is initiation, exemplified by the formation of the pre-initiation complex (PIC) on the promoter. This complex contains RNA pol II, the mediator complex, and several general transcription factor (GTF) complexes [25]. RNA pol II is composed of 12-subunits, RNA polymerase II subunit B (RPB) 1-12 [26]. There are six GTF complexes as part of the PIC; these are transcription factor II (TFII) A, TFIIB, TFIID, TFIIE, TFIIF, and TFIIH [21, 25]. The kinase module of the TFIIH complex contains CDK7 and its binding partner, cyclin H [27]. The last component of the PIC is the mediator complex, a large 1.2 MDa multi-protein complex comprised of 26 subunits [28]. Before PIC assembly, the mediator complex is typically found in complex with CDK8 and its binding partner cyclin C forming a 29 subunit CDK8-Mediator complex. Because the mediator complex initiates PIC assembly by promoting RNA pol II recruitment to the promoter, PIC assembly is inhibited by CDK8 [29, 30]. CDK8 blocks PIC formation

by competing for similar sites on the Mediator complex as RNA pol II [31]. For productive transcription to occur, RNA pol II must undergo promoter escape and phosphorylation of the C-terminal domain (CTD). The CTD of RNA polymerase II contains 52 heptapeptide tandem repeats for the consensus sequence Tyr-Ser-Pro-Thr-Ser-Pro-Ser ($Y_1S_2P_3T_4S_5P_6S_7$) [32]. CDK7, as part of the TFIIH complex, is responsible for phosphorylation of the CTD of RNA pol II on Ser5 and Ser7, which induce promotor clearance and productive transcription [33, 34].

The second step in RNA pol II-mediated transcription is pausing, which occurs after transcribing between 20 and 120 nucleotides downstream of the transcription start site and transcription halts [35]. Initially, after leaving the transcriptional start site, elongation factors bind to the polymerases. These elongation factors include the negative elongation factor (NELF) and 5,6-dichloro-1-β-D-ribofuranosylbenzimidazole (DRB) sensitivity-inducing factor (DSIF) [36]. NELF consists of four subunits: NELF-A, -B, -C, and -E [37]. DSIF consists of two subunits: Spt4 and Spt5 [38]. The association of NELF and DSIF is responsible for stabilizing paused RNA pol II and prevents the reassociation of transcription initiation factors [39].

The third phase in RNA pol II-mediated transcription is elongation, with paused RNA pol II release. The release of paused RNA pol II into productive elongation is facilitated by the positive transcription elongation factor b (p-TEFb). P-TEFb is a two subunit complex composed of CDK9 and one of its binding partners (cyclin T1, T2, or K) [40]. Before CDK9 can participate in transcription, it must first be activated via phosphorylation of Thr186 within the T-loop by CDK7 as part of the cyclin-dependent activating kinase (CAK) complex [11, 41]. Once CDK9 is activated, it then phosphorylates three primary substrates to facilitate productive elongation: (1) Ser2 residues of the CTD of RNA pol II, (2) the E-subunit of NELF, and (3) the Spt5 subunit of DSIF [42, 43]. The

phosphorylation of the E-subunit of NELF promotes the dissociation of NELF from RNA pol II, which, along with the phosphorylation of the Spt5 subunit of DSIF, turns DSIF into a positive elongation factor triggering the formation of an activated elongation complex [44, 45].

The fourth and final step in RNA pol II-mediated transcription is termination, starting with RNA pol II pausing at polyadenylation (poly(A)) sites. RNA pol II is halted when the cleavage and polyadenylation specificity factor (CPSF) recognizes and binds to the poly(A) signal sequence AAUAAA [46]. RNA pol II pausing allows for the CDK9-dependent (in some cases CDK12 mediated) phosphorylation of Ser2 of the CTD of RNA pol II, which recruits termination factors to the poly(A) sites and pause-release for proper termination [47, 48]. Additionally, the cleavage stimulatory factor (CstF) binds to glycine-rich processing signals where CPSF binds to it and accompanies it to the CTD of RNA pol II, causing CPSF-mediated cleavage [49]. The creation of an unprotected 5′ end by 3′-end processing endoribonuclease or other cleavage events downstream of the poly(A) sites allows for the 3′-end processing cleavage by the 5′–3′ exoribonuclease 2 (XRN2), whose enzymatic activity is enhanced by Thr439 CDK9-mediated phosphorylation, resulting in effective termination [50].

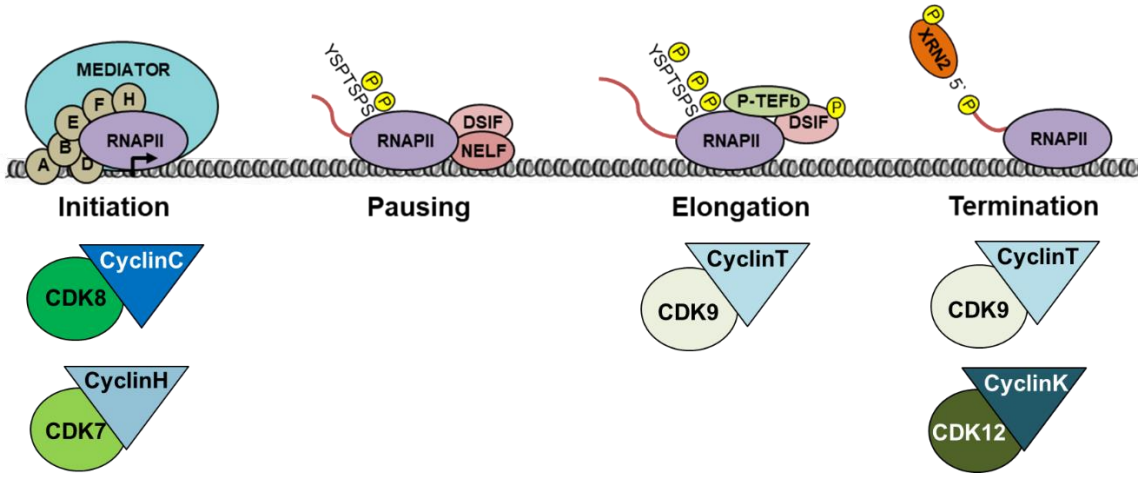

Figure 1. Known roles of transcription CDKs in RNA pol II gene transcription. *Modified from Galbraith et. al. (2019) Transcription.

CYCLIN-DEPENDENT 9

CDK9 was initially identified as the ubiquitously expressed PITALRE for its characteristic Pro-Ile-Thr-Ala-Leu-Arg-Glu motif in 1994 [51]. In 1998, PITALRE was further characterized as a serine/threonine proline-directed kinase which showed activity as a monomer [52]; however, when present in high molecular weight complexes, PITALRE activity was increased [53]. These high molecular weight complexes were later determined to be PITALRE and its cyclin partners via characterization of *Drosophila* p-TEFb [54]. Consequently, PITALRE was renamed CDK9. CDK9 has four cyclin partners: cyclin T1, cyclin T2a, cyclin T2b, and cyclin K [55]. The *CDK9* gene location is on chromosome 9q34; this gene includes seven exons that code for the two isoforms ($CDK9_{45}$ and $CDK9_{55}$) [56]. $CDK9_{55}$ has a 117-residue extension at the amino terminus resulting in the 10 kDa difference in molecular weight from $CDK9_{45,}$ 372 amino acids in length [57]. The structure of CDK9 in an unbound state has yet to be elucidated; however, co-crystallization reveals the kinase domain of CDK9 (residues 29 through roughly 186). The kinase domain contains the ATP binding site (T29-D167) and the threonine residue in the activation T-loop (T186) [58].

CDK9 forms active complexes with T- and K-type cyclins; each has different biological functions. CDK9/cyclin T exclusively plays a significant role in controlling basal gene transcription, detailed above in “Transcription and Cyclin-Dependent Kinases.” In brief, CDK9/cyclin T is responsible for releasing proximal promoter paused transcripts and transcriptional termination. CDK9/cyclin T phosphorylates DSIF, NELF, and Ser2 of the CTD of RNA pol II, releasing RNA pol II from its paused state and forming a productive elongation complex. Additionally, CDK9/cyclin T is also responsible for phosphorylating XRN2, which is necessary for transcriptional termination. CDK9/cyclin K can activate transcription via RNA but not DNA like its cyclin T counterpart [59]. Also, CDK9/cyclin K

has been implicated in replication stress response. Loss of CDK9 has been shown to increase DNA damage response signaling and a decreased ability to recover from replication stress. This activity was exclusively attributed to CDK9/cyclin K complexes [60]. Because of the critical role CDK9 plays in transcription, it is often dysregulated in transcriptional addicted cancer and is necessary for their pathogenesis.

CDK9 in Cancer

Most cancer cells rely on dysregulated gene expression to support their uncontrolled proliferation; these cells set high demands on transcriptional regulators, including oncogenic transcription factors. CDK9 is involved in these transcriptional addicted cancers due to its role in oncogenic-driven transcription. Representative examples of these cancers include MYC-driven pancreatic cancer [61], androgen receptor (AR) driven prostate cancer [62], and MCL-1 driven acute myeloid leukemia (AML) [63].

Pancreatic ductal adenocarcinoma (PDAC), which has a dismal 5-year survival rate of 8%, is genetically driven by the mutational activation of the *KRAS* oncogene [61]. *MYC* overexpression is sufficient to drive the development of metastatic PDAC, replicating the mutant KRAS phenotype [61]. KRAS-mutant pancreatic cancers are characterized by increased MYC expression, ultimately caused by the promotion of *MYC* gene transcription and prolonged MYC protein stability. Regarding *MYC* gene transcription, CDK9 is partially responsible for the productive transcription of MYC target genes, including MYC itself [64]. When it comes to MYC protein stabilization, CDK9 has been shown to phosphorylate Ser62 on MYC, which blocks MYC protein degradation [61]. Together, CDK9 regulates MYC at the transcriptional level and post-transcriptional level.

Prostate cancer is a type of hormone-driven cancer that will affect one in nine men. The androgen receptor (AR) drives the oncogenic signaling and downstream transcription of prostate cancer [62]. The AR is classified as a steroid receptor transcriptional factor.

The AR regulates genes required for prostate cell differentiation, metabolism, and proliferation [65]. Testosterone and dihydrotestosterone are the two androgens responsible for activating the androgen receptor in prostate cancer [66]. In addition to receptor activation, the AR is also regulated *via* phosphorylation of Ser81 on the androgen receptor, which prevents nuclear export and subsequent degradation. This residue phosphorylation is also crucial for AR promoter selectivity, modulating the genes transcribed by the AR and therefore affecting prostate cancer cell growth [65]. In summary, the post-translational modification of the AR by CDK9 contributes to the oncogenic-driven nature of prostate cancer.

Acute myeloid leukemia (AML) is a hematological malignancy representing 32% of all adult leukemia cases in the United States [63]. AML is characterized by deregulated expression of one or more apoptosis-controlling proteins. As a result, AML cells are critically dependent on the anti-apoptotic protein myeloid cell leukemia-1 (Mcl-1) for development, survival, and persistence [67]. Also, Mcl-1 contributes to resistance to chemotherapy [68]. The expression of Mcl-1 is critically regulated by CDK9 activity, mostly under super-enhancer mediated transcriptional control. In several AML models, inhibition of CDK9 has been directly correlated with decreased Mcl-1 expression resulting in apoptosis [63]. Ultimately, CDK9 is responsible for Mcl-1 expression in AML, thus contributing to its tumorigenicity.

CYCLIN-DEPENDENT 12

CDK12 was initially identified in 2001 as a ubiquitously expressed Cdc-2 related kinase (Crk) that contained an arginine/serine-rich domain (RS), consequently named CrkRS [69]. In 2006, CrkRS was renamed CDK12 based on its association with cyclin L1 and L2 [69, 70]. However, in 2010 experiments performed in yeast determined cyclin K was the CDK12 binding partner. The CDK12/cyclin K complex was further confirmed using

mammalian cells in 2011 [17, 71]. The *CDK12* gene is located on chromosome 17q12; this gene includes 14 exons which corresponds to two isoforms ($CDK12^S$ and $CDK12^L$) that differ only in the last exon. $CDK12^S$ is a 1481 amino acid protein that stops at exon 13. $CDK12^L$ is the full-length 1490 amino acid protein that splices directly from exon 13 to exon 14; this protein's molecular weight is 164 kDa [70]. CDK12 contains four functional domains: a central kinase domain with proline-rich motifs (PRM) on either side and an arginine/serine-rich (RS) domain at the N-terminus. There are 21 RS motifs within the first 400 amino acids at the N-terminus [72]. The kinase domain is roughly 300 amino acids (719-1051), consists of a threonine tyrosine residue at the beginning of the ATP binding site, and threonine in the activation T-loop, which gets phosphorylated by a CDK-activating kinase [73]. The CKD12/cyclin K complex serves many roles, though its primary function is transcriptional regulation, RNA splicing, and DNA damage response [74].

In transcription, the CDK12/cyclin K complex facilitates the transition between transcriptional initiation to elongation by phosphorylating the CTD of RNA pol II at Ser2 [72] and Ser5 [75]. Post-transcriptional modification of the CTD of RNA pol II has been shown to couple transcription termination with 3`end processing [71]. CDK12-dependent phosphorylation of the CTD of RNA pol II is involved in the recruitment of 3`end processing factors. For example, phosphorylation of Ser2 by CDK12 facilitates the recruitment of cleavage stimulating factor 77 (CstF77) for optimal 3`end processing of c-Myc [76]. Also, CDK12 depletion reduced cleave stimulating factor 64 (CstF64), which leads to the impaired 3`end processing of cellular Finkel-Biskis-Jinkins (FBJ) osteosarcoma virus (c-FOS) [77].

After transcription, the precursor (pre-)mRNA must transform into mature mRNA; this process is called RNA splicing. CDK12 is known to participate in RNA splicing in the following ways. CDK12 has been shown to localize to nuclear speckles, which are

subnuclear structures that store splicing factors [78]. Furthermore, CKD12 is known to co-localize with additional spliceosome components, including the spliceosome component called SC35 [69]. Besides its association with splicing components, exon junction complexes and RNA-binding proteins have also been co-immunoprecipitated with CDK12 [77, 79]. Tien et al. demonstrated that CDK12 regulates a specialized subtype of alternative mRNA splicing, called alternative last exon (ALE) splicing, in a gene- and cell-type-specific manner [79]. Typically spliceosomes regulatory factors regulate many forms, universally, of alternative splicing, making that quite unusual.

In the DNA damage response (DDR), CDK12 affects the expression of genes involved in homologous recombination (HR) [17, 80]. In CDK12 depleted cells, microarrays showed that only 2.67% of tested genes were altered. However, the downregulated genes were lengthy and contained large numbers of exons. Additionally, gene ontology analysis revealed enrichment for genes involved in DNA replication, recombination, and repair. These genes were centered around the breast and ovarian cancer type 1 susceptibility protein 1 (BRCA1) locus, resulting in lower levels of BRCA1, ataxia telangiectasia and Rad3-related (ATR), Fanconi anemia, complementation group I, (FANCI), and FA complementation group D2 (FANCD2) [17].

CDK12 in Cancer

CDK12 has been implicated in a variety of cancers, including ovarian cancer [81], breast cancer [82], prostate cancer [83], and gastric cancer [84]. CDK12 can act as either a tumor suppressor or oncogene in these cancers and potentially be a biomarker for DNA damaging response targeted therapies.

CDK12 was first implicated in high-grade serious ovarian cancer as a tumor suppressor. The Cancer Genome Atlas (TCGA) was able to identify nine mutations within the *CDK12* gene, five of which were either nonsense or indel, suggesting a loss of function.

The remaining four mutations were missense mutations located within the kinase domain (R882L, Y901C, K975E, and L996F). The mutation rate of *CDK12* is ~3% in ovarian cancer and has a similar prevalence rate of both *BRCA1* (3.5%) and *BRCA2* (3.2%) mutations [81]. The loss of function mutations in *CDK12* resulted in the abolishment of CDK12/cyclin K interaction causing the inactivation of CDK12 kinase activity [81, 85]. The subsequent loss of kinase activity has been shown to reduce *BRCA1* levels, disrupt HR repair, and sensitizes ovarian cells to poly(ADP-ribose) polymerase (PARP) inhibitors and DNA damaging agents [86].

CDK12 becomes dysregulated in a variety of breast cancer subtypes. In triple-negative breast cancer (TNBC), *CDK12* has a mutational rate of 1.5%, and *BRCA1* has a mutational rate of 30% [87]. Like ovarian cancer, in breast cancer *CDK12* mutations result in the loss of kinase activity. TNBC patients with HR deficiency (including the loss-of-function mutated CDK12) can potentially benefit from PARP inhibitors [87]. In estrogen receptor (ER) positive, CDK12 downregulation is part of the resistance mechanism to tamoxifen. *CDK12* expression is downregulated, resulting in the activation of the MAPK pathway and subsequent loss of ER dependency, causing tamoxifen resistance [88]. The last breast cancer subtype with CDK12 dysregulation is HER-2 positive breast cancer; this subtype is characterized by HER-2, located on chromosome 17q12, amplification which prompts the co-amplification of a 17q12-21 amplicon [89]. Since *CDK12* is located on chromosome 17q12, the HER-2 amplicon contains CDK12 in 71% of cases. An increase in CDK12 expression has been correlated to high tumor grade in breast cancer [90]. On the contrary, HER-2 amplicon rearrangement disrupts CDK12 gene expression in 13% of cases, resulting in CDK12 loss of function [91]. Additionally, alternative last exon splicing by CDK12 regulates both the DNA damage response activator ATM and DNAJB6 isoform in HER-2 positive breast cancer. These have been shown to influence cell invasion and

tumorigenesis in xenografts. Tien and colleagues found a direct correlation between DNAJB6, migration capacity, and tumor cell invasiveness with CDK12 levels [79]. In summary, breast cancer subtypes with loss of function mutations for CDK12 lead to genomic instability and PARP inhibitor susceptibility. In subtypes with CDK12 amplification, these cancers may depend on CDK12 expression and provide a new therapeutic target.

Prostate cancer is the second most commonly diagnosed cancer in men, with a 6.9% mutational rate for *CDK12*. Of the mutations found in prostate cancer, 83% result in the truncation of CDK12 resulting in the loss of the kinase domain [92]. However, unlike ovarian cancer, CDK12-defective prostate cancer did not affect *BRCA1* expression. These tumors show an up-regulation of genes involved in the inflammatory response. And down-regulation of genes involved in oxidative phosphorylation, hormone receptor signaling, and epithelial dedifferentiation [92]. CDK12 is also involved in gastric cancer, where again CDK12 is co-amplified with HER-2 [93]. HER-2 positive gastric patients with high expression of CDK12 show a lower overall survival rate than patients with low CDK12 expression [84]. In summary, CDK12 acts as a tumor suppressor in prostate cancer and as an oncogene in gastric cancer.

Furthermore, CDK12 can form synthetic lethal partners, which means inactivation of either of the two genes individually has little effect on cell viability, but the loss of function of both genes simultaneously leads to cell death. A siRNA functional genomic screen and synthetic lethal screen for the oncogene MYC in MYC-driven cancers discovered CDK12 as a synthetic lethal gene [94, 95]. MYC is a central driver for cancer, and targeting MYC using conventional means remains a challenge [96]. Hence, CDK12 may provide a new target for MYC-driven cancers because of the overlapping cellular functions of MYC and

CDK12. MYC is known to accelerate DNA replication by inducing replicative stress; this shows how DDR is a weakness in MYC-driven cancers [97].

The fusion protein EWS/FLI is an essential transcriptional activator and transforming gene found to be pathogenic in Ewing sarcoma. Similar to MYC, EWS/FLI fusion makes cancer cells suspectable to DDR [98]. Genes that drive cancer, such as MYC and EWS/FLI fusions, are great therapeutic targets; however, targeting these proteins remains a challenge, however targeting their synthetic lethal partners, in this case, CKD12, is a viable therapeutic option. Additionally, this synthetic lethal relationship also indicates that CDK12 is an essential component in oncogene-driven tumorigenesis.

PHARMACOLOGICAL WAYS TO TARGET CYCLIN-DEPENDENT KINASES

ATP-Competitive Inhibitors

Cyclin-dependent kinases have been shown to contribute to the development of cancer. Therefore, medicinal chemists both in academia and pharmaceutical companies have focused their efforts on developing small-molecular inhibitors that target this protein kinase family [4, 99, 100]. There have been various types of inhibitors designed to perturb kinase activity; particularly, most inhibitors that have been developed for CDK inhibition bind to the ATP binding site [18, 101, 102]. These small molecular inhibitors are called ATP-competitive inhibitors and mimic ATP when inhibiting the kinase activity. The ATP binding pocket is positioned in-between the N- and C-terminal lobes [6]. When the kinase is active, the adenosine ring within ATP forms three hydrogen bonds with the kinase's hinge region. The ATP ribose and triphosphate groups then bind to the hydrophilic channel near the substrate-binding site, making it accessible for catalysis [99]. ATP-competitive inhibitors are designed to mimic ATP within the active site. These inhibitors bind within the ATP binding pocket and mirror the hydrogen bond network. The ATP competitive inhibitors

block ATP binding and the subsequent transfer of the γ-phosphate to downstream substrates, thus inhibiting the downstream signaling pathway [99].

Non-Covalent Inhibitors

Non-covalent inhibitors are designed to transiently interact with their target kinase to suppressing the enzymatic activity or disrupting protein-protein interactions by binding to the ATP binding pocket or hot spot, respectively. These inhibitors form reversible hydrogen bonds between the inhibitor functional groups and the protein active site residues, creating an equilibrium between bound and unbound states of the protein-inhibitor complex (**Figure 2**) [102, 103]. The potency of non-covalent inhibitors is correlated to their target binding affinity, which is referred to as the dissociation constant (K_i) [104]. In 2001, Imatinib (Gleevec) was the first kinase inhibitor approved by the FDA to treat Philadelphia chromosome-positive chronic myeloid leukemia targeting Bcr-Abl [105]. As of 2018, 37 non-covalent kinase inhibitors have received FDA approval to treat several malignancies [106].

A.

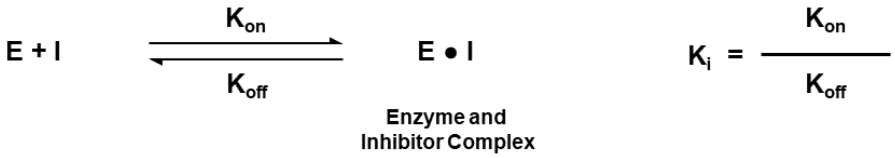

B.

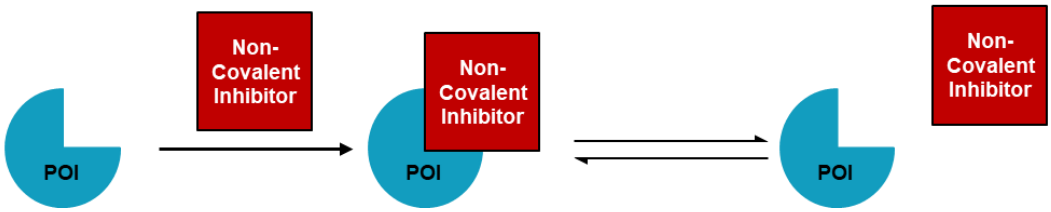

Figure 2. Mechanism of Action of Non-covalent inhibitors. **A)** Generic mechanism of non-covalent inhibitors (E=enzyme, I=inhibitor). **B)** Mechanism of action of non-covalent inhibitors which transiently interact with their target.

The use of non-covalent ATP-competitive small molecule kinase inhibitors has been the primary approach to CDK inhibition over the last 25 years [103], which has resulted in the development of several first-generation CDK inhibitors as potential cancer therapeutics. The first-generation inhibitors have been tested in numerous clinical trials for several different cancer types [20]. The first-generation inhibitors that were developed were relatively non-specific and were often classified as ‘pan-CDK’ inhibitors; these include the well-studied CDK inhibitors flavopiridol, roscovitine, and olomoucine [18, 107-109]. Flavopiridol inhibits CDK1, CDK2, CDK4, CDK6, CDK7, and CDK9, and as a result, induces cell cycle arrest in G1 and G2 phases, as well as suppresses transcription [107]. Flavopiridol showed nM potency *in vitro* activity and suppressed tumor growth in animal models; thus, it was tested in over 60 clinical trials in a broad spectrum of cancer types where it showed substantially less activity *in vivo.* Therefore, drug development of flavopiridol was discontinued in 2021 [20]. Like flavopiridol, roscovitine inhibited CDK1, CDK2, CDK5, CDK7, and CDK9 and failed to demonstrate clinical potential in clinical trials [108]. Unlike roscovitine and flavopiridol, olomoucine was not developed commercially, but it was used as a chemical tool; olomoucine inhibits CDK1, CDK2, CDK7, and CDK9 [110]. First-generation CDK inhibitors showed good anti-cancer properties, but due to the non-specific nature of inhibition, many of these compounds had significant toxicity and failed to meet pharmaceutical expectations when advanced to the clinic.

Since first-generation CDK inhibitors lacked clinical efficacy, the discovery and development of new CDK inhibitors with enhanced selectivity and potency were necessary. In 2004, a new class of ATP-competitive CDK inhibitors was discovered through high-throughput screening (HTS) towards CDK2 inhibition. This screen identified 3-aminopyrazoles as potent CDK2 inhibitors which contain an aminopyrazole core [111]. Due to the small nature of the core and the ability to easily modify the substituents, this

class of molecules has rapidly expanded. This class was further developed using structure-activity relationship (SAR) studies to generate the CDK2 inhibitor PNU-292137 [111]. The ability of PNU-292137 to inhibit CDK2 was elucidated using X-ray and crystallographic studies, which revealed that the trio of hydrogen bonds undergo a donor-acceptor-donor relationship between the nitrogen residues on the aminopyrazole core and the Glu81-Lue83 residues of CDK2 in the hinge region [111]. The aminopyrazole core can be functionalized at two positions, one that occupies the shallow hydrophobic pocket and the other is solvent-exposed. SAR studies illustrate that modifying the aminopyrazole core substituents could lead to more potent and selective CDK inhibitors. Since this scaffold discovery, several other aminopyrazole based CDK inhibitors have been developed and evaluated in clinical trials. For example, the pan-CDK inhibitor AT7519 targets CDK1, CDK2, CDK4, CDK6, and CDK9 inhibitor and is currently being investigated in combination therapy with onalespib, a small-molecule inhibitor of heat shock protein 90, in a clinical trial to treat advanced and metastatic malignant solid neoplasm (NCT02503709) (https://clinicaltrials.gov/) [20, 111].

Despite the promiscuity of first-generation and second-generation inhibitors and failed clinical trials, later generations have obtained FDA approval. Currently, there are only three FDA-approved CDK inhibitors, Palbociclib, Ribociclib, and Abemaciclib. Palbociclib, an orally bioavailable inhibitor that targets CDK4/6, became the first CDK inhibitor to receive FDA approval for the treatment of HR+, HER2– breast cancer in February of 2015 [112, 113]. Ribociclib, another CDK4/6 inhibitor, received its first FDA approval in March 2017 to treat hormone receptor-positive, ErbB2/HER2-negative advanced breast cancer [114]. Abemaciclib, the more recent CDK4/6 inhibitor, obtained FDA approval in September 2017 to treat ER-positive, HER2-negative advanced breast cancer as a monotherapy and in combination with fulvestrant, an estrogen receptor

antagonist [105]. Each of these inhibitors binds to the ATP binding pocket of CDK4 and CDK6. Palbociclib and ribociclib are classified as 2-amino-pyrrolo[2,3-d]pyrimidine derivatives and abemaciclib is classified as an amino-pyrimidine-benzimidazole derivative. These scaffolds enable their amino groups to form a hydrogen bond with the carbonyl group of V101 on CDK4/CDK6. The pyrimidine forms a hydrogen bond with the N-H group of V101 within the hinge region, effectively blocking ATP from binding to CDK4/6 [115]. Inhibition of CDK4/CDK6 results in the inhibition of retinoblastoma protein phosphorylation during the G1 phase of the cell cycle leading to cell cycle arrest, suppressing DNA replication, and decreased tumor cell proliferation [116]. As our understanding of CDK biology continues to progress, inhibitors designed to target them have also improved, making it easier to develop selective and potent CDK inhibitors for other members of the CDK family, including CDK9 and CDK12.

Covalent Inhibitors

Covalent inhibitors are designed to form a covalent bond with a specific molecular target to provide a prolonged therapeutic response due to the increased drug occupancy. Like non-covalent inhibitors, covalent inhibitors initially bind reversibly with their target. Following this initial interaction, they form a covalent bond with the target protein resulting in an irreversible drug-protein complex (**Figure 3**) [117]. Covalent inhibitors have been used in pharmacology for over a decade. The first known covalent inhibitor was acetylsalicylic acid, better known as aspirin, which has been on the market since 1899 [118]. Currently, there are more than 50 covalent inhibitors that have obtained FDA approval representing about 30% of marketed drugs [104].

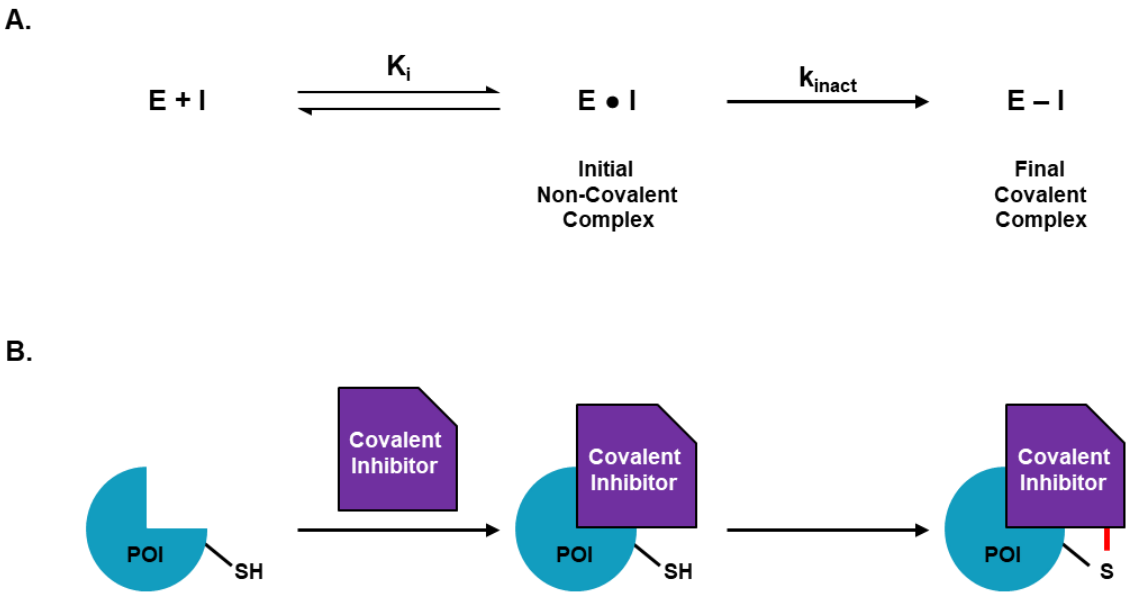

Figure 3. Mechanism of Action of Covalent Inhibitors. **A)** A two-step mechanism of inhibition, where E represent the enzyme, I is the inhibitor, E●I is the initial reversibly bound enzyme inhibitor complex, and E – I represents the final covalent complex between the enzyme and inhibitor. K_{inact} is the maximum potential rate of inactivation. **B)** Mechanism of action of irreversible covalent inhibitors which targets a cysteine residue on the protein of interest (POI) . *Modified from Sutanto, Konstantiniduo, and Dömling (2020) RSC Medicinal Chemistry.

Despite the use and development of covalent inhibitors for more than a decade, the first CDK covalent inhibitor was not developed until 2014 with the discovery of THZ1 [119]. THZ1 was characterized as a phenylaminopyrimidine bearing a cysteine-reactive acrylamide moiety. Mass spectrometry analysis was able to identify the covalent modification site as cysteine 312. This residue is located outside the kinase domain of CDK7, making THZ1 the first inhibitor to target a cysteine residue outside of the kinase domain [119]. To further validate the cysteine residue, THZ1 docked into the crystal structure of CDK7, determined a C-terminal extension bearing C312 traverses the ATP binding pocket in the kinase domain; furthermore, it predicted the C312 residue would be directly adjacent to the reactive acrylamide moiety of THZ1. Additionally, Gray and colleagues showed that mutation from cysteine to serine (C312S) prevented THZ1 from covalently binding to CDK7 [119]. Sequence alignment of the CDK family determined that CDK12 and CDK13 possess cysteine residues within four amino acids of C312, but C312 is unique to CDK7. Due to the similarity, they found that THZ1 inhibited CDK12 kinase activity, however, at slightly higher concentrations. THZ1 ability to concurrently bind to the ATP-binding pocket and covalently interact with a cysteine residue characterized it as an ATP-competitive, allosteric covalent inhibitor. THZ1 was initially tested in a diverse panel of 1,000 cancer cell lines to evaluate its anti-proliferative activity. THZ1 exhibited IC_{50} values of less than 200 nM against 53% of the cancer cell lines tested, demonstrating its therapeutic potential. However, THZ1 is unsatisfactory for further clinical development due to its cross-reactivity to CDK12 and CDK13; also, its poor bioavailability and dismal half-life *in vivo* [119].

Considering the poor clinical potential of THZ1 but the high therapeutic potential of a selective covalent CDK7 inhibitor, Hu and colleagues utilized the THZ1 scaffold to design a suitable compound for clinical development [120]. They sought to improve

potency, selectivity, and metabolic stability. After numerous modifications, this group synthesized SY-1365. SY-1365 engages the same cysteine residue as THZ1, cysteine 312. THZ1 had an EC_{50} of 38 nmol/L, and SY-1365 has an EC_{50} of 8 nmol/L in terms of potency. THZ1 had an EC_{50} of 101 nmol/L in terms of selectivity towards CDK7, and SY-1365 has an EC_{50} of 13 nmol/L. In terms of metabolic stability, THZ1 had a plasma clearance value of 129 mL/min/kg, and SY-1365 has a plasma clearance value of 5.6 mL/min/kg [120]. They were indeed able to improve upon THZ1, making a compound suitable for clinical development. And in 2017, the clinical trial of SY-1365 for ovarian and breast cancer treatment started (NCT03134638). However, on March 9, 2021, the clinical trial was terminated, citing a business decision (https://clinicaltrials.gov/).

Covalent inhibitors have also been designed against CDK12. Utilizing the structure of THZ1, Gray and colleagues made chemical modifications to alter the acrylamide moiety orientation to target CDK12, resulting in THZ531 [106]. The C-terminal domain of CDK12 traverses the kinase domain, positioning a cysteine residue near the ATP-binding pocket. THZ531 binds to the active site of CDK12 and CDK13, inhibiting the enzymatic activity of both kinases. Additionally, THZ531 covalently interacts with cysteine 1039 on CDK12, which is located outside the kinase domain. Like THZ1, THZ531 weakly inhibits other CDK family members' enzymatic activity, in this case, CDK7 and CDK9 [121]. THZ531 represents the first covalent inhibitor to target CDK12 and CDK13.

Ferguson and colleagues were the first to synthesis a covalent inhibitor for CDK14. This lab employed *in vitro* assays to identify potential CDK14 targeted scaffolds, from which they identified AT7519, a pan-CMGC kinase inhibitor. The piperidine moiety of AT7519 was replaced with acrylamide-bearing groups, while the hinge-binding scaffold (aminopyrazole core) of AT7519 remained. Through extensive analog synthesis, they identified FMF-04-159-2 as a potent Pan-TAIRE CDK inhibitor that covalently binds to

CDK14 on Cys218, a uniquely CDK14 cysteine residue [3]. Since little is known about CDK14, this compound is a valuable tool in further characterizing CDK14 kinase function. In summary, covalent inhibitors have been designed against CDK7, CDK12/13, and CDK14 so far.

PROTEOLYSIS-TARGETING CHIMERA

Classical drug discovery is based on the occupancy-driven pharmacological model; the inhibitors designed using this approach are generally covalent and non-covalent inhibitors [122]. As discussed earlier, these inhibitors require binding to the active site to suppress the enzymatic activity of their target. Non-covalent inhibitors bind reversibly, requiring higher continuous systemic drug administration to ensure maximum occupancy of the active site for optimal therapeutic efficacy, leading to dose-limiting toxicity. Furthermore, covalent inhibitors can cause drug-induced toxicity or have unexpected toxicity or hypersensitivity [104]. Additionally, the need for a binding niche limits the number of proteins in which this approach can effectively target. Currently, only about 7% of the human proteome is considered pharmaceutically accessible via the classical methods [123].

Due to the occupancy-driven model's current limitations, an alternative approach has been gaining attention over the last few decades, called the event-driven pharmacological model. This approach encompasses several different methods, including hydrophobic tagging, ligand-induced degradation, molecular glues, and proteolysis-targeting chimeras [122]. These methods result in irreversible protein function inhibition by inducing protein degradation by engaging the ubiquitin/proteasome system (UPS). The UPS is a cellular quality control system used to maintain protein homeostasis by removing misfolded and damaged proteins [124]. This control mechanism can be rudimentarily broken down into two steps, 1) ubiquitin covalently binds to lysine residues of a target

protein, and 2) degradation of the target protein is facilitated by the 26S proteasome. Step 1 of this process is facilitated by a series of three enzymes. An activation enzyme, E1, transfers the ubiquitin to a carrier E2 enzyme, which in turn tags ubiquitin to the doomed substrate with the assistance of the E3 enzymes [125].

PROteolysis TArgeting Chimera, coined PROTAC by Craig Crews, are hetero-bifunctional molecules comprised of two different ligands connected via a linker. One ligand is required for binding to the protein of interest (POI). The other ligand is essential to bind to an E3 ubiquitin ligase, resulting in a ternary complex formation [122, 126, 127]. The formation of this stable ternary complex allows the E3-ligase to ubiquitinate the POI, which is subsequently degraded by the proteasome. The release of the PROTAC from the POI resulting from target degradation enables the PROTAC to be recycled. As a result, the rate-limiting step in this process is the formation of the ternary complex (**Figure 4**). However, at high PROTAC concentrations, unproductive binary complexes can be observed, and this phenomenon is referred to as the hook effect. Due to the catalytic process, the amount of drug (PROTAC) required is less than the abundance of the target protein in the cell, which addresses the dose-limiting toxicity problem associated with traditional inhibitors.

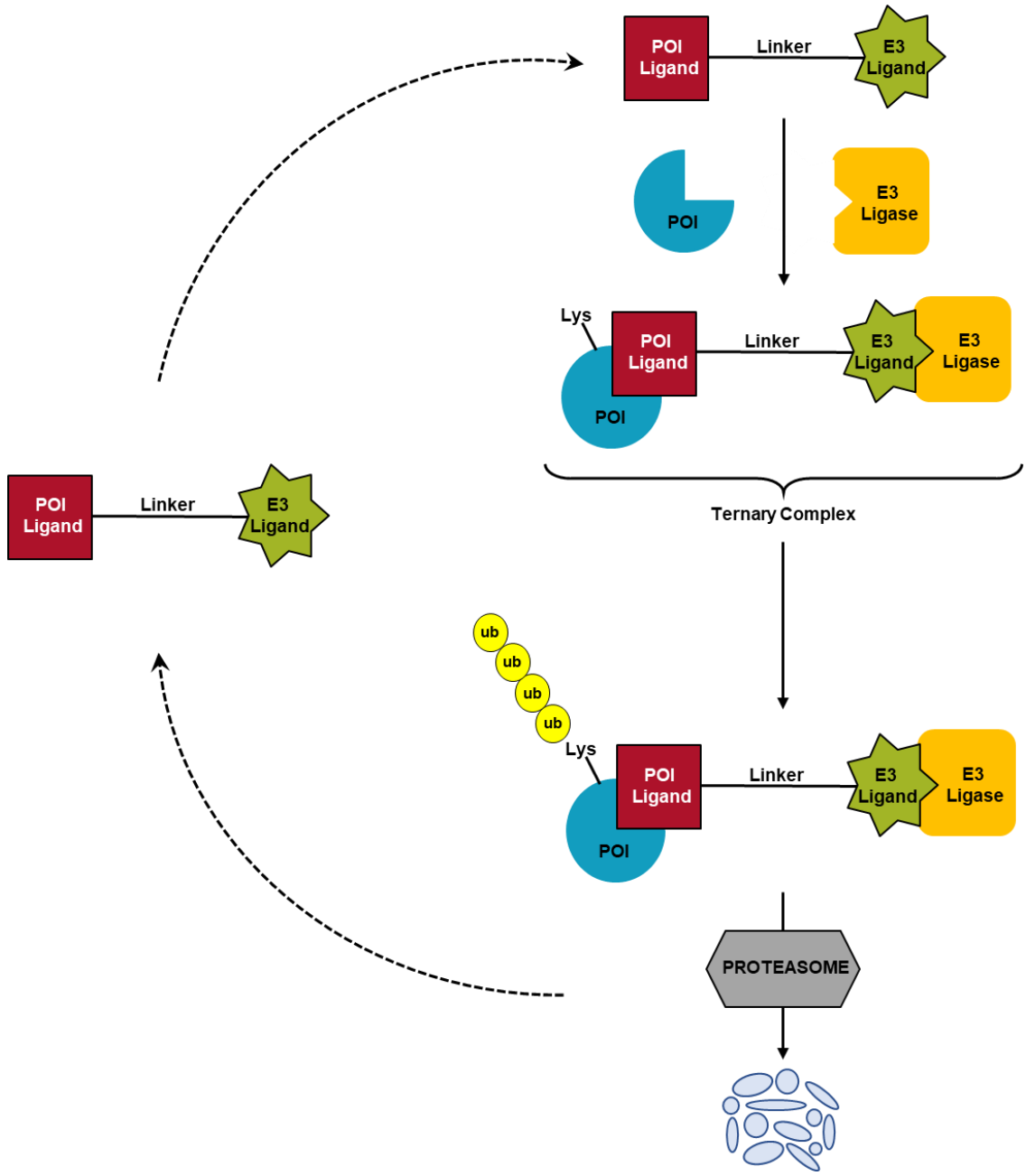

Figure 4. PROTAC Mechanism of Action.

History

The PROTAC approach to targeted protein degradation was first proven utilizing a peptide-based PROTAC, called PROTAC-1 [126]. PROTAC-1 was synthesized using ovalicin, a covalent angiogenesis inhibitor, as the POI ligand to bind methionine aminopeptidase-2 covalently. The E3 ligand was a ten amino acid peptide of IκBα, DRHDSGLDSM, used to recruit the Skp1-Cullin-F box E3 complex ($SCF^{\beta\text{-}TRCP}$) [126]. When tested in *Xenopus* extracts, PROTAC-1 successfully degraded methionine aminopeptidase-2, validating that an E3 ligase can accept neo-substrates. However, the large size of the IκBα phosphopeptide within PROTAC-1 fundamentally resulted in low cell permeability, labile peptide bonds, and low potency, which hindered further pharmacological development [122, 126].

After this foundation experiment, a considerable effort was made to generate new small-molecule PROTACs with improved cellular penetrance and stability. In 2008, the first all small-molecule PROTAC was reported [128]. This PROTAC was synthesized using a selective non-steroidal androgen receptor ligand (SARM) as the POI to interact with the androgen receptor. The E3 ligand was a type of compound, called nutlins, to recruit the E3 ligase MDM2. A PEG-based linker connected the nutlin ligand and SARM ligand. The SARM-nutlin PROTAC could degrade the androgen receptor at 10 μM HeLa cells after a 7-hour treatment. They were able to show a blockade of degradation when pre-treated with a proteasome inhibitor, proving degradation is proteasome-dependent. While this new class of PROTACs was able to overcome the cell permeability issues of the peptide-based PROTACs, it still had relatively low potency for further pharmacological development [128].

In 2010, another new class of small-molecule PROTACs was discovered. This class utilized bestatin ester analogs, which bind to the baculoviral IAP repeat domains of

the E3 ligase cIAP1 [129]. The POI ligand used was the *all-trans* retinoic acid, a derivative of vitamin A, to target CRABP-I and II (cellular retinoic acid-binding proteins-I and II). CRABP-II levels were reduced in neuroblastoma IMR-32 cells when treated with this PROTAC, illustrating its ability to induce ubiquitination and degradation of the intracellular CRABP-I/II proteins. This type of PROTAC possessed sufficient permeability and stability in cells, but, like MDM2 based PROTACs, these cIAP1-based PROTACs lacked selectivity and activity [129].

Arguably the most significant development in PROTAC technology was the use of cereblon and Von-Hippel-Lindau (VHL) recruiting moieties in small-molecule PROTAC design. Cereblon (CRBN) based PROTACs started with the discovery of the molecular target of thalidomide. In 2010, Ito *et al*. discovered that the immunomodulatory drug thalidomide interacts with the E3 ubiquitin ligase, cereblon. Previously, thalidomide was used as an anti-nauseous medication for pregnant women, but it caused severe congenital disabilities. Presumably, treatment with thalidomide triggered the degradation of critical genes necessary for proper development [130]. This key discovery proved thalidomide to be a valuable ligand to target E3 ubiquitin ligases.

Exploiting this discovery, researchers repurposed thalidomide to target the degradation of disease-driving proteins for the first time in 2015 [131]. Lu *et al.* synthesized ARV-825, a small-molecule BRD4 targeting PROTAC using OTX015, a BRD4 non-covalent inhibitor, as the POI binding moiety and pomalidomide, a third-generation immunomodulatory drug, as the E3 ligase cereblon binding moiety. When tested for potency in Burkitt's lymphoma cell lines, ARV-825 achieved a DC_{50} for BRD4 below 1 nM, fundamentally increasing the potency seen by other classes of PROTACs [131].

Before 2015, VHL ligands were used in peptide-based PROTACs where it demonstrated better cellular permeability but still lacked potency like other peptide-based

PROTACs [132]. However, in 2015 VHL ligands were utilized in two small-molecule PROTACs designed to target ERRα and RIPK2 [133]. PROTAC_ERRα demonstrated dose-dependent reduction of ERRα in MCF-7 breast cancer cells, demonstrating a DC_{50} ~100 nM. Similarly, PROTAC_RIPK2 exhibited a DC_{50} of 1.4 nM in human THP-1 monocytes illustrating a stable, dose-dependent RIPK2 degradation. These two small molecule-based VHL PROTACs were capable of explicitly reducing protein levels by >90% at nanomolar concentrations, clearly demonstrating the improved potency of the PROTAC technology [133].

More recently, a family of antitumor sulfonamides has been shown to recruit DCAF15 E3 ligase. In 2017, Han *et al.* discovered that the splicing inhibitor sulfonamide drug indisulam interacts with the E3 ubiquitin ligase, DCAF15 [134]. Utilizing this discovery, Zoppi and colleagues in 2018 synthesized the first DCAF15 based PROTACs designed to target BRD7 and BRD9. However, these PROTACs were unable to degrade either target [135]. In 2020, the first successful DCAF15 PROTAC was synthesized to target BRD4. Li *et al.* synthesized DP1, utilizing the BET inhibitor JQ1 as the POI binding moiety, and a biotinylated photosensitive sulfonamide E7820 probe, as the E3 ligase DCAF15 binding moiety. DP1 obtained a DC_{50} value of $10.84 \pm 0.92\,\mu M$ for BRD4; however, it demonstrated a dose-dependent degradation of BRD2 and BRD3 as well [136]. This study proves DCAF15 based PROTACs can be used; however, this class needs the development of new DCAF15 ligands with higher affinity and specificity to improve their potency.

In summary, since the technologies conception in 2001, the PROTAC field has robustly expanded and improved. The field went from peptide-based PROTACs that lacked cellular permeability and potency to small-molecule-based PROTACs with nanomolar potency.

Applications

Since 2001, molecules have been designed against a whole host of protein kinases, including some of the “undruggable” proteome (**Table 1**). More than 40 targets have been degraded by PROTACs so far utilizing one of the five E3 ubiquitin ligases that have been exploited so far with this technology; these include $SCF^{\beta\text{-}TRCP}$, MDM2, cIAP1, VHL, CRBN, and DCAF15. These molecules have been designed to target proteins related to various diseases, including cancer, viral infections, immune disorders, and neurodegenerative diseases [137]. In general, PROTACs are great research tools with the potential to be therapeutic agents.

E3 Ligase	Molecule Name	Protein Target	Reference
cIAP1	DAS-IAP	BRC-ABL	[138]
CRBN	TL13-12	ALK	[139]
	C5	BCL2	[140]
	PROTAC 9	BCL6	[141]
	DAS-6-2-2-6-CRBN	BCR-ABL	[142]
	dBET1	BRD4	[143]
	dBRD9	BRD9	[144]
	L18I	BTK	[145]
	BSJ-04-132	CDK4	[146]
	PROTAC 6	CDK6	[147]
	JH-XI-10-02	CDK8	[148]
	PROTAC 3	CDK9	[149]
	TL13-117	FLT3	[150]
	dMCL1-2	Mcl-1	[151]
	Compound D	PI3K	[152]
	SD-36	STAT3	[153]
DCAF15	DP1	BRD4	[136]
	Compound 9	BRD7	[135]
MDM2	SARM-nutlin PROTAC	AR	[128]
	Compound 3	PARP1	[154]
VHL	Api-PROTAC-II	AHR	[127]
	ARCC-4	AR	[155]
	DAS-6-2-2-6-VHL	BCR-ABL	[142]
	ARV-771	BET	[156]
	VZ185	BRD9/7	[135]
	Brequinar-PROTAC	DHODH	[157]
	ERD-308	ER	[158]
	PROTAC_ERRα	ERRα	[133]
	PROTAC-3	FAK	[159]
	UNC6852	PRC	[160]
	PROTAC_RIPK2 3	RIPK2	[133]
	DAT8	SGK3	[161]
	PROTAC	Smad3	[162]
	Compound 3i	TBK1	[163]
	dTRIM24	TRIM24	[164]

Table 1. Representative table of current small-molecule PROTAC.Including exploited E3 ligase, compound name, and compound targets. *Modified from Sun et.al. (2019) Nature.

The PROTAC strategy holds several advantages over traditional inhibitors. First, they can degrade the “undruggable” protein targets. It is estimated that only about 7% of the human proteome is pharmaceutically accessible to traditional inhibition. These “undruggable” proteins typically lack catalytic activity and/or have catalytic independent functions. These include transcription factors, protein skeleton function, and mutated proteins. The PROTAC technology has been successfully employed to target the Signal Transducer and Activator of Transcription 3 (STAT3), which was previously considered undruggable; this case confirms the ability of PROTAC technology to target these proteins [153]. Next, PROTACs can eliminate both the enzymatic and nonenzymatic functions of kinases, while traditional inhibitors only inhibit the enzymatic activity. For example, Craig M. Crews’ group developed a highly effective and selective FAK PROTAC, which inhibited both the kinase-dependent and kinase-independent function of FAK [159]. Thus proving, PROTACs can expand the druggable space, which was previously considered difficult to control by traditional inhibitors.

Furthermore, PROTACs can be a valuable tool for the fast and reversible chemical knockdown of proteins. Current genetic protein knockout technologies are associated with high costs, are irreversible, and take a lot of time to develop. Additionally, PROTACs provide an advantage when studying embryonic-lethal genes *in vivo* since PROTACs knock down proteins directly rather than acting at the genome level, making them suitable for functional studies of embryonic-lethal proteins in adult organisms. Lastly, PROTACs have been proven to overcome drug resistance in cancers. For example, the androgen receptor targeting PROTAC ARCC-4 does overcome enzalutamide-resistant prostate cancer [155]. In summary, PROTACs possess several advantages that can help advance drug development.

Since PROTACs offer added benefits compared to traditional inhibitors, it begs the question, are they pharmaceutically as potent as their inhibitor counterparts? A study from Nathanael Gray's group at the Dana-Farber Cancer Institute was the first to investigate the difference between CDK9 inhibition (NVP-2 and SNS-032) and CDK9 degradation (THAL-SNS-032) [165]. First, they synthesized THAL-SNS-032, which uses thalidomide as the E3 ligand, and SNS-032, a pan-CDK inhibitor, as the POI ligand. SNS-032 targets CDK1, CDK2, CDK7, and CDK9 at low nanomolar concentrations (4-398 nM) [165]. Next, they investigated the ability of THAL-SNS-032 to degraded CDK9 in MOLT4 cells. They performed a time-course experiment which determined THAL-SNS-032 induced robust degradation of CDK9 as soon a 1 hour and persisted for at least 24 hours, obtaining an IC_{50} of 50 nM [165]. Furthermore, they characterized the pan-CDK inhibitor SNS-032 for comparison with THAL-SNS-032, which they determined has an IC_{50} of 173 nM [165]. Head-to-head comparison of apoptotic ability both SNS-032 and THAL-SNS-032 induced PARP cleavage by 4 hours; however, THAL-SNS-032 reduced Mcl-1 levels by 4 hours while SNS-032 did not reduce Mcl-1 levels. When compared head-to-head for anti-proliferative effects, THAL-SNS-032 treatment resulted in a more profound decrease in viability after washout when compared to SNS-032. Furthermore, they determined that compound washout significantly reduced the induction of apoptosis caused by SNS-032; this was not the case for THAL-SNS-032. This illustrates the prolonged effect of degradation over inhibition [165].

Since PROTAC's conception in 2001, significant advances have been made in the field. Consequently, two PROTACs are being evaluated in clinical trials. ARV-110 is an orally bioavailable androgen receptor targeting small molecule PROTAC degrader [166]. In *in vitro* analyses, ARV-110 is a sub-nanomolar selective AR degrader capable of suppressing the AR-target gene PSA expression, inhibiting AR-dependent cell

proliferation, and induces apoptosis. In *in vivo* analysis, ARV-110 degraded 90% of the androgen receptor with once-a-day oral administration of 1 mg/kg dose [166]. ARV-110 is currently being tested in phase II clinical trials for the treatment of metastatic castration-resistant prostate cancer. ARV-471 is an orally bioavailable estrogen receptor targeting small molecule PROTAC degrader [167]. In ER-positive breast cancer cell lines, ARV-471 achieves nanomolar degradation of the ER, decreasing ER-target genes' expression and inhibiting cell proliferation. Additionally, ARV-471 can degrade the known ER mutated variants Y537S and D538G. In *in vivo* experiments, ARV-471 demonstrated >90% ER degradation and led to significant tumor volume regressions when administered oral, once-a-day at 3 mg/kg and 10 mg/kg [167]. ARV-471 is currently in Phase 1b combination trial with Palbociclib for the treatment of advancer or metastatic ER+/HER2- breast cancer.

As promising as the PROTAC technology is, several challenges need to be addressed/understood. PROTACs are catalytic, meaning traditional methods of evaluating pharmacokinetics (PK) and pharmacodynamics (PD) properties cannot be accurately used. As a result, new PK and PD evaluation systems need to be designed for PROTACs. Furthermore, predicting degradation activity, selectivity, and possible off-target effects of PROTACs is still poorly understood, making rational drug design difficult. As mentioned early, only six E3 ubiquitin ligases have been used to develop PROTACs so far, even though the human genome encodes more than 600. Expanding the number of E3 ubiquitin ligase used is another challenge PROTACs must overcome. Moreover, quick and effective screening of PROTAC POI ligands needs to be developed. Lastly, there is no way to distinguish between PROTAC mediated degradation and “molecular glue” mediated degradation. “Molecular glues” stabilize protein−protein interactions through small molecule modulators of E3 ligases, which some PROTACs have been reported to function as to cause degradation [168].

CHAPTER 2: MATERIALS AND METHODS

CHEMISTRY

General Methods

All reagents were purchased from commercial sources and were used without further purification. Flash chromatography was carried out on silica gel (200–400 mesh). Thin-layer chromatography (TLC) was performed on pre-coated silica gel 60 (Å) F_{254} plates (EMD Millipore) and observed under UV light at 254 nm and stained with basic potassium permanganate dip. Column chromatography was performed with silica gel (230-400 mesh, grade 60, Fisher Scientific, USA). ^{1}H NMR (500 MHz) and ^{13}C NMR (125 MHz) spectra were recorded in DMSO-D_6 or chloroform-d ($CDCl_3$) on a Varian-500 and Varian-600 spectrometer (DMSO-D_6 was 2.50 ppm for ^{1}H and 39.55 ppm for ^{13}C, $CDCl_3$ was 7.27 ppm for ^{1}H and 77.23 ppm for ^{13}C). Proton and carbon chemical shifts were reported in ppm relative to the residual solvent proton and carbon signal. The compound's final purity was determined by analytical HPLC and was found to be ≥95% pure. Analysis of sample purity was performed on a Waters Alliance 2695 HPLC system equipped with a Waters 2996 photodiode array detector and an auto-sampler with Phenomenex Luna RP-C18 column (5 µm, 4.6 mm × 250 mm, 100 Å). HPLC conditions: solvent A, H_2O containing 0.1% formic acid (FA); solvent B, CH_3CN (acetonitrile) containing 0.1% FA; gradient, 10% B to 100% B over 15 min followed by 100% B over 2 min; flow rate, 1 mL/min. Purity was determined at λ=254 nm. Retention times for each final compound are provided in the synthesis section. High-resolution mass spectrometry (HRMS) for the compounds was generated on an Agilent 6230 LC/TOF system with a UV detector (254 nm).

Synthesis of Compounds

All the compounds were synthesized in-house by Dr. Sandeep Rana as follows.

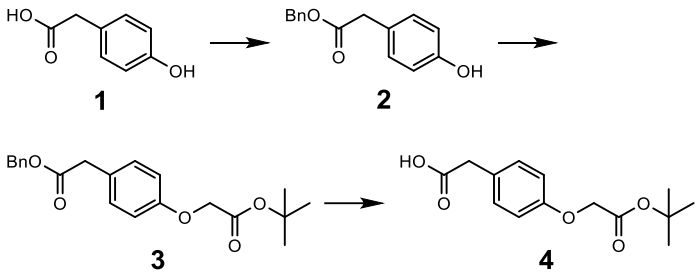

Synthesis of 2 (benzyl 2-(4-hydroxyphenyl)acetate) [169]:

Synthesis of 3 (benzyl 2-(4-(2-(tert-butoxy)-2-oxoethoxy)phenyl)acetate): A solution of compound **2** (700 mg, 2.89 mmol) in DMF was added to K_2CO_3 (798 mg, 5.78 mmol), the solution was heated at 60 °C for 10 minutes followed by addition of tert-butyl 2-bromoacetate (677 mg, 3.47 mmol). The reaction mixture was stirred for 4 hours. The crude mixture was then poured into brine, extracted with ethyl acetate, and the organic phase was collected and extracted consecutively with water and dried with $MgSO_4$. Evaporation of the solvent gave a residue which was purified by column chromatography to produce compound **3** in a quantitative yield as a yellow oil. ^{1}H NMR (500 MHz, $CDCl_3$) δ (ppm) 7.35 – 7.30 (m, 5H), 7.21 (d, 2H, J = 8.5 Hz), 6.85 (d, 2H, J = 8.5 Hz), 5.12 (s, 2H), 4.50 (s, 2H), 3.61 (s, 2H), 1.49 (s, 9H). ^{13}C NMR (125 MHz, $CDCl_3$) δ (ppm) 171.47, 167.91, 157.03, 135.79, 130.29, 128.45, 128.11, 128.02, 126.81, 114.65, 82.23, 66.47, 65.70, 40.35, 27.96.

Synthesis of 4 (2-(4-(2-(tert-butoxy)-2-oxoethoxy)phenyl)acetic acid): Compound **3** (1.16 g) was placed in a round bottom flask, and 20 mL of dry ethyl acetate was added via syringe. Pd/C (116 mg, 5 % by weight on activated carbon) was added to the reaction mixture, and argon gas was bubbled through the reaction mixture for about 10 minutes. The reaction mixture was gently vacuumed and was kept under a hydrogen atmosphere

for 16 hours. After completing the reaction, the mixture was passed through a bed of celite and column chromatographed using hexane and ethyl acetate gradient to obtain compound **4** (870 mg) as a white solid. ^{1}H NMR (500 MHz, $CDCl_3$) δ (ppm) 7.18 (d, 2H, J = 8.5 Hz), 6.84 (d, 2H, J = 8.5 Hz), 4.49 (s, 2H), 3.56 (s, 2H), 1.48 (s, 9H). ^{13}C NMR (125 MHz, $CDCl_3$) δ (ppm) 177.03, 167.98, 157.24, 130.44, 126.23, 114.80, 82.39, 65.77, 39.98, 28.03.

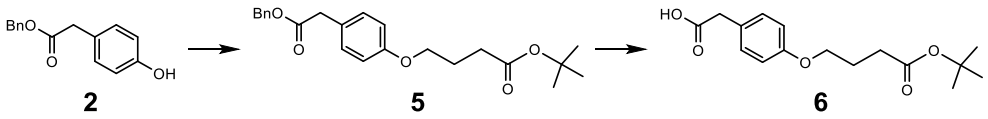

2 **5** **6**

Synthesis of 5 (tert-butyl 4-(4-(2-(benzyloxy)-2-oxoethyl)phenoxy)butanoate): A solution of compound **2** (500 mg, 2.00 mmol) in DMF was added to K_2CO_3 (553 mg, 4.00 mmol), the solution was heated at 60 °C for 15 minutes followed by addition of tert-butyl 4-bromobutanoate (553 mg, 2.47 mmol). The reaction mixture was stirred for 6 hours. The crude mixture was then poured into brine, extracted with ethyl acetate, and the organic phase was collected and extracted consecutively with water, and dried with $MgSO_4$. Evaporation of the solvent gave a residue which was purified by column chromatography to yield compound **5** (510 mg, 64%). ^{1}H NMR (500 MHz, $CDCl_3$) δ (ppm) 7.35 – 7.31 (m, 5H), 7.19 (d, 2H, J = 8.5 Hz), 6.85 (d, 2H, J = 8.5 Hz), 5.13 (s, 2H), 3.98 (t, 2H, J = 6.0 Hz), 3.60 (s, 2H), 2.42 (t, 2H, J = 7.5 Hz), 2.09 – 2.03 (m, 2H), 1.46 (s, 9H). ^{13}C NMR (125 MHz, $CDCl_3$) δ (ppm) 172.50, 171.69, 158.04, 135.88, 130.32, 130.27, 128.55, 128.50, 128.16, 128.09, 125.95, 114.94, 114.59, 80.32, 66.87, 66.51, 40.41, 32.00, 28.09, 24.74.

Synthesis of 6 (tert-butyl 4-(4-(2-(benzyloxy)-2-oxoethyl)phenoxy)butanoate): Compound **5** (500 mg) was placed in a round bottom flask and 10 mL of dry ethyl acetate was added via syringe. Pd/C (70 mg, 5 % by weight on activated carbon) was added to the reaction mixture and argon gas was bubbled though the reaction mixture for about 10

minutes. The reaction mixture was gently vacuumed and kept under hydrogen atmosphere for 16 hours. After completion of the reaction, mixture was passed through a bed of celite, and column chromatographed using hexane and ethyl acetate gradient to obtain compound **6** (381 mg) as a white solid. ^{1}H NMR (500 MHz, $CDCl_3$) δ (ppm) 7.17 (d, 2H, J = 8.5 Hz), 6.84 (d, 2H, J = 8.5 Hz), 3.96 (t, 2H, J = 6.0 Hz), 3.57 (s, 2H), 2.41 (t, 2H, J = 7.5 Hz), 2.07 – 2.02 (m, 2H), 1.44 (s, 9H). ^{13}C NMR (125 MHz, $CDCl_3$) δ (ppm) 177.70, 172.60, 158.18, 130.36, 125.34, 114.64, 80.40, 66.86, 60.41, 40.08, 32.00, 28.08, 24.73, 21.00, 14.16.

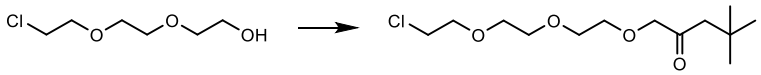

7 **8**

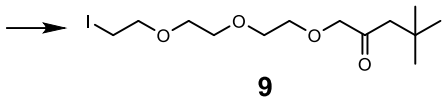

9

Synthesis of 8 (1-(2-(2-(2-chloroethoxy)ethoxy)ethoxy)-4,4-dimethylpentan-2-one) [170] : ^{1}H NMR (500 MHz, $CDCl_3$) δ (ppm) 4.00 (s, 2H), 3.75 – 3.73 (m, 2H), 3.70 – 3.66 (m, 8H), 3.62 – 3.60 (m, 2H), 1.45 (s, 9H). ^{13}C NMR (125 MHz, $CDCl_3$) δ (ppm) 169.58, 81.45, 71.29, 70.66, 70.62, 70.58, 70.54, 68.99, 42.62, 28.04, 27.93.

Synthesis of 9 (1-(2-(2-(2-iodoethoxy)ethoxy)ethoxy)-4,4-dimethylpentan-2-one): To a solution of compound **8** (473 mg, 1.76 mmol) in acetone (10 ml), sodium iodide (NaI) was added (754 mg 5.29 mmol). The reaction mixture was stirred at reflux temperature for 24 hours. The solvent was removed under vacuum, and the crude product was dissolved in ethyl acetate and washed with aqueous 10% $NaHSO_3$, brine, dried ($MgSO_4$), and evaporated under vacuum to yield compound **9** (quantitative yield). ^{1}H NMR (500 MHz, $CDCl_3$) δ (ppm) 3.90 (s, 2H), 3.64 – 3.54 (m, 10H), 3.14 (s, 2H), 1.35 (s, 9H). ^{13}C NMR (125 MHz, $CDCl_3$) δ (ppm) 169.16, 80.96, 71.51, 70.28, 70.17, 69.77, 68.61, 27.74.

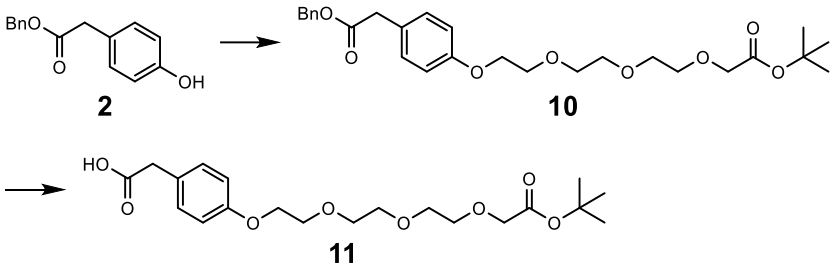

Synthesis of 10 (benzyl 2-(4-((13,13-dimethyl-11-oxo-3,6,9,12-tetraoxatetradecyl)-oxy)phenyl)acetate): A solution of compound **2** (323 mg, 1.34 mmol) in DMF was added to K_2CO_3 (370 mg, 2.68 mmol), the solution was heated at 60 °C for 10 minutes followed by addition of tert-butyl 2-(2-(2-(2-iodoethoxy)ethoxy)ethoxy)acetate (600 mg, 1.60 mmol). The reaction mixture was stirred for additional 16 hours at 60 °C. The crude mixture was then poured into brine, extracted with ethyl acetate, and the organic phase was collected and extracted consecutively with water, and dried with $MgSO_4$. Evaporation of the solvent gave a residue which was purified by column chromatography yielding compound **10** (510 mg, 78%) as colorless oil. ^{1}H NMR (500 MHz, $CDCl_3$) δ (ppm) 7.35 – 7.30 (m, 5H), 7.18 (d, 2H, J = 8.5 Hz), 6.86 (d, 2H, J = 8.5 Hz), 4.11 (t, J = 5.0 Hz), 4.02 (s, 2H), 3.84 (t, 2H, J = 5.0 Hz), 3.74 – 3.68 (m, 8H), 3.59 (s, 2H), 1.47 (s, 9H). 2.42 (t, 2H, J = 7.5 Hz), 2.09 – 2.03 (m, 2H), 1.46 (s, 9H). ^{13}C NMR (125 MHz, $CDCl_3$) δ 171.59, 169.57, 157.88, 135.82, 130.20, 128.44, 128.10, 128.02, 126.07, 114.66, 81.41, 70.72, 70.65, 70.57, 70.56, 69.64, 68.96, 67.37, 66.44, 40.35, 28.03.

Synthesis of 11 (2-(4-((13,13-dimethyl-11-oxo-3,6,9,12-tetraoxatetradecyl)oxy)-phenyl)acetic acid): Compound **10** (510 mg) was placed in a round bottom flask and 10 mL of dry ethyl acetate was added via syringe. To the reaction mixture was added Pd/C (70 mg, 5 % by weight on activated carbon) and argon gas was bubbled though the reaction mixture for about 10 minutes. The reaction mixture was gently vacuumed and was kept under hydrogen atmosphere for 16 hours. After completion of reaction, mixture

was passed through a bed of celite and column chromatographed using hexane and ethyl acetate gradient to obtain compound **11** (420 mg, quantitative yield). ^{1}H NMR (500 MHz, $CDCl_3$) δ (ppm) 7.15 (d, 2H, J = 8.5 Hz), 6.84 (d, 2H, J = 8.5 Hz), 4.11 – 4.07 (m, 2H), 4.00 (s, 2H), 3.82 (t, 2H, J = 5.0 Hz), 3.72 – 3.66 (m, 8H), 3.55 (s, 2H), 1.45 (s, 9H). 2.42 (t, 2H, J = 7.5 Hz), 2.09 – 2.03 (m, 2H), 1.46 (s, 9H). ^{13}C NMR (125 MHz, $CDCl_3$) δ 177.05, 169.66, 157.93, 130.27, 125.63, 114.69, 81.52, 70.67, 70.62, 70.53, 70.50, 69.62, 68.93, 67.32, 60.36, 40.04, 28.01, 20.94, 14.09.

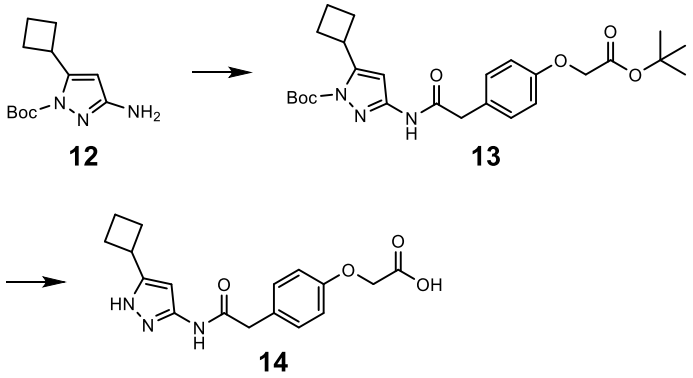

Synthesis of 12 [149]:

Synthesis of 13 (tert-butyl 3-(2-(4-(2-(tert-butoxy)-2-oxoethoxy)cyclohexa-1,5-dien-1-yl)acetamido)-5-cyclobutyl-1H-pyrazole-1-carboxylate): To a stirred solution of compound **4** (25 mg, 0.10 mmol), tert-butyl 3-amino-5-cyclobutyl-1H-pyrazole-1-carboxylate (compound **12**, 15 mg, 0.06 mmol) in dichloromethane (1 mL) was added and triethyl amine (32 mg, 0.32 mmol). The reaction mixture was stirred for 10 minutes followed by addition of 50% T3P in ethyl acetate (30 mg, 0.09 mmol). The reaction was stirred overnight, and the progress of the reaction was monitored by thin layer chromatography (TLC). The crude mixture was dissolved in dichloromethane, washed in brine. The organic phase was collected, dried with $MgSO_4$ and the solvent was evaporated and purified by flash column chromatography with hexane/ethyl acetate to give compound **13** (27 mg,

90% yield) as white solid. ^{1}H NMR (500 MHz, CDCl3) δ (ppm) 10.23 (s, 1H), 7.28 (d, 2H, J = 3.0 Hz), 6.92 (d, 2H, J = 3.0 Hz), 6.87 (s, 1H), 4.52 (s, 2H), 3.71 (s, 2H), 3.56 – 3.51 (m, 1H), 2.34 – 1.88 (m, 6H), 1.63 (s, 9H), 1.51 (s, 9H). ^{13}C NMR (125 MHz, $CDCl_3$) 167.88, 161.06, 157.48, 150.93, 141.35, 130.52, 126.62, 115.18, 95.49, 86.26, 82.35, 65.82, 43.62, 34.33, 28.38, 28.03, 27.92, 18.68.

Synthesis of 14 (2-((4-(2-((5-cyclobutyl-1H-pyrazol-3-yl)amino)-2-oxoethyl)-cyclohexa-2,4-dien-1-yl)oxy)acetic acid): To a stirred solution of compound **13** (220 mg) in CH_2Cl_2 (2 mL) at 0 °C was added 1 mL of trifluoroacetic acid dropwise and reaction mixture was stirred for 2 hours. After completion, the reaction mixture was concentrated in vacuo to produce compound **14** in quantitative yield, which was dissolved in 3 mL of dry DMF and stored at -20 °C.

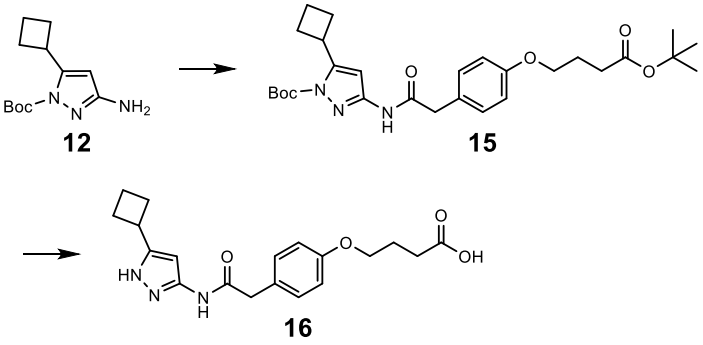

Synthesis of 15 (tert-butyl 3-(2-(4-(4-(tert-butoxy)-4-oxobutoxy)cyclohexa-1,5-dien-1-yl)acetamido)-5-cyclobutyl-1H-pyrazole-1-carboxylate): To a stirred solution of amine **12** (31 mg, 0.13 mmol), 2-(4-(4-(tert-butoxy)-4-oxobutoxy)phenyl)acetic acid (compound **6**, 50 mg, 0.17 mmol) in dichloromethane (2 mL) was added and triethyl amine (66 mg, 0.65 mmol). The reaction mixture was stirred for 10 minutes, followed by dropwise addition of 50% T3P in ethyl acetate (120 μL, 0.19 mmol). The reaction was stirred for 4 hours and the progress of the reaction was monitored by thin layer chromatography (TLC). The crude mixture was dissolved in dichloromethane, washed in brine. The organic phase

was collected, dried with $MgSO_4$ and the solvent was evaporated and purified by flash column chromatography with hexane/ethyl acetate to give compound **15** (59 mg, 88% yield) as off-white solid. ^{1}H NMR (500 MHz, CDCl3) δ (ppm) 10.19 (s, 1H), 7.22 (d, 2H, J = 8.5 Hz), 6.89 (d, 2H, J = 3.0 Hz), 6.84 (s, 1H), 3.99 (t, 2H, J = 6.0Hz), 3.68 (s, 2H), 3.56 – 3.49 (m, 1H), 2.42 (t, 2H, 7.5 Hz), 2.32 – 1.86 (m, 6H), 1.60 (s, 9H), 1.45 (s, 9H). ^{13}C NMR (125 MHz, $CDCl_3$) 172.48, 168.12, 161.09, 158.47, 150.92, 141.41, 130.50, 125.70, 115.09, 95.44, 86.23, 80.36, 67.00, 43.65, 34.34, 32.02, 28.40, 28.11, 27.92, 24.74, 18.69.

Synthesis of 16 (4-((4-(2-((5-cyclobutyl-1H-pyrazol-3-yl)amino)-2-oxoethyl)-cyclo-hexa-2,4-dien-1-yl)oxy)butanoic acid): To a stirred solution of **15** (59 mg) in CH_2Cl_2 (2 mL) at 0 °C was added 1 mL of trifluoroacetic acid dropwise and reaction mixture was stirred for 2 hours. After completion, the reaction mixture was concentrated in vacuo to give 52 mg of compound **16,** dissolved in 2 mL of dry DMF, and stored at -20 °C.

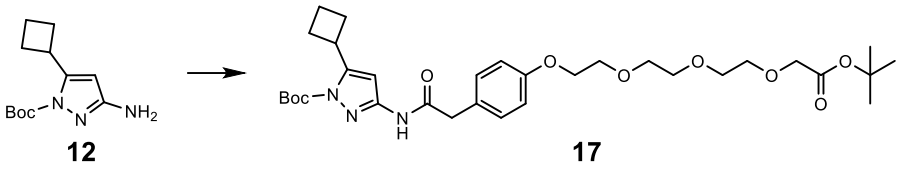

12

17

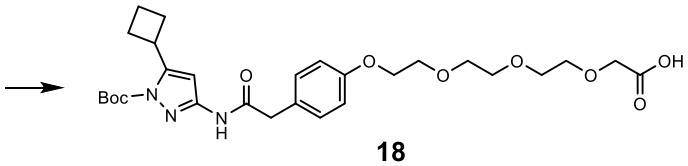

18

Synthesis of 17: To a stirred solution of compound **12** (71 mg, 0.30 mmol), 2-(4-((13,13-dimethyl-11-oxo-3,6,9,12-tetraoxatetradecyl)oxy)phenyl)acetic acid (compound **11**, 150 mg, 0.38 mmol) in dichloromethane (5 mL) was added and triethyl amine (46 mg, 0.45 mmol). The reaction mixture was stirred for 10 minutes followed by dropwise addition of 50% T3P in ethyl acetate (1 mL, 1.5 mmol). The reaction was stirred for 4 hours and the progress of the reaction was monitored by thin layer chromatography. The crude mixture

was dissolved in dichloromethane, washed in brine. The organic phase was collected, dried with $MgSO_4$ and the solvent was evaporated and purified by flash column chromatography with hexane/ethyl acetate to give compound **17** (110 mg, 59% yield) as off-white solid. ^{1}H NMR (500 MHz, CDCl3) δ (ppm) 10.19 (s, 1H), 7.22 (d, 2H, J = 8.5 Hz), 6.91 (d, 2H, J = 8.5 Hz), 6.84 (s, 1H), 4.13 – 4.11 (m, 2H), 4.01 (s, 2H), 3.88 – 3.85 (t, 2H), 3.73 – 3.68 (m, 10H), 3.55 – 3.49 (m, 1H), 2.31 – 2.25 (m, 2H), 2.21 – 2.14 (m, 2H), 2.04 – 1.86 (m, 2H), 1.60 (s, 9H), 1.46 (s, 9H). ^{13}C NMR (125 MHz, $CDCl_3$) 169.61, 168.05, 161.04, 158.32, 150.87, 141.38, 130.44, 125.85, 115.19, 95.43, 86.25, 81.48, 70.79, 70.70, 70.62, 70.61, 69.66, 69.01, 67.50, 43.63, 34.30, 28.37, 28.08, 27.91, 18.67.

Synthesis of 18 (2-(2-(2-(2-((4-(2-((1-(tert-butoxycarbonyl)-5-cyclobutyl-1H-pyrazol-3-yl)amino)-2-oxoethyl)cyclohexa-2,4-dien-1-yl)oxy)ethoxy)ethoxy)ethoxy)acetic acid): To a stirred solution of **17** (110 mg) in CH_2Cl_2 (5 mL) at 0 °C 2 mL of trifluoroacetic acid was added dropwise and reaction mixture was stirred for 3 hours. After completion, the reaction mixture was concentrated in vacuo to give 98 mg of compound **18** which was dissolved in 3 mL of dry DMF and stored at -20 °C.

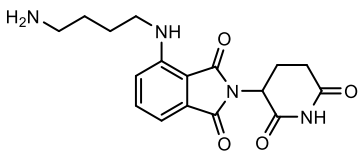

19

Compound 19 (4-((4-aminobutyl)amino)-2-(2,6-dioxopiperidin-3-yl)isoindoline-1,3-dione) [147]

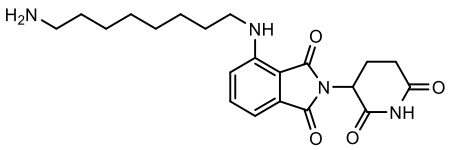

20

Compound 20 (4-((8-aminooctyl)amino)-2-(2,6-dioxopiperidin-3-yl)isoindoline-1,3-dione) [147]

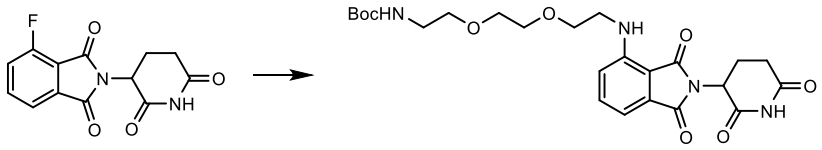

21 **22**

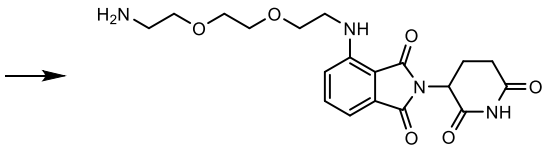

23

Synthesis of 22 (tert-butyl (2-(2-(2-((2-(2,6-dioxopiperidin-3-yl)-1,3-dioxoisoindolin-4-yl)amino)ethoxy)ethoxy)ethyl)carbamate): To a stirred solution of compound **21** (100 mg, 0.36 mmol) in DMA (2 mL) tert-butyl(2-(2-(2-aminoethoxy)ethoxy)ethyl)carbamate (90 mg, 0.35 mmol) and DIPEA (0.2 mL, 1.08 mmol) was added. The reaction mixture was stirred at 90 °C for 2 hours. The mixture was cooled to room temperature, poured into brine, extracted twice with ethyl acetate, and dried with $MgSO_4$. After filtration and evaporation, the crude residue was purified by column chromatography to give compound **22** (50 mg, 27%) as green solid. ^{1}H NMR (500 MHz, CDCl3) δ (ppm) 8.53 (s, 1H), 7.48 (t, 1H, 8.0 Hz), 7.09 (d, 1H, 7.0 Hz), 6.89 (d, 1H, 8.0 Hz), 6.50 (s, 1H), 5.05 – 4.9 (m, 2H), 3.72 - 3.30 (m, 12H), 2.87 – 2.72 (m, 3H), 2.12 – 2.10 (m, 1H), 1.41 (s, 9H). ^{13}C NMR (125 MHz, $CDCl_3$) 171.14, 171.10, 169.29, 168.43, 167.56, 156.03, 146.76, 135.99, 132.51, 116.67, 111.63, 110.36, 79.22, 70.71, 70.32, 70.11, 69.34, 60.34, 48.85, 42.29, 40.36, 31.35, 28.37, 22.80, 20.99, 14.15.

Synthesis of 23 (4-((2-(2-(2-aminoethoxy)ethoxy)ethyl)amino)-2-(2,6-dioxopiperidin-3-yl)isoindoline-1,3-dione): To a stirred solution of compound **22** (50 mg) in CH_2Cl_2 (1 mL) at 0 °C 1 mL of trifluoroacetic acid was added dropwise and reaction mixture was stirred for 3 hours. After completion, the reaction mixture was concentrated in vacuo to give 55 mg of compound **23,** which was dissolved in 3 mL of dry DMF and stored at -20 °C.

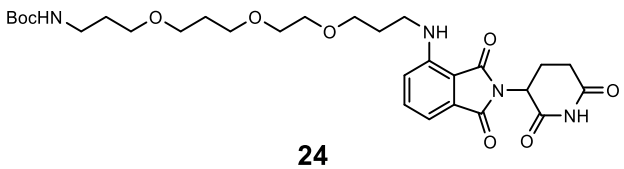

24

Compound 24 (4-((3-(2-(3-(3-aminopropoxy)propoxy)ethoxy)propyl)amino)-2-(2,6-dioxopiperidin-3-yl)isoindoline-1,3-dione) [147]

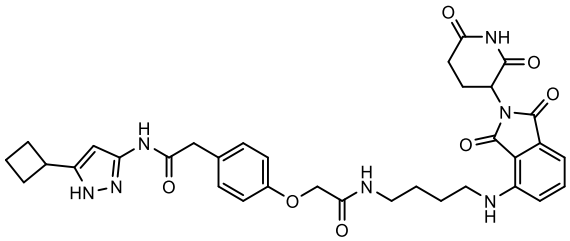

PROTAC 1

PROTAC 1 (N-(5-cyclobutyl-1H-pyrazol-3-yl)-2-(4-(2-((4-((2-(2,6-dioxopiperidin-3-yl)-1,3-dioxoisoindolin-4-yl)amino)butyl)amino)-2-oxoethoxy)phenyl)acetamide): A solution of acid **14** (10 mg, 0.03 mmol) and amine 19 (10 mg, 0.023 mmol) in DMF (1 mL) was stirred followed by adding EDC (8.5 mg, 0.04 mmol), HOBT (6.6 mg, 0.04 mmol) and NEt_3 (20 µL, 0.04 mmol) and stirred overnight at the ambient temperature. The mixture was rotavated and purified by reverse phase HPLC (5-95% CH_3CN in H2O) to give **PROTAC 1** as a light green solid. ^1H NMR (500 MHz, CD_3OD) δ (ppm) 7.51 (t, 1H, J = 6.0 Hz), 7.28 (br, 2H), 7.07 – 6.94 (m, 4H), 5.07 – 5.04 (m, 1H), 3.97 (t, 2H, J = 5.5 Hz), 4.50

(s, 2H), 3.65 – 3.62 (m, 2H), 3.52 (br, 1H), 2.88 – 2.66 (m, 3H), 2.36 – 2.34 (m, 2H), 2.19 – 2.16 (m, 2H), 2.10 – 2.02 (m, 2H), 1.94 – 1.93 (m, 2H), 1.66 – 1.54 (m, 4H), 0.96 – 0.88 (m, 3H). HRMS-ESI (+) calcd (calculated) *m/z* for $C_{34}H_{38}N_7O_7^+$ 656.2827 $(M+H)^+$, found 656.2830. HPLC purity ≥95%, t_R= 13.77 min.

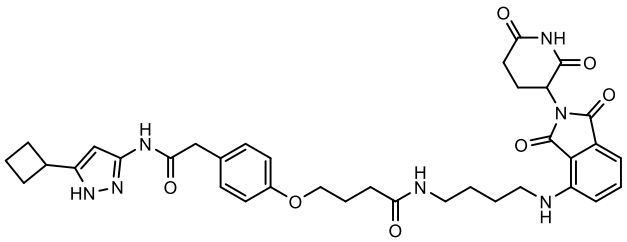

PROTAC 2

PROTAC 2 (4-(4-(2-((5-cyclobutyl-1H-pyrazol-3-yl)amino)-2-oxoethyl)phenoxy)-N-(4-((2-(2,6-dioxopiperidin-3-yl)-1,3-dioxoisoindolin-4-yl)amino)butyl)butanamide): ^{1}H NMR (500 MHz, CD_3OD) δ (ppm) 7.55 – 7.47 (m, 1H), 7.23 (br, 2H), 7.01 – 7.00 (m, 2H), 6.88 (br, 2H), 5.07 – 5.03 (m, 1H), 3.97 (t, 2H, J = 5.5 Hz), 3.65 – 3.61 (m, 1H), 3.28 – 3.20 (m, 4H), 2.95 – 2.66 (m, 3H), 2.39 – 2.36 (m, 4H), 2.19 (br, 2H), 2.09 – 2.04 (m, 4H), 1.94 (br, 1H), 1.66 – 1.54 (m, 4H), 1.32 – 1.29 (m, 2H). HRMS-ESI (+) calcd *m/z* for $C_{36}H_{42}N_7O_7^+$ 684.3140 $(M+H)^+$, found 684.3141. HPLC purity ≥95%, t_R= 13.20 min.

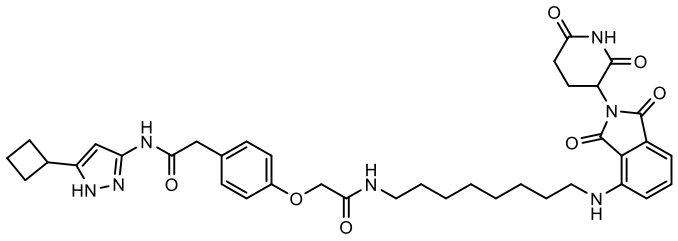

PROTAC 3

PROTAC 3 (N-(5-cyclobutyl-1H-pyrazol-3-yl)-2-(4-(2-((8-((2-(2,6-dioxopiperidin-3-yl)-1,3-dioxoisoindolin-4-yl)amino)octyl)amino)-2-oxoethoxy)phenyl)acetamide): ^{1}H NMR (500 MHz, CD_3OD) δ (ppm) 7.52 (t, 1H, J = 7.5 Hz), 7.28 – 7.26 (m, 2H), 7.02 – 7.00 (m, 2H), 6.95 – 6.94 (m, 2H), 6.28 (br, 1H), 5.06 – 5.02 (m, 1H), 4.48 (s, 1H), 3.65 – 3.54

(m, 3H), 3.30 – 3.23 (m, 8H), 2.86 – 2.65 (m, 4H), 2.38 – 2.36 (m, 2H), 2.24 – 2.16 (m, 2H), 2.10 – 2.04 (m, 2H), 1.94 – 1.92 (m, 1H), 1.66 – 1.60 (m, 2H), 1.54 – 1.48 (m, 2H), 1.40 – 1.29 (m, 8H). HRMS-ESI (+) calcd *m/z* for $C_{40}H_{50}N_7O_{10}^+$ 712.3453 $(M+H)^+$, found 712.3457. HPLC purity ≥95%, t_R= 15.11 min.

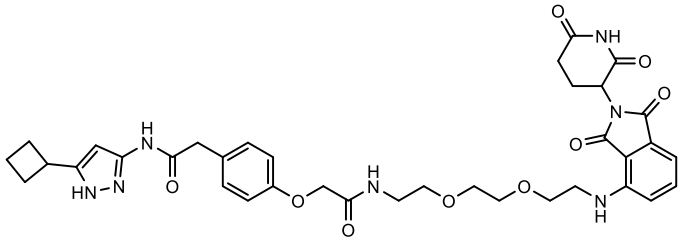

PROTAC 4

PROTAC 4 (N-(5-cyclobutyl-1H-pyrazol-3-yl)-2-(4-(2-((2-(2-(2-((2-(2,6-dioxopiperidin-3-yl)-1,3-dioxoisoindolin-4-yl)amino)ethoxy)ethoxy)ethyl)amino)-2-oxoethoxy)-phenyl)acetamide): ^{1}H NMR (500 MHz, CD_3OD) δ (ppm) 7.49 (t, 1H, J = 7.5 Hz), 7.29 – 7.22 (m, 2H), 7.01 – 6.99 (m, 2H), 6.91 – 6.89 (m, 2H), 6.28 (br, 1H), 5.04 – 5.00 (m, 1H), 4.45 (s, 1H), 3.70 – 3.68 (m, 2H), 3.60 – 3.57 (m, 8H), 3.47 – 3.42 (m, 4H), 2.86 – 2.63 (m, 3H), 2.39 – 2.34 (m, 2H), 2.22 – 2.16 (m, 2H), 2.09 – 2.04 (m, 2H), 1.95 – 1.92 (m, 1H). HRMS-ESI (+) calcd *m/z* for $C_{36}H_{42}N_7O_9^+$ 716.3039 $(M+H)^+$, found 716.3039. HPLC purity ≥95%, t_R= 12.90 min.

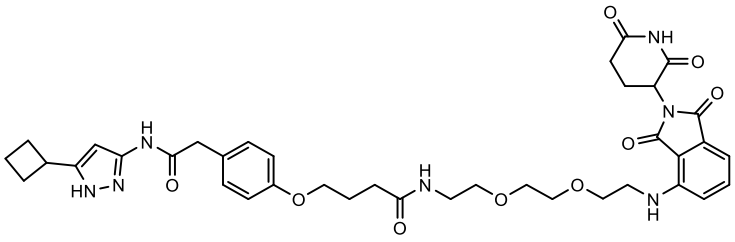

PROTAC 5

PROTAC 5 (4-(4-(2-((5-cyclobutyl-1H-pyrazol-3-yl)amino)-2-oxoethyl)phenoxy)-N-(2-(2-(2-((2-(2,6-dioxopiperidin-3-yl)-1,3-dioxoisoindolin-4-yl)amino)ethoxy)ethoxy)-ethyl)butanamide): ^{1}H NMR (500 MHz, CD_3OD) δ (ppm) 7.52 (t, 1H, J = 7.5 Hz), 7.22 –

7.20 (m, 2H), 7.05 – 7.02 (m, 2H), 6.86 – 6.84 (m, 2H), 6.28 (br, 1H), 5.05 – 5.02 (m, 1H), 3.94 (t, 2H, J = 6.0 Hz), 3.67 (t, 2H, J = 5.0 Hz), 3.60 – 3.57 (m, 4H), 3.52 (t, 2H, J = 5.0 Hz), 3.45 (t, 2H, J = 5.0 Hz), 3.35 (t, 2H, J = 5.0 Hz), 2.86 – 2.64 (m, 3H),2.36 – 2.33 (m, 4H), 2.23 – 2.16 (m, 2H), 2.09 – 2.00 (m, 4H). HRMS-ESI (+) calcd *m/z* for $C_{38}H_{46}N_7O_9^+$ 744.3352 $(M+H)^+$, found 744.3355. HPLC purity ≥95%, t_R= 12.90 min.

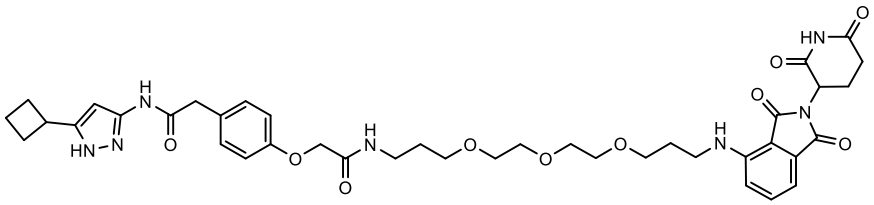

PROTAC 6

PROTAC 6 (N-(5-cyclobutyl-1H-pyrazol-3-yl)-2-(4-((16-((2-(2,6-dioxopiperidin-3-yl)-1,3-dioxoisoindolin-4-yl)amino)-2-oxo-7,10,13-trioxa-3-azahexadecyl)oxy)phenyl)-acetamide): ^{1}H NMR (500 MHz, CD_3OD) δ (ppm) 7.51 (t, 1H, J = 7.5 Hz), 7.28 – 7.27 (m, 2H), 7.04 – 6.99 (m, 2H), 6.95 – 6.94 (m, 2H), 6.28 (br, 1H), 5.05 – 5.01 (m, 1H), 4.46 (s, 2H), 3.65 – 3.51 (m, 10H), 3.47 (t, 2H, J = 6.0 Hz), 3.40 (t, 2H, J = 6.5 Hz), 3.35 (t, 2H, J = 6.5 Hz), 2.74 – 2.65 (m, 3H), 2.38 – 2.36 (m, 2H), 2.24 – 2.18 (m, 2H), 2.09 – 2.04 (m, 2H), 1.90 – 1.85 (m, 2H), 1.78 – 1.73 (m, 2H). HRMS-ESI (+) calcd *m/z* for $C_{40}H_{50}N_7O_{10}^+$ 788.3614 $(M+H)^+$, found 788.3619. HPLC purity ≥95%, t_R= 13.41 min.

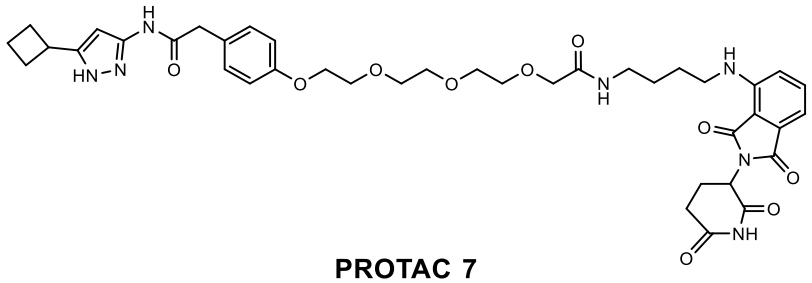

PROTAC 7

PROTAC 7 (N-(5-cyclobutyl-1H-pyrazol-3-yl)-2-(4-((16-((2-(2,6-dioxopiperidin-3-yl)-1,3-dioxoisoindolin-4-yl)amino)-11-oxo-3,6,9-trioxa-12-azahexadecyl)oxy)phenyl)-acetamide): ^{1}H NMR (500 MHz, CD_3OD) δ (ppm) 7.51 (t, 1H, J = 7.5 Hz), 7.28 – 7.27 (m,

2H), 7.02 – 6.99 (m, 2H), 6.89 (br, 2H), 5.06 – 5.02 (m, 1H), 4.43 – 4.08 (m, 2H), 3.95 (s, 2H), 3.85 – 3.79 (m, 3H), 3.66 – 3.64 (m, 12H), 2.88 – 2.68 (m, 3H), 2.66 (s, 1H), 2.37 (br, 2H), 2.20 (br, 2H), 2.10 – 2.08 (m, 2H), 1.62 (br, 4H). HRMS-ESI (+) calcd *m/z* for $C_{40}H_{50}N_7O_{10}^+$ 788.3614 $(M+H)^+$, found 788.3618. HPLC purity ≥95%, t_R= 12.66 min.

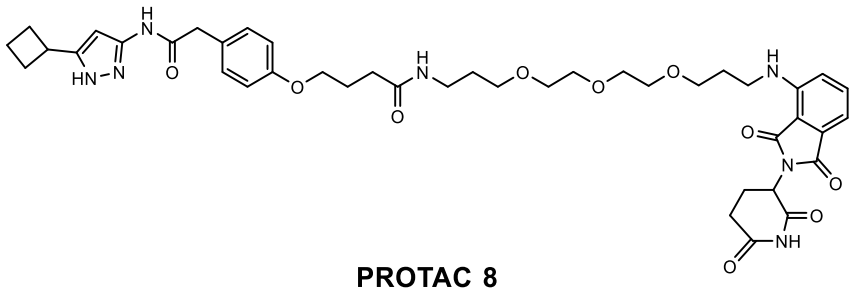

PROTAC 8

PROTAC 8 (4-(4-(2-((5-cyclobutyl-1H-pyrazol-3-yl)amino)-2-oxoethyl)phenoxy)-N-(3-(2-(2-(3-((2-(2,6-dioxopiperidin-3-yl)-1,3-dioxoisoindolin-4-yl)amino)propoxy)-ethoxy)ethoxy)propyl)butanamide): ^{1}H NMR (500 MHz, CD_3OD) δ (ppm) 7.53 (t, 1H, J = 7.5 Hz), 7.23 (br, 2H), 7.06 – 7.01 (m, 2H), 6.89 (br, 2H), 5.06 – 5.02 (m, 1H), 3.96 (t, 2H, J = 5.5 Hz), 3.67 – 3.40 (m, 13H), 3.24 (t, 2H, J = 7.0 Hz), 2.86 – 2.66 (m, 3H), 2.37 – 2.34 (m, 2H), 2.00 (br, 1H), 2.06 – 2.02 (m, 2H), 1.90 – 1.88 (m, 2H), 1.74 – 1.69 (m, 2H). HRMS-ESI (+) calcd *m/z* for $C_{42}H_{54}N_7O_{10}^+$ 816.3927 $(M+H)^+$, found 816.3928. HPLC purity ≥95%, t_R= 13.44 min.

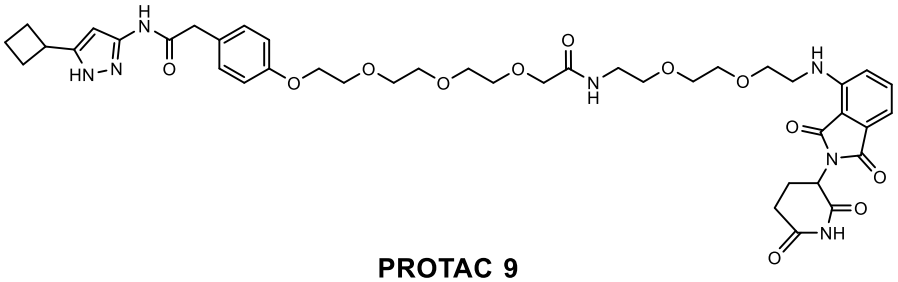

PROTAC 9

PROTAC 9 (N-(5-cyclobutyl-1H-pyrazol-3-yl)-2-(4-((1-((2-(2,6-dioxopiperidin-3-yl)-1,3-dioxoisoindolin-4-yl)amino)-10-oxo-3,6,12,15,18-pentaoxa-9-azaicosan-20-yl)-oxy)phenyl)acetamide): ^{1}H NMR (500 MHz, CD_3OD) δ (ppm) 7.56 – 7.51 (m, 1H), 7.23

(br, 2H), 7.06 – 7.04 (m, 2H), 6.88 (br, 2H), 5.05 – 5.02 (m, 1H), 4.09 (m, 2H), 3.94 (br, 2H), 3.81 – 3.80 (m, 2H), 3.65 – 3.61 (m, 14H), 3.55 (t, 2H, J = 5.0 Hz), 3.47 – 3.39 (m, 4H), 2.89 – 2.66 (m, 3H), 2.36 (br, 2H), 2.19 (br, 2H), 2.09 – 2.02 (m, 2H). HRMS-ESI (+) calcd *m/z* for $C_{42}H_{54}N_7O_{12}^+$ 848.3825 $(M+H)^+$, found 848.3822. HPLC purity ≥95%, t_R= 13.83 min.

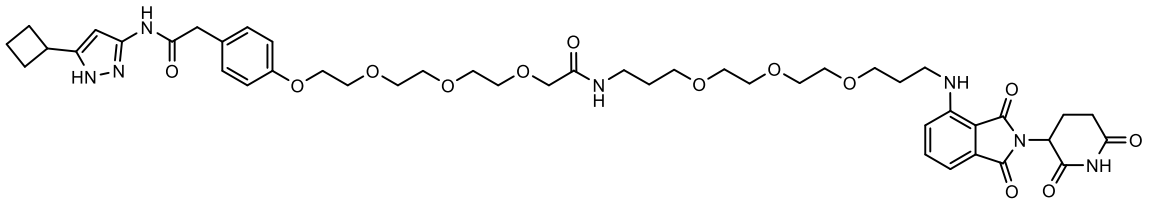

PROTAC 10

PROTAC 10 (N-(5-cyclobutyl-1H-pyrazol-3-yl)-2-(4-((25-((2-(2,6-dioxopiperidin-3-yl)-1,3-dioxoisoindolin-4-yl)amino)-11-oxo-3,6,9,16,19,22-hexaoxa-12-azapentacosyl)-oxy)phenyl)acetamide): ^{1}H NMR (500 MHz, CD_3OD) δ (ppm) 7.53 (t, 1H, J = 7.0 Hz), 7.24 (br, 2H), 7.06 – 7.02 (m, 2H), 6.90 (br, 2H), 5.06 – 5.02 (m, 1H), 4.11(br, 2H), 3.94 (br, 2H), 3.83 – 3.82 (m, 2H), 3.70 – 3.54 (M, 18H), 3.48 (T, 2H, J = 6.0 Hz), 3.42 (T, 2H, J = 6.0 Hz), 2.89 – 2.66 (m, 3H), 2.36 (br, 2H), 2.19 (br, 2H), 2.10 – 2.01 (m, 2H), 1.94 – 1.88 (m, 2H), 1.75 (t, 2H, J = 6.0 Hz). HRMS-ESI (+) calcd *m/z* for $C_{46}H_{62}N_7O_{13}^+$ 920.4400 $(M+H)^+$, found 920.4404. HPLC purity ≥95%, t_R= 13.58 min.

HPLC Chromatograms of PROTACs

PROTAC 1

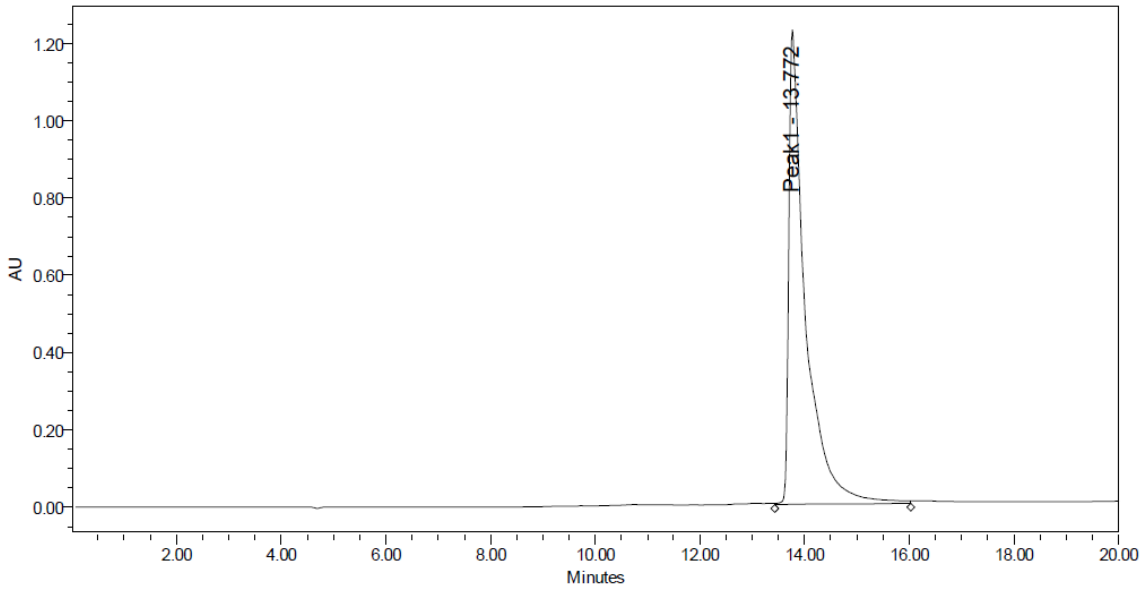

	Peak Name	RT	Area	% Area	Height
1	Peak1	13.772	27045156	100.00	1229550

PROTAC 2

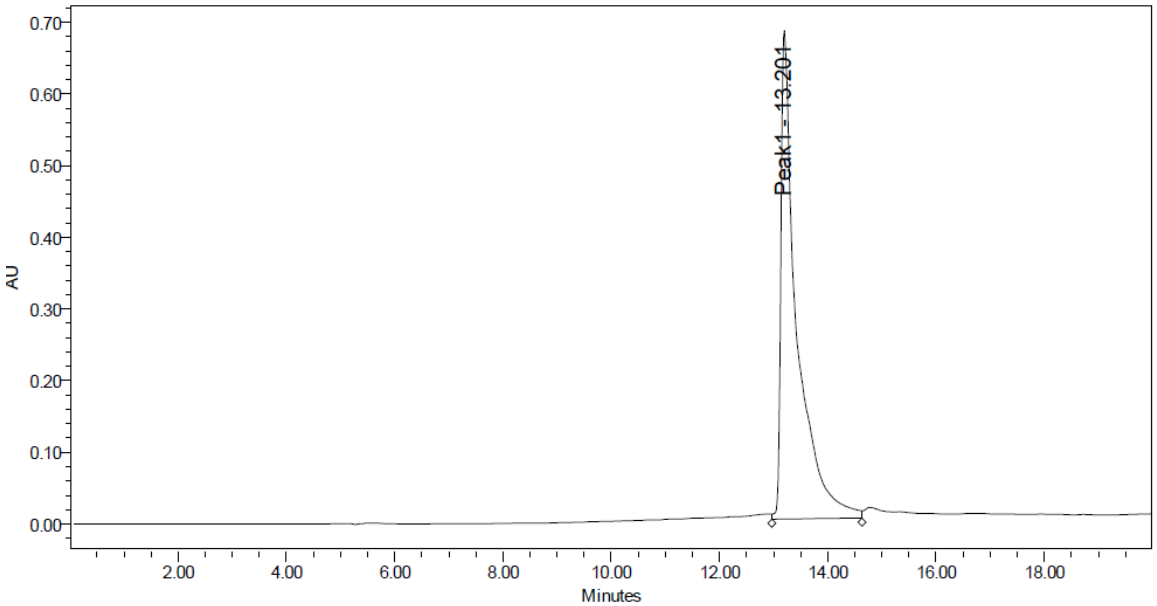

	Peak Name	RT	Area	% Area	Height
1	Peak1	13.201	13952550	100.00	682379

PROTAC 3

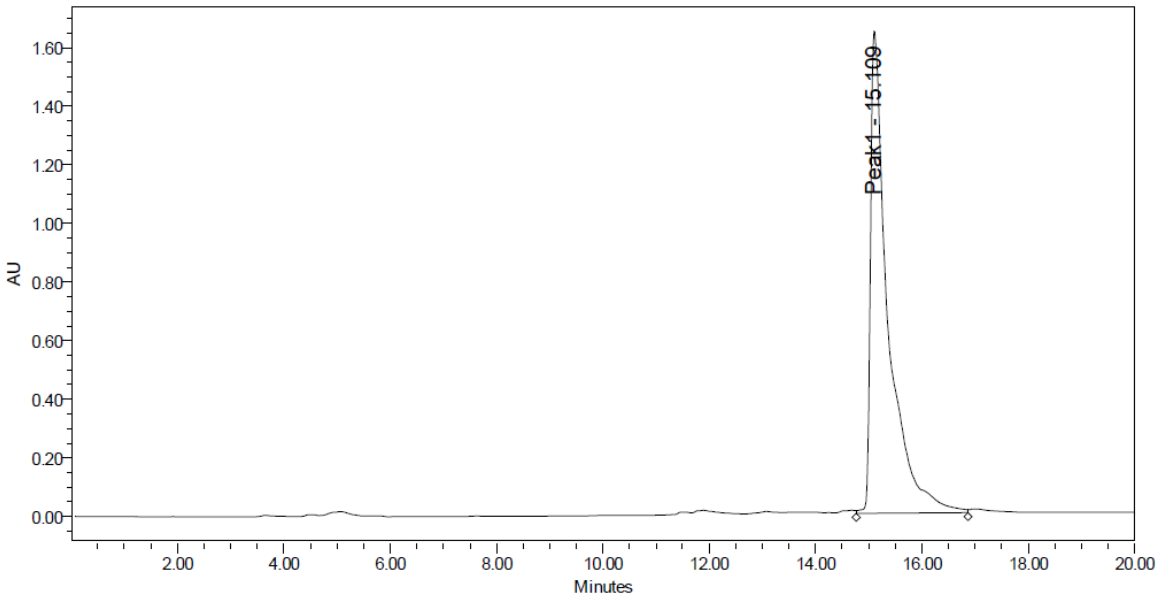

	Peak Name	RT	Area	% Area	Height
1	Peak1	15.109	37942251	100.00	1656077

PROTAC 4

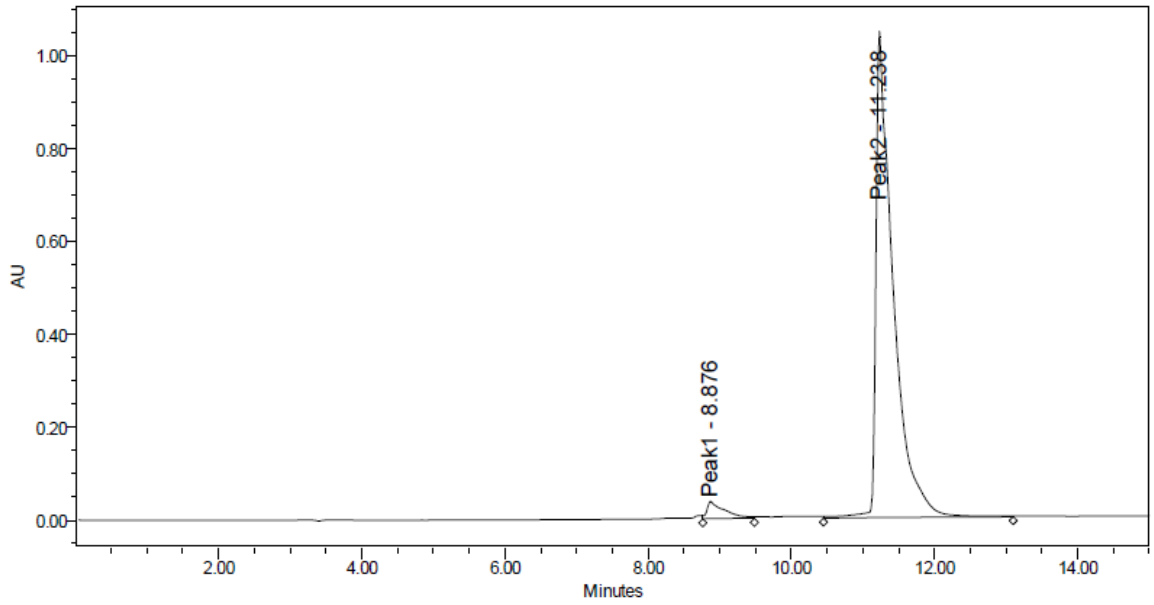

	Peak Name	RT	Area	% Area	Height
1	Peak1	8.876	620795	3.43	37245
2	Peak2	11.238	17463814	96.57	1047549

PROTAC 5

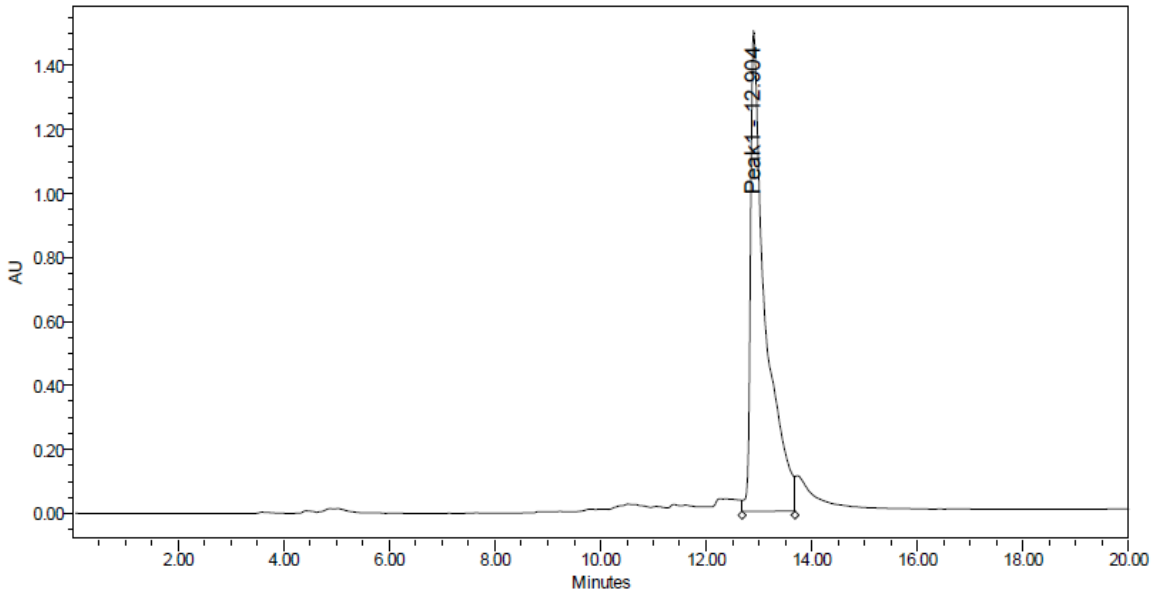

	Peak Name	RT	Area	% Area	Height
1	Peak1	12.904	29175730	100.00	1505342

PROTAC 6

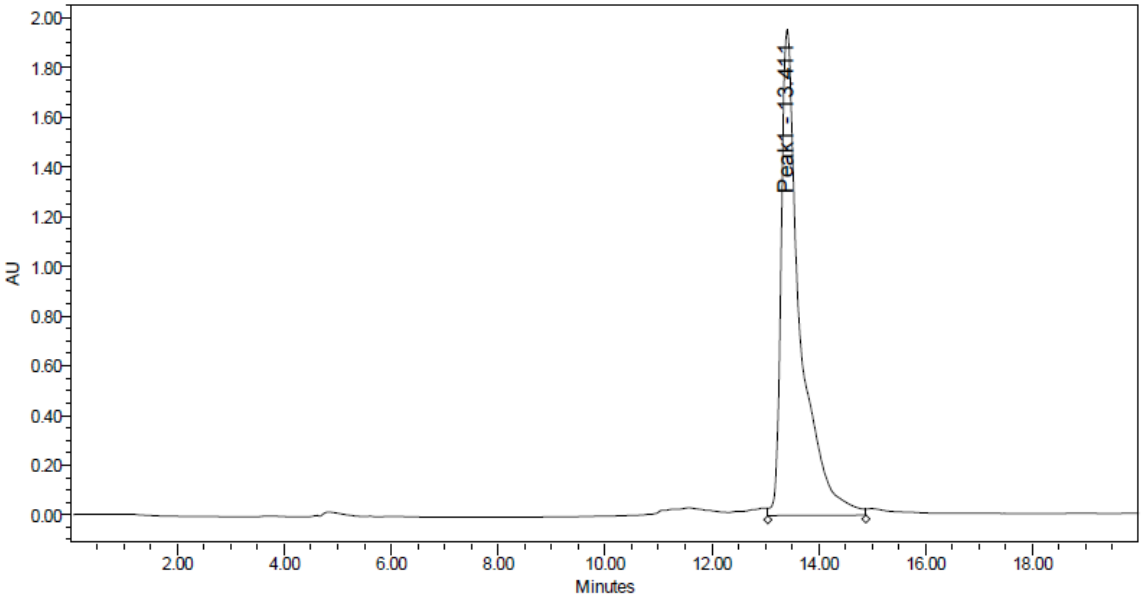

	Peak Name	RT	Area	% Area	Height
1	Peak1	13.411	48297839	100.00	1957110

PROTAC 7

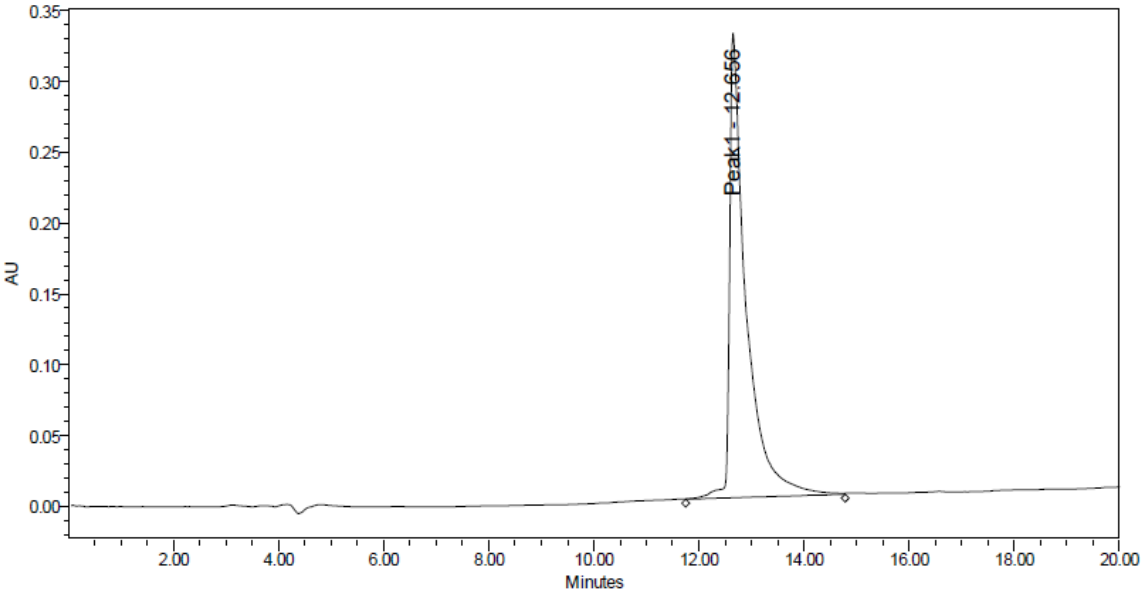

	Peak Name	RT	Area	% Area	Height
1	Peak1	12.656	7159901	100.00	329245

PROTAC 8

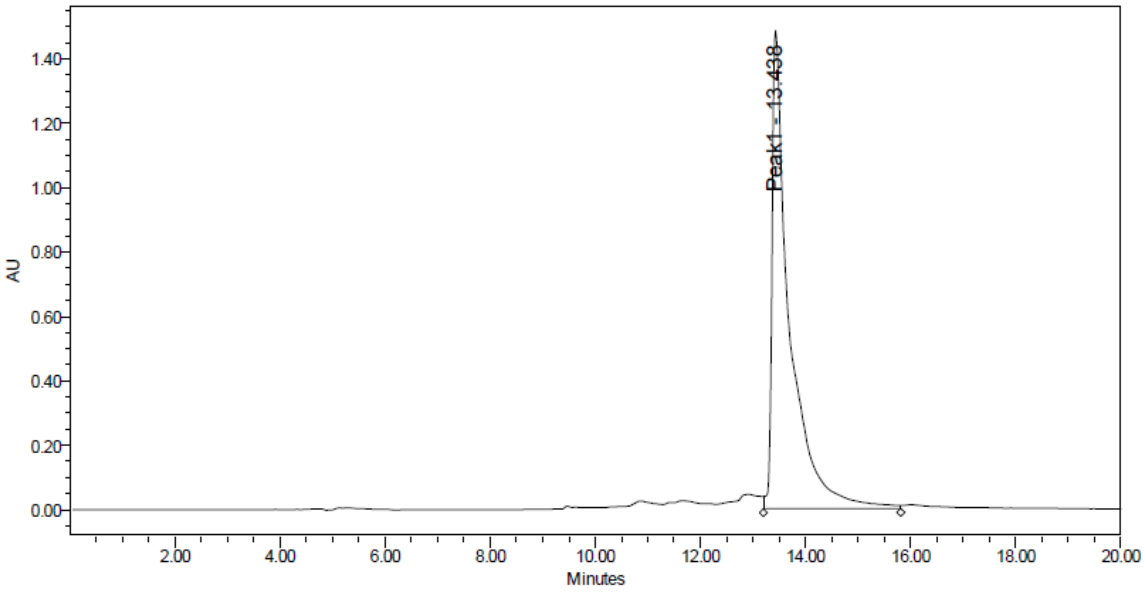

	Peak Name	RT	Area	% Area	Height
1	Peak1	13.438	34398998	100.00	1488526

PROTAC 9

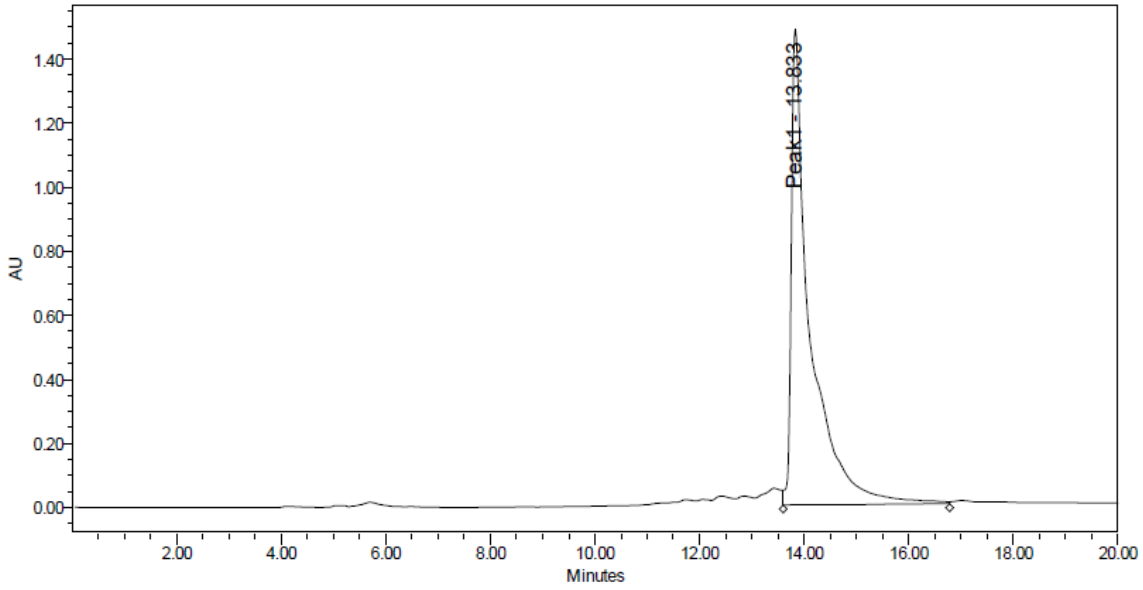

	Peak Name	RT	Area	% Area	Height
1	Peak1	13.833	37197550	100.00	1486187

PROTAC 10

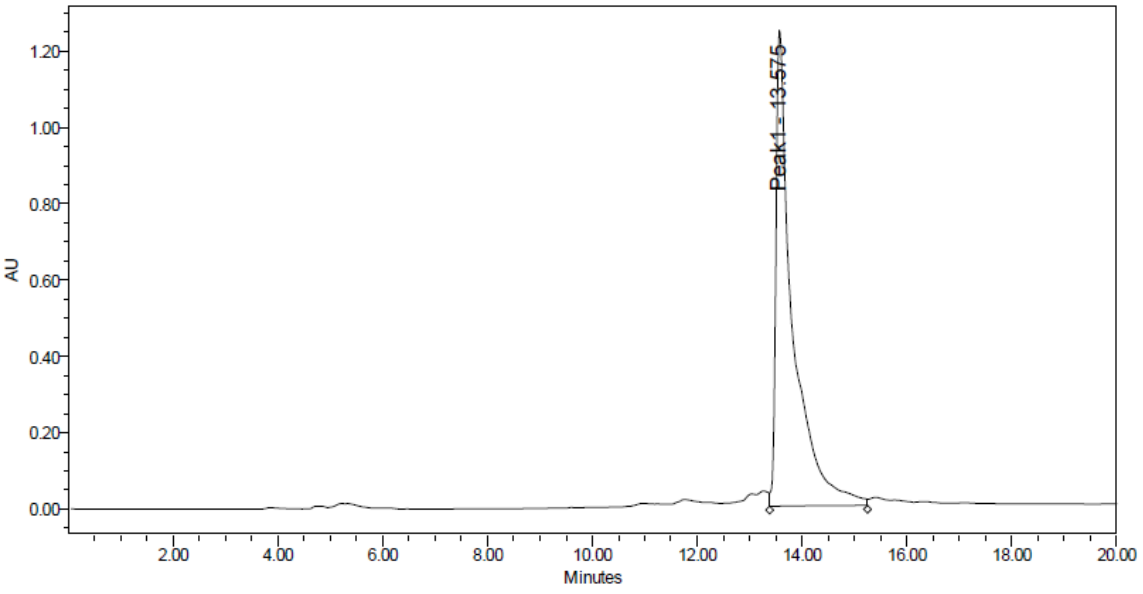

	Peak Name	RT	Area	% Area	Height
1	Peak1	13.575	27631082	100.00	1254601

CELL-FREE SYSTEM ANALYSIS

We sent samples to Reaction Biology Corporation for cell-free analysis. Kinase profiling of compound **11** and PROTAC **2** were tested against three kinases: CDK2/cyclin E, CDK5/p35, and CDK9/cyclin T1. The enzymatic activity was determined by measuring ATP hydrolysis. Compounds were tested using dose-response studies containing ten concentrations, beginning at 20 μM with 3-fold dilutions, in the presence of 10 μM ATP. IC_{50} values were generated by fitting the dose-response curves. Furthermore, samples were also sent to Eurofins Discover X for KINOMEscan direct binding analysis. Binding affinity was determined for compound **11**, PROTAC **2,** and PROTAC **4;** we tested against four kinases: CDK2, CDK5, CDK9, and CDK12.

CELL LINES & MATERIALS

This dissertation's cancer cell lines are HEK293, MiaPaCa2, S2-013, SKOV3, A673, Jurkat, and HCT116 cells. HEK293, MiaPaCa2, S2-013, SKOV3, and A673 cells were grown in Dulbecco's Modified Eagle Medium (DMEM) with High Glucose (HyClone #SH30022.FS) supplemented with 10% Fetal Bovine Serum (Gibco by Life Technologies #26140-079) and 1x penicillin-streptomycin (HyClone #SV30010). HCT116 and Jurkat cells were cultured in RPMI-1640 Medium (HyClone #SH30027.01) supplemented with 10% FBS and 1x Penicillin-Streptomycin (HyClone #SV30010). All cells were maintained at 37°C and 5% CO_2.

WESTERN BLOT ANALYSIS

Following treatment, cells were washed three times with cold 1X phosphate-buffered saline (PBS, HyClone #SH30028.02) and scraped before being lysed in a buffer comprised of radioimmunoprecipitation assay (RIPA) buffer (Thermo Scientific #89900), sodium orthovanadate (Na3VO4), sodium fluoride (NaF), β-glycerophosphate and 1mM

phenylmethylsulfonyl fluoride (PMSF). Samples were then incubated on ice for 30 minutes, vortexed in 10-minute intervals, and pelleted by centrifugation at 14,000 g for 10 minutes at 4°C. The supernatant was collected, and protein quantification was determined using BCA Protein Assay (Pierce #23225). 40µg of total protein was loaded per well and run on a 4-15% gradient gel (BioRad) in 1X TRIS-Glycine-SDS Buffer (Research Products International Corporation #T32080) at 120V for ~80 minutes and separated by SDS-PAGE (sodium dodecyl sulfate-polyacrylamide gel) electrophoresis. The proteins were transferred onto a polyvinylidene fluoride (PVDF) methanol-activated membrane using a semi-dry transfer method (ThermoScientific #35035) run at 18V for 35 minutes. Membranes were blocked by shaking in a solution of 5% (w/v) non-fat dry milk in 1X-Tris Buffered Saline with 0.1% Tween (1xTBST) for 1 hour at room temperature. Membranes were incubated in primary antibodies (listed below) in 5% milk in 1xTBST at 4°C overnight with gentle rocking. Complimentary HRP-conjugated secondary antibodies diluted at 1:10,000 or 1:5,000 incubated in 5% milk in 1xTBST, rocked at room temperature for 1 hour. The membranes were then incubated with ECL Prime (Cytiva #RPN2236) to detect protein expression. Membranes were developed 1) on film (ThermoScientific #34090) using the KODAK X-OMAT 2000 Processor system or 2) ChemiDoc MP Imaging System. Developed films were scanned as JPEG image files. ChemiDoc images were processed using the Image Lab software (version 6.0.1). And ImageJ was used for the quantification of the western blots.

ANTIBODIES

Antibody	Company	Catalog #	Lot #	Dilution of 1º Antibody	Source
α-tubulin	Cell Signaling	3873	7	1:5,000	Mouse
CDK9	Cell Signaling	2316	7	1:1,000	Rabbit
CDK12	Cell Signaling	11973	2	1:1,000	Rabbit
CDK8	Cell Signaling	17395	1	1:1,000	Rabbit
CDK7	Cell Signaling	2916	4	1:2,000	Mouse
CDK6	Cell Signaling	13331	3	1:1,000	Rabbit
CDK5	Cell Signaling	2506	2	1:1,000	Rabbit
CDK4	Cell Signaling	12790	4	1:1,000	Rabbit
CDK2	Cell Signaling	2546	33	1:2,000	Rabbit
CDK1	Cell Signaling	77055	2	1:1,000	Rabbit
Cyclin K	Bethyl Labor.	A301-939A	4	1:1,000	Mouse
EGFR	Santa Cruz	SC-03	H0409	1:800	Rabbit
IKKβ	Cell Signaling	2678	4	1:1000	Rabbit
RB	Cell Signaling	9309	9	1:2,000	Mouse
ERK	Cell Signaling	9302	2	1:1,000	Rabbit
FAK	Cell Signaling	3285	9	1:1,000	Rabbit
AKT	Cell Signaling	9272	25	1:2,000	Rabbit

Table 2. Antibody information.

CELL VIABILITY

MiaPaCa2 and HCT116 cells were plated at a density of 4,000 cells/well in a 96-well plate (Thermo Scientific #249946) and allowed to adhere overnight at 37 °C, 5% CO_2. The following day, cells were treated with the indicated concentration of inhibitors. For MiaPaCa2 cells, after the 72-hour drug incubation, PrestoBlue cell viability (10 µL) reagent (Invitrogen #A13262) was added to cells and incubated for 15 min at 37°C to assess the growth inhibition. Fluorescence (560ex/590em) was measured using the SpectraMax M5e instrument to determine the growth inhibition. For HCT116, the plate was analyzed at 3-hour intervals for 114 hours using an IncuCyte live-cell imager. The readout was phase area object average (μm^2). For both cell lines, percentage growth inhibition was calculated using 100 – [100 x (samples – T_0)/(T_{100}-T_0)], whereT_0 is the vehicle control reading immediately following the addition of the drug and T_{100} is the vehicle control reading at the end of the 72-hr incubation.

CALCUSYN

To determine the fraction affected as a decimal of 1, the percent growth inhibition data was divided by 100. If a value exceeded 100%, 0.999 was assumed. If a negative value was observed, a value of 0.001 was assumed. Using CalcuSyn software, combination index (CI) values were calculated as a mean of CI values calculated for each clinically relevant effect dose. The clinically relevant effect doses and their corresponding CI values were determined from the following ED values: ED_{50}, ED_{75}, and ED_{90}, where ED_{75} is the dose at which 75% of the cells are affected.

STATISTICAL ANALYSIS

Graphs and figures were generated using SigmaPlot 11.0 and Graphpad Prism statistical software (GraphPad Software, Inc). The student’s t-test was used to compare

differences between means between two groups. One-way analyses of variance (ANOVA) with a post-test for linear trend were used to compare two or more groups. For all analyses, significance was inferred at $P < 0.05$, and P values were two-sided.

PROTEOMICS ANALYSIS

Sample preparation for label-free & TMT mass spectrometry experiments

Samples were provided to the UNL core in a buffer comprised of radioimmunoprecipitation assay (RIPA) buffer (Thermo Scientific #89900), sodium orthovanadate (Na3VO4), sodium fluoride (NaF), β-glycerophosphate, and 1mM phenylmethylsulfonyl fluoride (PMSF). Extracted protein samples for both label-free quantitation (LFQ) and TMT experiments were acetone precipitated and washed to remove detergent before redissolving in 8 M urea, 100 mM tris/HCl, pH 7.8 (for LFQ experiments) and 7M urea, 2M thiourea, 0.5M triethylammonium bicarbonate (TEAB) buffer, pH 8.5 (for TMT experiments). Samples were assayed for protein, and 100µg (LFQ)/200µg (TMT) was reduced and alkylated, then digested using Lys-C and trypsin. Before labeling digests with TMT 10plex reagents (Thermofisher Scientific) according to the manufacturer's instructions, samples were desalted using Sep-Pak® C18 SPE columns (Waters Corp, Milford, MA). Labels were randomized within each 10plex set. Labeling efficiency was calculated as >99.3% labeled for both 10plex sets. 200 µg of the combined 10-plex mix was sub-fractionated offline into 96 fractions using high pH reverse phase C18 chromatography (ACQUITY UPLC® BEH C18, 1.7µm, 2.1 x 150mm, Waters Corp) in ammonium formate, pH 10. The 96 fractions were recombined to give a total of 12 fractions according to the concatenated strategy of Yang *et al.* (2012) [171]. For each LFQ analysis, 3µg of peptides were analyzed by mass spectrometry, and for each TMT fraction, 2.5µg of peptides was analyzed.

LC-MS/MS analysis of label-free & TMT-labeled samples

LC-MS/MS analyzed peptide samples on an RSLCnano system (ThermoFisher Scientific) coupled to a Q-Exactive HF mass spectrometer (ThermoFisher Scientific). The samples were first injected onto a trap column (Acclaim PepMap™ 100, 75µm x 2 cm, ThermoFisher Scientific) before switching in-line with the main column (Acquity UPLC® M-class, Peptide CSH™ 130A, 1.7µm 75µm x 250mm, Waters Corp). Mass spectra were acquired on a Q Exactive HF mass spectrometer in data-dependent mode using a mass range of m/z 375–1500 and MS1 resolution of 120,000. Data-dependent MS2 spectra were acquired by HCD. For the label-free samples, the MS2 settings were: 15,000 resolution, AGC target 1e5 ions, maximum ion time 250msec, top20 with a dynamic exclusion time of 60sec. For the TMT, MS2 settings were: 45,000 resolution, AGC target 5e5 ions, maximum ion time 86 msec, top10 with a dynamic exclusion time of 30sec, and the isolation window set to 0.7 m/z to reduce co-isolation.

Data analysis

Data were analyzed in Proteome Discoverer 2.4 software (ThermoFisher Scientific). Mascot 2.6.2 was used to search the databases; the common contaminants database cRAP (116 entries, www.theGPM.org) and the Human Reference Proteome UniProtKB (74,034 entries from 10/24/2019). For the LFQ approach used for the MiaPaCa2 cells experiment, methionine oxidation, asparagine and glutamine deamidation, protein N-terminal acetylation, cysteine carbamidomethylation, and serine, threonine, tyrosine phosphorylation was set as variable modifications. The same variable modifications were used for the TMT-labeled experiment used for the HEK293 cells except for the phosphorylation, while TMT10plex (K) and TMT10plex (N-term) were specified as fixed modifications. The search included a maximum of two trypsin missed cleavages with the precursor mass tolerance set to 10 ppm and the fragment mass tolerance to 0.02 Da,

respectively. Peptide validations were done by Percolator with a 0.01 posterior error probability (PEP) threshold. The data were searched using a decoy database to set the false discovery rate to 1% (high confidence). The peptides for MiaPaCa2 cells were quantified using the precursor abundance based on intensity. The peak abundance was normalized for differences in sample loading using total peptide amount, where the peptide group abundances are summed for each sample, and the maximum sum across all runs is determined. The significance of differential expression reported as log2 fold change is tested using an ANOVA test, which provides adjusted p-values using the Benjamini-Hochberg method for all the calculated ratios. The peptide quantification for HEK293 cells was processed using the TMT reporter ion's peak intensity in the MS2 spectrum, with the co-isolation threshold set to 50% and the average S/N to 10.

CHAPTER 3: DEGRADATION OF CDK9 BY PROTAC

Portions of the content covered in this chapter are the subject of an article at Bioorganic & Medicinal Chemistry Letters by King HM *et al.* 2021 Apr 23;43:128061.

Synthesis of aminopyrazole-based PROTACs for CDK9 degradation:

Aminopyrazole analogs were synthesized and evaluated as CDK2 inhibitors initially, but in practice, been demonstrated as pan-CDK inhibitors [111, 172]. Our laboratory and others have utilized this structure, along with aminothiazole and 4*H*-chromen-4-one cores, to generate CDK9 selective PROTACs Compound **3**, THAL-SNS-032, and Wogonin-based 11c, respectively [149, 165, 173]. Our laboratory reported the first CDK9 degrader, Compound **3**, which showed excellent selectivity for CDK9 degradation but unremarkable potency (DC_{50}= 7.8 μM) (**Figure 5A**) [149]. When designing PROTACs, optimization of linker length and composition has been increasingly crucial to the degrader's pharmacological potential [174]. Due to the dependence on linker length and composition for potency, we hypothesized modulation of one or both could result in a more potent CDK9 degrader.

To test this hypothesis, we synthesized ten aminopyrazole-based PROTACs with varying linker length and composition (**Figure 5B**). We utilized the same POI ligand and E3 ligand as Compound **3** but increased linker length and varied the composition. The linker lengths range from 9 atoms to 27 atoms. And the design of these linkers are based on two parameters: the number of oxygen atoms present in the linker and the amide group's position within the linker. For example, PROTAC **3** and PROTAC **4** have the same linker length and amide position; however, the number of oxygen atoms varies from 1 to 3. In PROTAC **9** and PROTAC **10,** the amide position is identical; however, their linker

length and oxygen atoms vary. PROTAC **6**, PROTAC **7**, and PROTAC **8** have the same number of oxygen atoms, but they differ in amide position and length.

A.

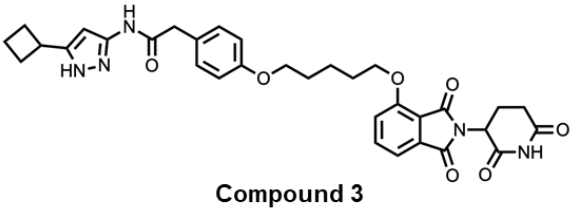

Compound 3
Linker Atoms = 7
Oxygen Atoms = 2
CDK9 DC_{50} = 7802 nM

B.

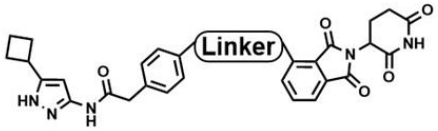

PROTAC	Linker Structure	# Linker Atoms	# Oxygen Atoms	Amide Position
1	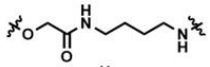	9	1	3
2	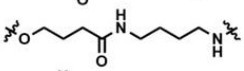	11	1	5
3	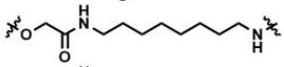	13	1	3
4	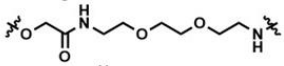	13	3	3
5	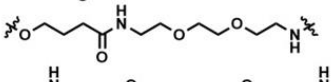	15	3	5
6	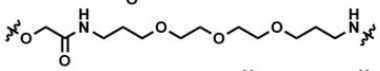	18	4	3
7	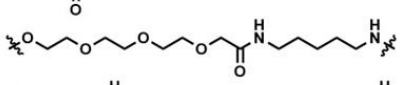	19	4	12
8	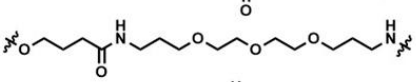	20	4	5
9	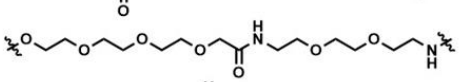	22	6	12
10	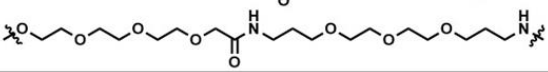	27	7	12

Figure 5. Structure of aminopyrazole-based PROTACs.

Evaluation of PROTAC panel in a dose-response and a time-course study for CDK9 degradation:

To determine the optimal linker for inducing CDK9 degradation, we screened the panel of PROTACs in a dose-response and a time-course study. For the dose-response analysis, we subjected HEK293 cells to increasing concentrations (0.1 – 10 μM) of each PROTAC for 24 hours (**Figure 6**). We observed CDK9 degradation with four of the PROTACs: PROTAC **1**, PROTAC **2**, PROTAC **3**, and PROTAC **4**. Degradation of CDK9 was minimal at the 10 μM dose of PROTAC **3** and PROTAC **4**. The most robust degradation of CDK9 was at 1 μM of PROTAC **1** and PROTAC **2**. For the time-course study, HEK293 cells were treated with 1 μM of each PROTAC in the panel for 0, 4, 8, and 24 hours (**Figure 7**). We see the degradation of CDK9 in three of the PROTACs: PROTAC **1**, PROTAC **2**, and PROTAC **3,** starting at the 4-hour time point. No visible degradation of CDK9 was observed with PROTAC **4** in the time-course study. The remaining PROTACs (**5-10**) showed no activity towards CDK9 in either study.

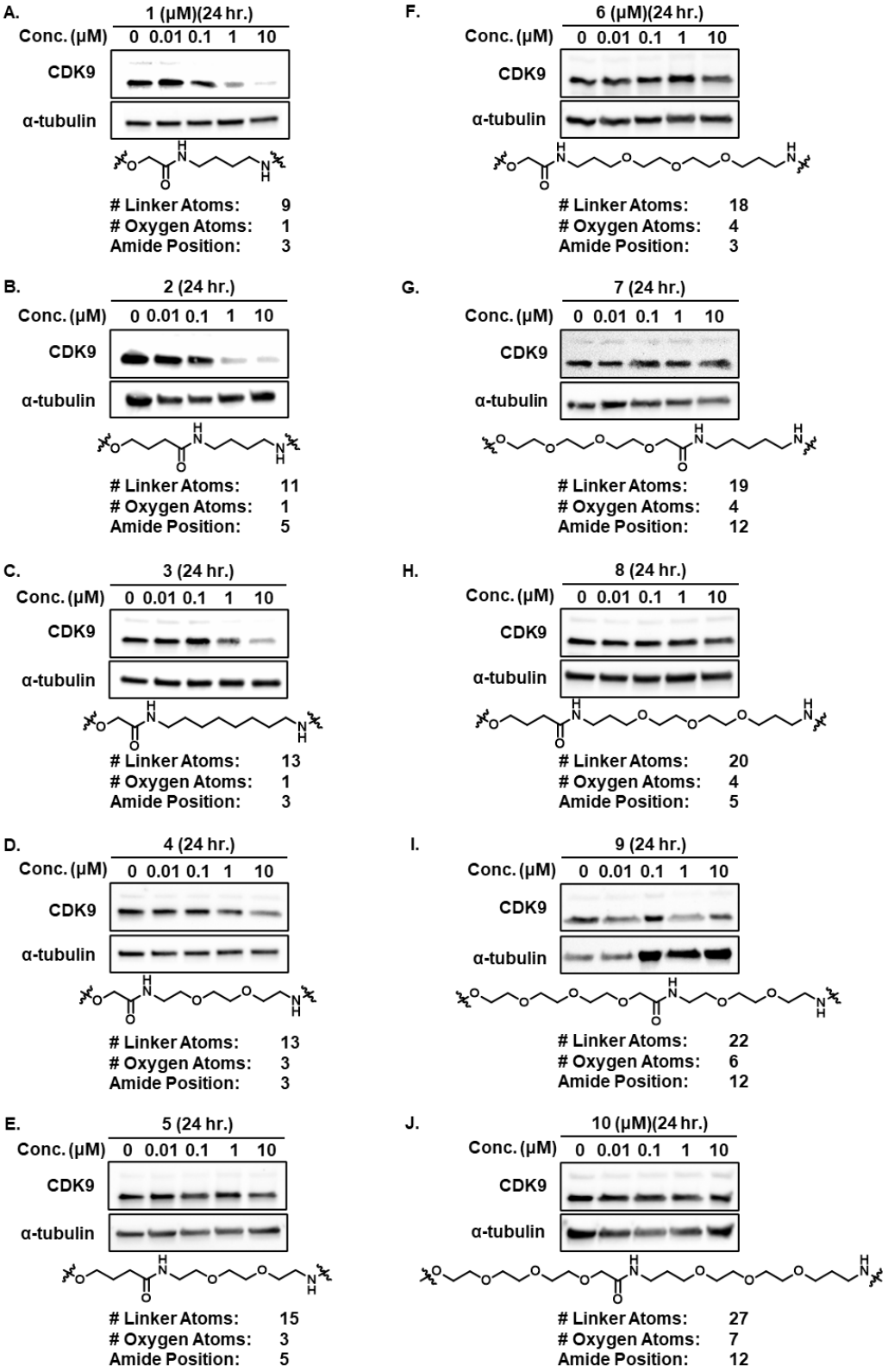

Figure 6. Screening of aminopyrazole-based PROTACs for CDK9 degradation. **A-J)** Dose-response studies examined after 24-hour treatment with the PROTACs in HEK293 cells.

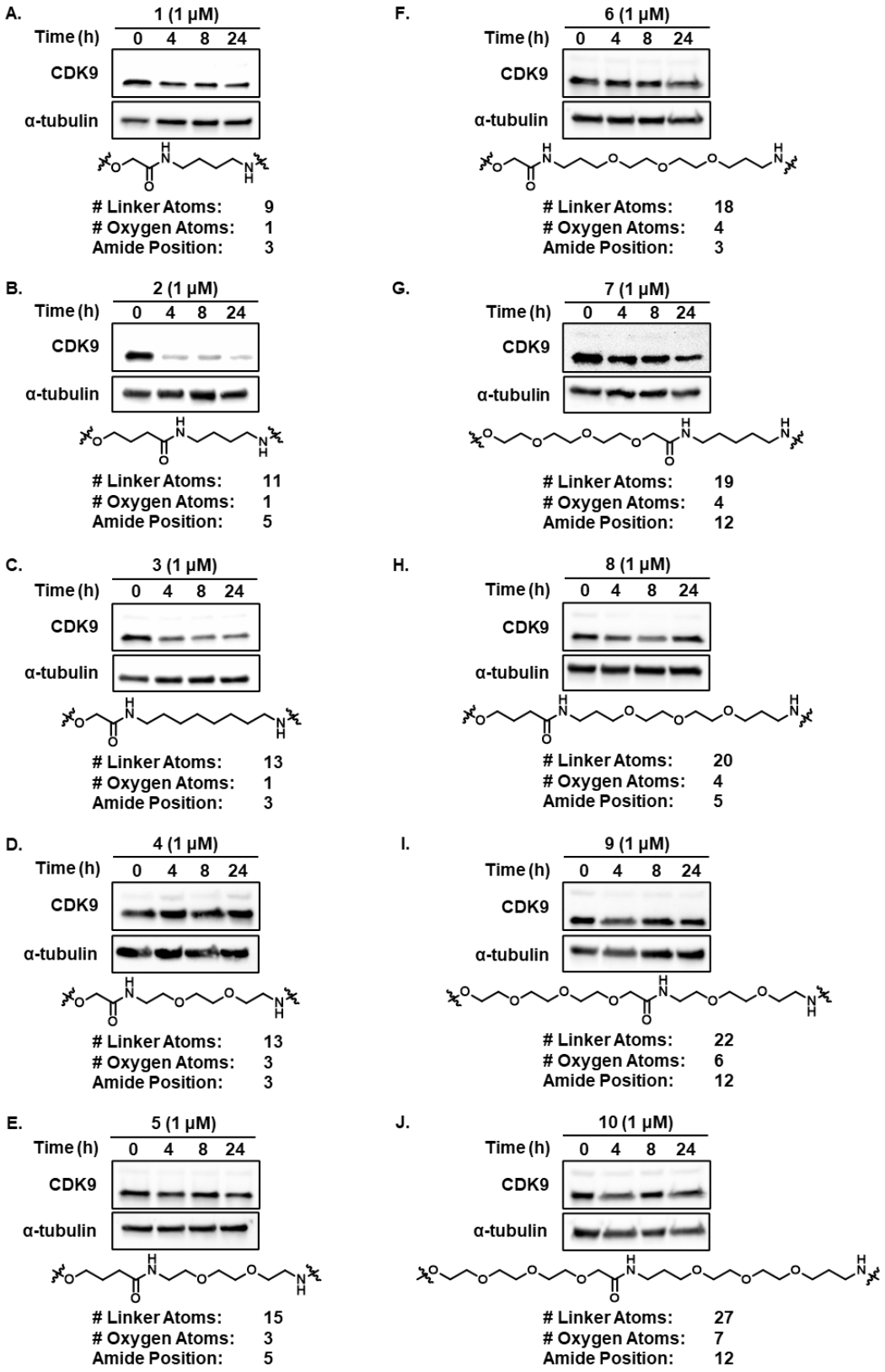

Figure 7. Time-course of aminopyrazole-based PROTACs. **A-J)** Time-course studies examined with 1 μM treatment with the PROTACs in HEK293 cells.

Selection of lead PROTAC based on cellular potency towards CDK9:

PROTAC **1** and PROTAC **2** showed robust degradation of CDK9 at 1 μM in the dose-response study. Also, they both showed degradation of CDK9 starting at 4 hours in the time-course study. To further characterize and decide on a lead compound, we quantified CDK9 expression in the dose-response study to determine which compound had the lowest DC_{50} (**Figure 8**). We established the DC_{50} of PROTAC **1** to be ~1μM and PROTAC **2** to be 158 ± 6 nM, demonstrating PROTAC **2** to be the most potent. Therefore, designating it as our lead compound. Interestingly, decreasing the linker length by 2-carbon atoms (PROTAC **1)** resulted in a significant decrease in potency.

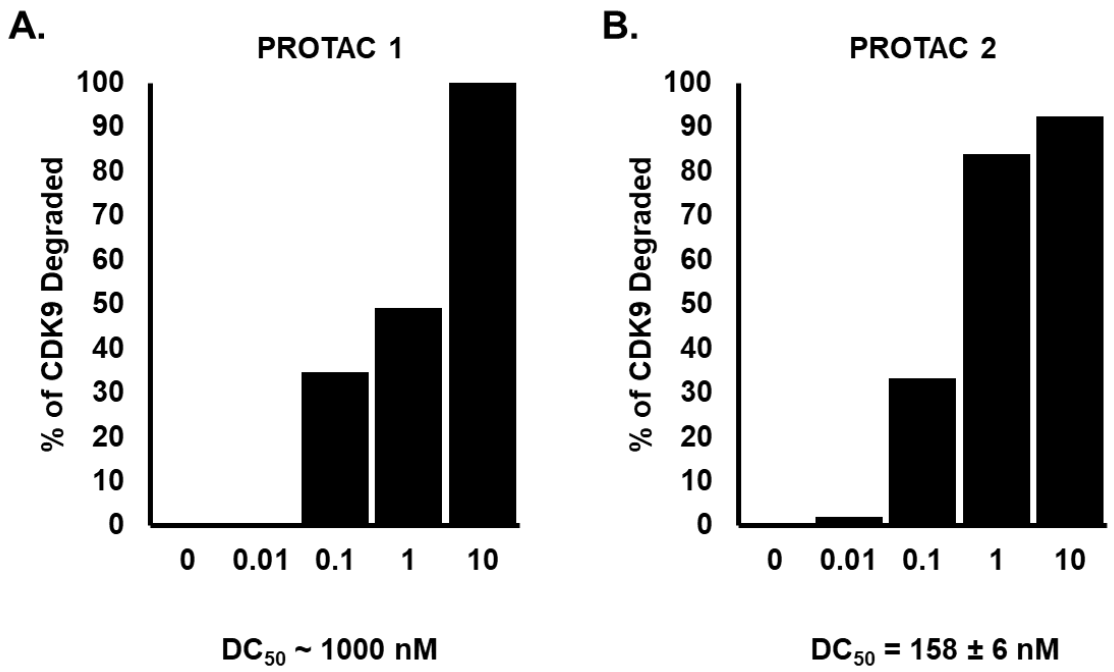

Figure 8. Quantification of dose-response. **A-B)** Quantification of PROTAC **1** and PROTAC **2** dose-response showing percentage of CDK9 degraded, respectively. (Quantify the blot in 10D and you can add error bars to PROTAC 2 bar graph)

Determining the CDK selectivity of PROTAC 2:

Due to the promiscuous nature of aminopyrazole analogs (known as CDK2/5 inhibitors) [172], we next evaluated the selectivity of PROTAC **2** across other CDK family members. First, PROTAC **2** was administered to HEK293 cells in a dose-dependent manner (**Figure 9A**). Cells were harvested after a 24-hour incubation, lysates were subjected to western blot analyses and probed for expression of indicated CDKs. In this study, PROTAC **2** selectively degraded CDK9 without affecting the levels of other CDK family members. Next, HEK293 cells were subjected to PROTAC **2** in a time-dependent (**Figure 9B**) manner. Cells were treated with 1 μM of PROTAC **2** for either 0, 4, 8, or 24 hours. These samples were subjected to western blot analyses and probed for various CDKs. In this analysis, we determined PROTAC **2**, again, selectively degrades CDK9 over other CDK family members. These two studies demonstrate the selective dose- and time-dependent degradation of CDK9 by PROTAC **2**.

To determine if the selectivity of PROTAC **2** was the result of decreased binding to the other CDK family members, we evaluated PROTAC **2** and its parent inhibitor, inhibitor **11**, in *in vitro* cell-free kinase assays. We determined PROTAC **2** exhibited greater potency (IC_{50}) and binding affinity (K_D) towards CDK2 and CDK5 over CDK9 (**Figure 9C-D**). However, the conversion from inhibitor to PROTAC did reduce the potency towards CDK2 while increasing the potency towards CDK9 and CKD5. Furthermore, PROTAC **2** lost binding affinity for CDK2 and CDK5 while having a slight increase in binding affinity for CDK9. In conclusion, since the kinase activity and affinity profile of PROTAC **2** and inhibitor **11** are similar, we can conclude the selectivity of PROTAC **2** is not due to selective binding. However, it can be attributed to the differential distribution of surface-exposed lysine residues among CDK2, CDK5, and CDK9 [149].

A.

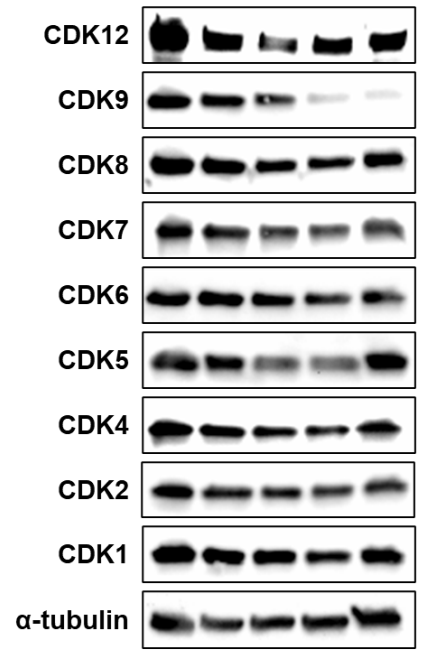

B.

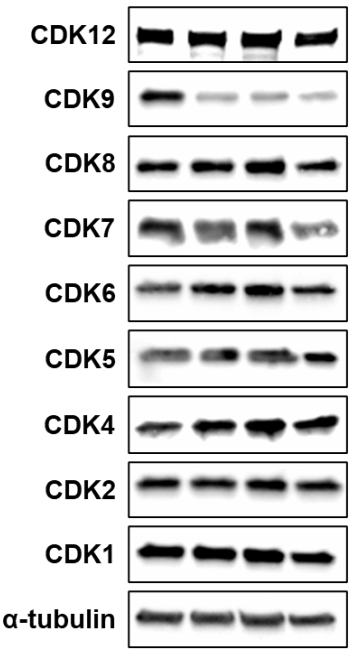

C.

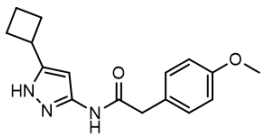

11

Code	IC_{50} (nM)		
	CDK2 / cyclin E	CDK5 / p25	CDK9 / cyclin T1
11	44 ± 11	32 ± 8	1080 ± 190
2	155 ± 46	7 ± 1	530 ± 50

D.

Code	K_D (nM)		
	CDK2 / cyclin E	CDK5 / p25	CDK9 / cyclin T1
11	135 ± 21	230 ± 14	1065 ± 191
2	385 ± 78	815 ± 134	1055 ± 205

Figure 9. Selectivity profile of lead PROTAC. **A)** Time-dependent effects of PROTAC **2** on CDK family members. **B)** Dose-dependent effect of PROTAC **2** on CDK family members. *In vitro* cell free **(C)** IC_{50} and **(D)** K_D profling of inhibitor **11** and PROTAC **2** respectively.

Elucidating the mechanism of action of PROTAC 2:

Now that we have validated the molecular targets of PROTAC **2**, we next needed to elucidate its mechanism of action. The formation of a stable ternary complex, CDK9—PROTAC **2**—cereblon, is essential for PROTAC **2** mediated CDK9 degradation [127]. To validate this mechanism of action, we conducted a series of competition experiments. First, we wanted to confirm the E3 ligand thalidomide's engagement with cereblon using a thalidomide analog, pomalidomide. HEK293 cells were treated with either 10 μM of pomalidomide alone and in combination with 1 μM of PROTAC **2** for 24 hours, and the lysates were subjected to western blot analysis (**Figure 10A**). We observed no degradation of CDK9 in the pomalidomide alone treated samples, but we did block CDK9 degradation in the combination-treated samples. Additionally, we saw no change in CDK7 levels; a transcriptional CDK, we used a control.

Next, we wanted to validate the POI ligand's engagement with CDK9 using a known CDK9 inhibitor, flavopiridol. Flavopiridol is an ATP-competitive inhibitor, so it should engage CDK9 in the same binding pocket as PROTAC **2**. HEK293 cells were treated with either 10 μM of flavopiridol alone and in combination with 1 μM of PROTAC **2** for 8 hours, and the lysates were subjected to western blot analysis (**Figure 10B**). The results showed that flavopiridol by itself did not affect CDK9 levels but could block PROTAC **2** mediated degradation of CDK9 when treated in combination. At the same time, no change was observed in CDK7 protein levels. Both competition studies demonstrated the need for simultaneous engagement of CDK9 and a CRBN E3 ligase (ternary complex) by PROTAC **2** to facilitate CDK9 degradation.

Lastly, protein targets must undergo PROTAC-mediated ubiquitination, which results in its proteasomal-mediated degradation. We also subjected HEK293 cells to increasing concentrations of the proteasome inhibitor MG132 with PROTAC **2** for 24 hours

to validate this mechanism. MG132 blocks the proteolytic activity of the 26S proteasome complex [175]. In the presence of MG132, we observed an abrogation in the degradation of CDK9 (**Figure 10C**). Membranes were also probed for CDK1 and CDK12 as controls, where no such change was observed.

Collectively, these studies confirmed the formation of a stable ternary complex between CDK9—PROTAC **2**—CRBN. Followed by CDK9 ubiquitination and subsequent proteasomal degradation as the mechanism of action of PROTAC **2**, which is similar to our previous report of a CDK6 selective PROTAC [147]. Additionally, we performed western blot analysis on cyclin K to ensure the degradation profile was not due to the disruption of CDK9 binding partners. We observed no change in cyclin K expression levels when treated with PROTAC **2**.

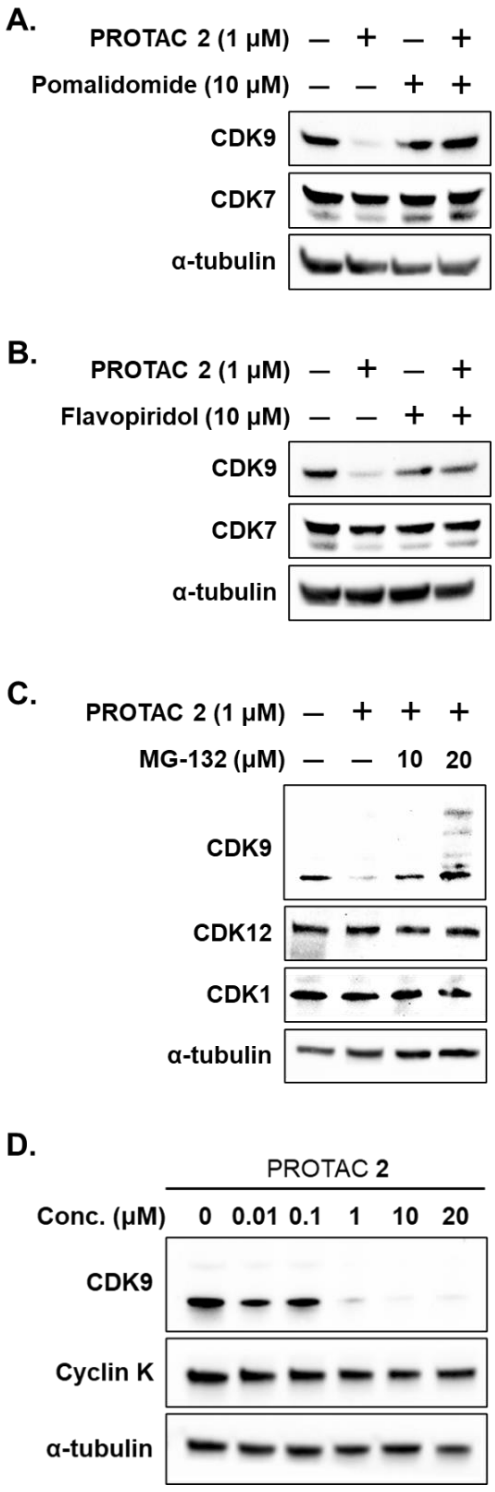

Figure 10. PROTAC 2 Mechanism of action. **A)** Western blot analysis showing **Pomalidomide** induced inhibition of CDK9 degradaion. **B)** Western blot analysis showing **Flavopiridol** induced inhibition of CDK9 degradaion.**C)** Western blot analysis showing **MG132** induced inhibition of CDK9 degradaion. **D)** Western blot analysis demonstrating no effect on cyclin K expression.

Determining the activity of PROTAC 2 in pancreatic cancer cell lines:

CDK9 plays a role in several transcriptional addicted cancers, mainly because of its role in oncogenic-driven transcription. Recently, CDK9 has been implicated in MYC transcription and stabilization in MYC-driven pancreatic cancer [61]. As a result, we wanted to evaluate the ability of PROTAC **2** to degrade CDK9 in two pancreatic cancer cells. We subjected two pancreatic cancer cell lines, MiaPaCa-2 and Suit-2, to PROTAC **2** (0-1 μM) for 24 hours (**Figure 11A-B**). Additionally, we treated HEK293 cells with PROTAC 2 for 24 hours to serve as a technical control (**Figure 11C**). At 1 μM, we observed CDK9 degradation in all three cell lines tested, MiaPaCa-2, Suit-2, and HEK293. Although, CDK9 degradation was most robust in HEK293 cells.

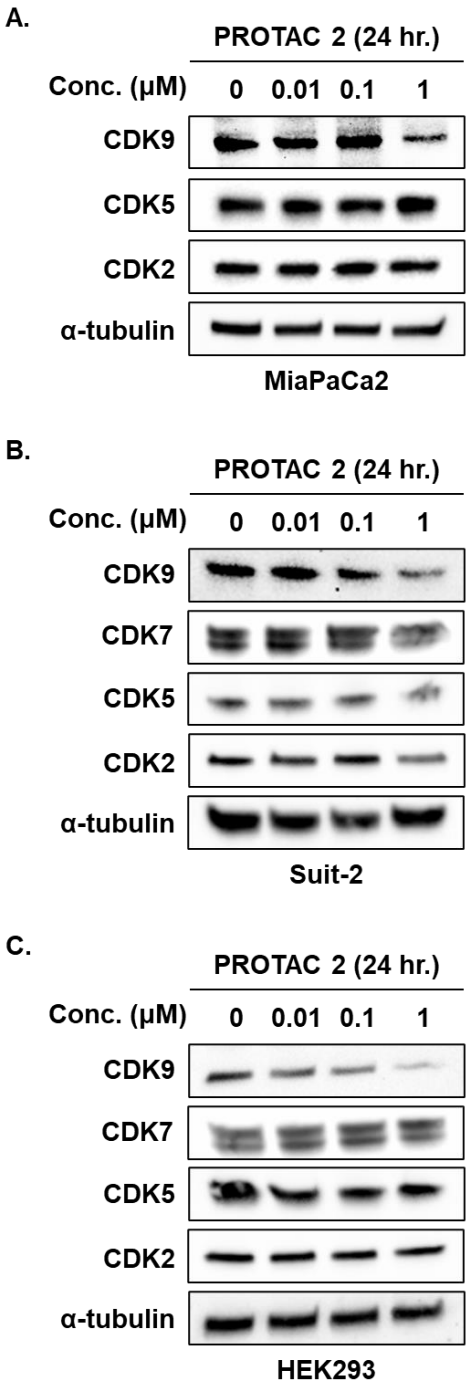

Figure 11. PROTAC **2** mediated CDK9 degradation in pancreatic cancer cell lines. Western blot analysis of PROTAC **2** treated (A) MiaPaCa-2, (B) Suit-2, and (C) HEK293 cell lines exhibiting CDK9 degradation.

Proteome and kinome profiling of PROTAC 2:

PROTAC **2** has been shown to mediate CDK9 selective degradation in both human embryonic kidney (HEK293) and pancreatic cancer (MiaPaCa-2 & Suit-2) cell lines when compared to other CDK family members. Next, we wanted to determine the proteome-and kinome-wide profile of PROTAC **2**. Quantitative mass spectrometry (MS) proteomic analysis has been successfully employed to profile 243 clinical kinase inhibitors' specificity and potency. We hypothesized this approach could be used to profile PROTAC **2** [176]

To examine the kinome and proteome selectivity of PROTAC **2**, we performed quantitative mass spectrometry with lysates from HEK293 (**Figure 12A**) and MiaPaCa-2 (**Figure 12B**) cell lines treated with PROTAC **2** for 24 hours (**Figure 12C**). We were able to quantify 229 unique kinases, including 13 CDKs in the HEK293 lysate and CDK9 was the only kinase identified as a hit with a 1.5-fold change and a significance threshold of $P < 0.001$ (**Figure 12D**). We were able to quantify 3433 proteins in the MiaPaCa2 lysate, and three kinases, CDK9, CDK2, and RPS6KA1, were identified as hits with a 1.5-fold change and a significance threshold of $P < 0.001$ (**Figure 12E**). MiaPaCa2 cell line was selected for the proteome-wide profiling because they were previously used to validate CDK9 as a therapeutic target for pancreatic cancers and showed PROTAC **2** mediated degradation of CDK9 [61].

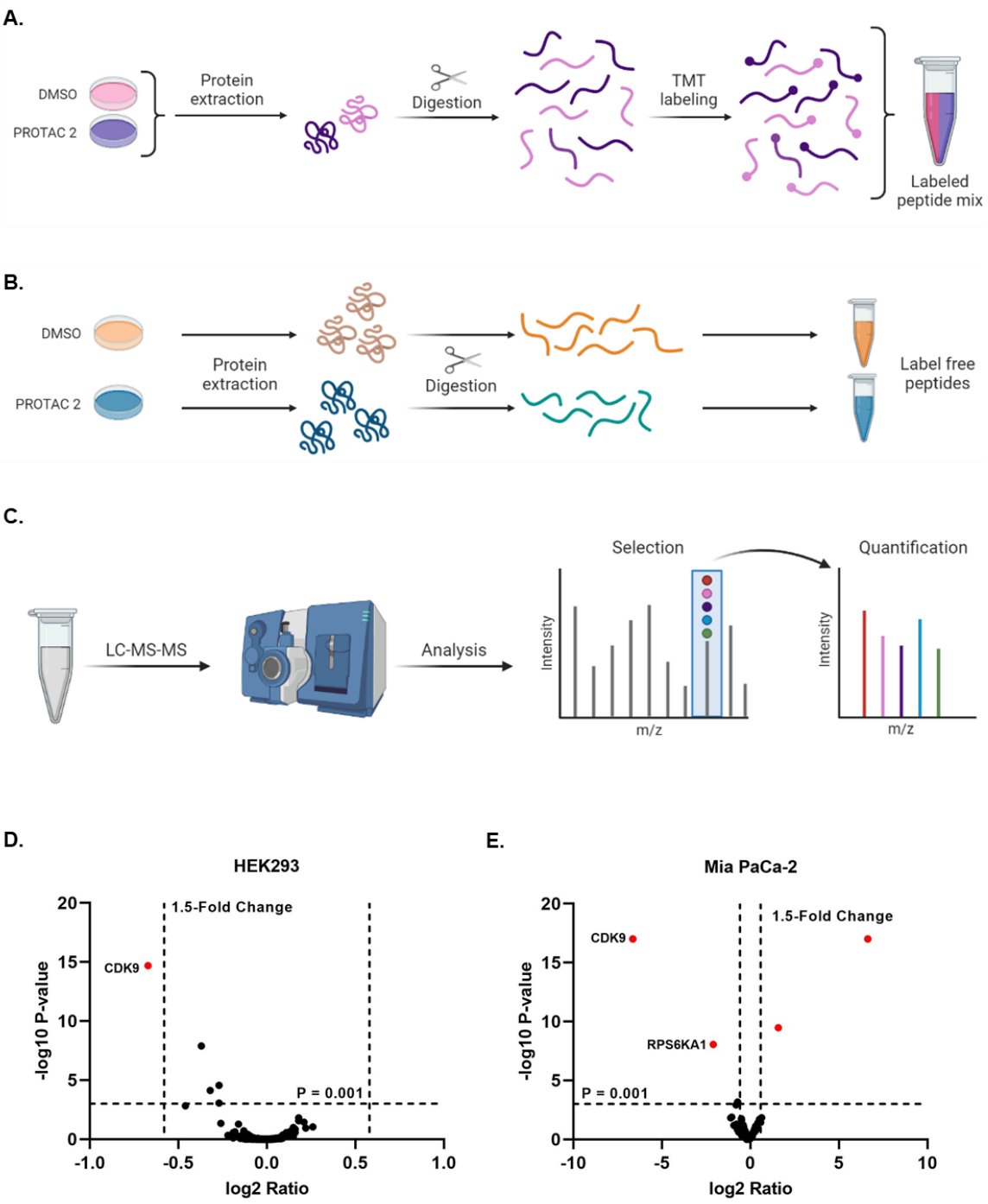

Figure 12. Kinome and proteome-wide profile of PROTAC 2. **A)** Overview of sample preparation of TMT labeled proteomics. **B)** Overview of sample preparation for label-free proteomics.**C)** Overview of sample anlaysis for both TMT labeled and label-free proteomics. **D)** Volcano plot of the kinome in HEK293 cells treated with 1 μM of PROTAC **2** and incubated for 24 hours. **E)** Volcano plot of the proteome in MiaPaCa2 cells treated with 1 μM of PROTAC **2** and incubated for 24 hours.

Exploring synergism with Bcl2 inhibitors through combination studies:

Recent studies demonstrated that concurrent inactivation of Mcl-1 and Bcl-xL, the two major anti-apoptotic Bcl-2 family members, results in the robust activation of apoptosis[149, 172, 177-184]. As a result, targeting Mcl-1 and Bcl-xL is considered a therapeutic strategy for pancreatic cancer therapy [180]. However, upon blockade of Bcl-xL, an increase in the expression of Mcl-1 has been observed, indicating Mcl-1 is a crucial player in resistance [185]. In addition, Mcl-1 inactivation sensitizes cancer cells to Bcl-2 inhibitors [186, 187]. Since CDK9 is known to regulate the expression of Mcl-1, we hypothesized PROTAC **2** would sensitize pancreatic cancer cell lines to Bcl2 inhibition.

To test this hypothesis, we selected three Bcl2 inhibitors that Abbott Laboratories successfully developed as direct inhibitors of Bcl-xL/Bcl2/Bcl-w. ABT-263 (Navitoclax), a clinical candidate, is characterized as a Bcl2/Bcl-xL/Bcl-w inhibitor that underwent a phase II trial. ABT-199 (Venetoclax) is an FDA-approved Bcl2 inhibitor. And WEHI-539, an experimental Bcl-xL inhibitor (**Figure 13A**). We performed a 72-hour growth inhibition assay to determine if PROTAC **2** sensitizes MiaPaCa2 cells to the above Bcl2 inhibitors. MiaPaCa2 cells were treated individually with ABT-263 (Bcl2/BclxL/Bcl-w), ABT-199 (Bcl2), WEHI-537 (Bcl-xL), PROTAC **2**, and the combination with the Bcl2 inhibitors and PROTAC **2**, respectively.

When examined as single agents, the selective compounds PROTAC **2**, ABT199, and WEHI-539 showed minimal growth inhibition at equimolar concentration. However, the non-selective inhibitor ABT-263 induced ~50% growth inhibition. When examined in combination, PROTAC **2** sensitized MiPaCa2 cells to ABT-263 and ABT-199. Interestingly, PROTAC **2** did not sensitize MiaPaCa2 to the Bcl-xL selective inhibitor WEHI-539 (**Figure 13B**). Next, we determined the combination index (CI) values using CalcuSyn at effective doses (ED) 50, 75, and 90, which demonstrated that PROTAC **2**

exhibited strong synergism with ABT-263 and ABT-199 but not with WEHI-539 (**Figure 13C**). Together, this data confirms that PROTAC **2** potently sensitizes MiaPaCa2 cells to the FDA-approved Bcl2 inhibitor Venetoclax.

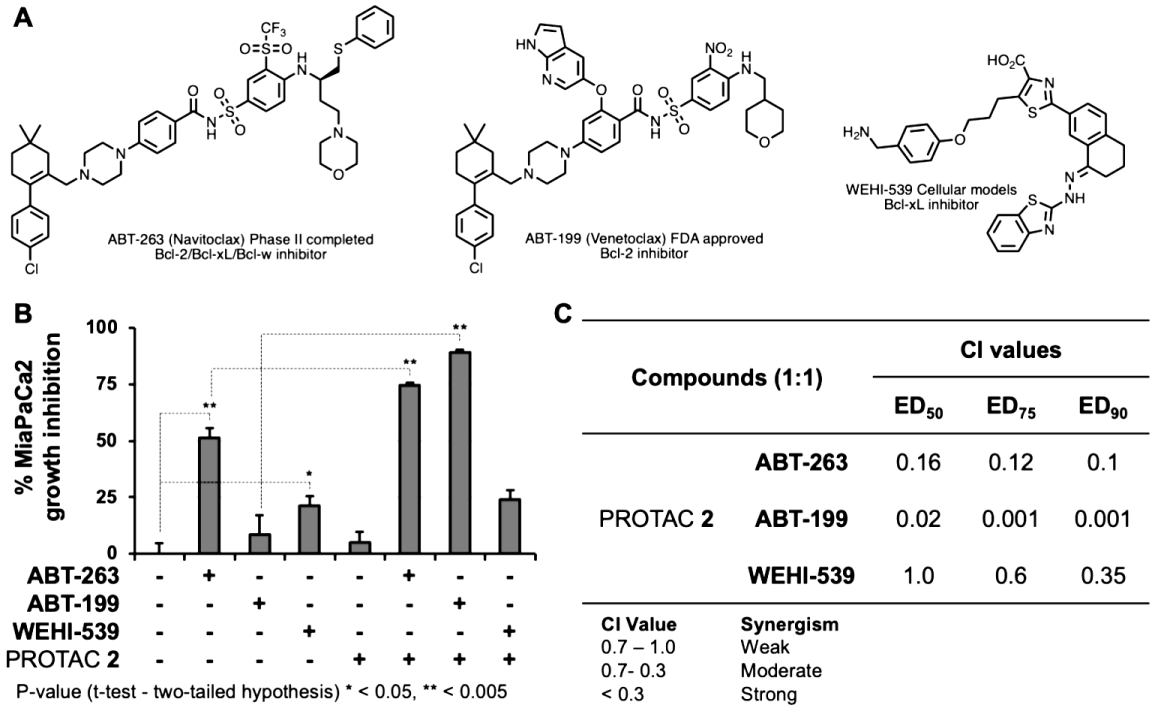

C

Compounds (1:1)		CI values		
		ED_{50}	ED_{75}	ED_{90}
	ABT-263	0.16	0.12	0.1
PROTAC **2**	**ABT-199**	0.02	0.001	0.001
	WEHI-539	1.0	0.6	0.35

CI Value	**Synergism**
0.7 – 1.0	Weak
0.7- 0.3	Moderate
< 0.3	Strong

Figure 13. Synergism studies using BCL inhibitors and PROTAC 2. **A)** Structure of Bcl2 inhibitors: ABT-263 (Navitoclax), ABT-199 (Venetoclax); WEHI-539. **B)** Growth inhibitory effects of different inhibitor combinations tested at 5 μM. **C)** Combination index (CI) values for the three Bcl2 inhibitor:PROTAC **2** combinations.

CHAPTER 4: DEGRADATION OF CDK12 BY PROTAC

Screening of aminopyrazole based degrader in several cancer types:

Our laboratory synthesized a panel of ten aminopyrazole degraders designed to selectively and potently target CDK9 (**Figure 5Figure 5.** Structure of aminopyrazole-based PROTACs.). However, when initially tested in HEK293 cells, only four compounds triggered CDK9 degradation, PROTAC **2** being the most potent (**Figure 6**). Then, when we used PROTAC **2** in pancreatic cancer cell lines, we observed a decrease in the potency of PROTAC **2**. Which led us to hypothesize these degraders might have improved potency in a different cell type.

Compound **3**, our original CDK9 degrader, was initially tested in the colorectal cancer cell line HCT116. As a result, we evaluated the degraders' effect on a panel of cyclin-dependent kinases and non-CDK kinases in HCT116 colorectal cancer cell line. We treated HCT116 cells to 1 μM treatment of each of the ten aminopyrazole based PROTACs for 24 hours (**Figure 14**). Surprisingly, we saw no analog caused robust degradation of CDK9; however, PROTAC **4** showed potent and selective degradation of CDK12.

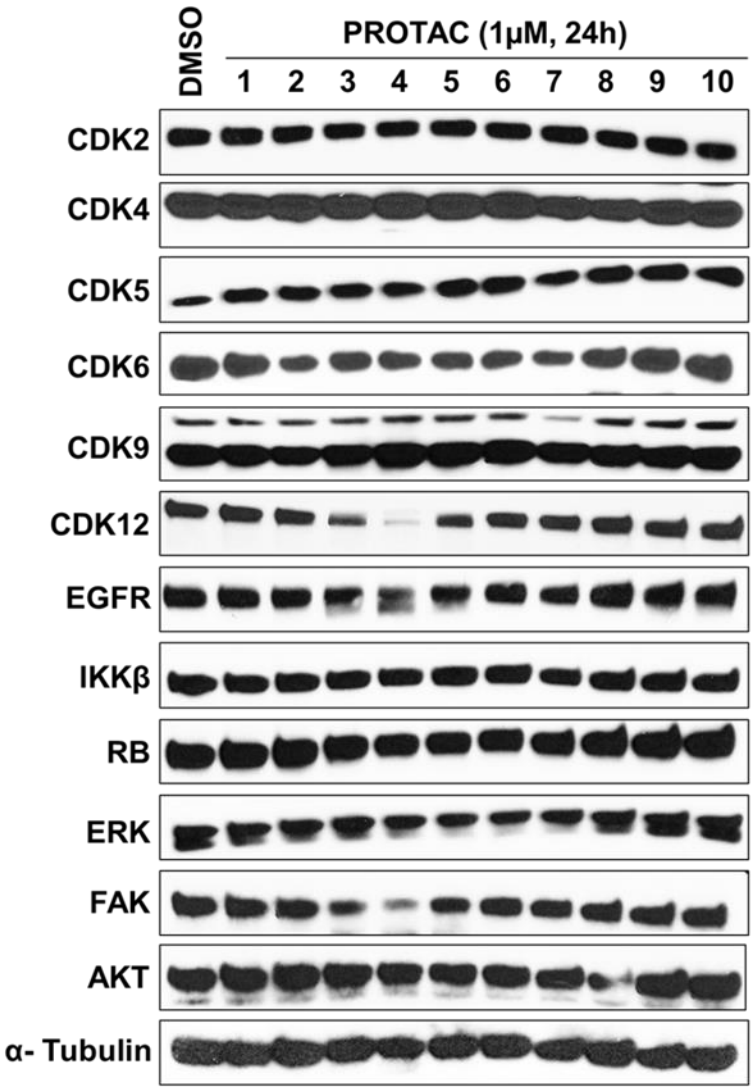

Figure 14. Screening of PROTAC panel in HCT116. Western blot analysis of HCT116 cells with single dose treatment (1 μM) of PROTAC panel.

PROTAC 4 degrades CDK12 only in colorectal cancer cell lines:

Since we saw varying potency between cell line types, we decided to examine PROTAC **4** in several different cancer types. We treated a panel of cancer cell lines with all ten degraders at 1 μM for 24 hours. SW620 and HCT116 are colorectal cancer cell lines where PROTAC **4** showed CDK12 degradation (**Figure 15**). S2013 and Mia PaCa-2 (MP2) are pancreatic cancer cell lines, SKOV3 is an ovarian cancer cell line, A673 is an Ewing Sarcoma cell line, and Jurkat is an acute myeloid leukemia cell line. None of these other cell lines showed CDK12 degradation with any of the degraders. Our preliminary studies suggest PROTAC **4** is a colorectal-specific CDK12.

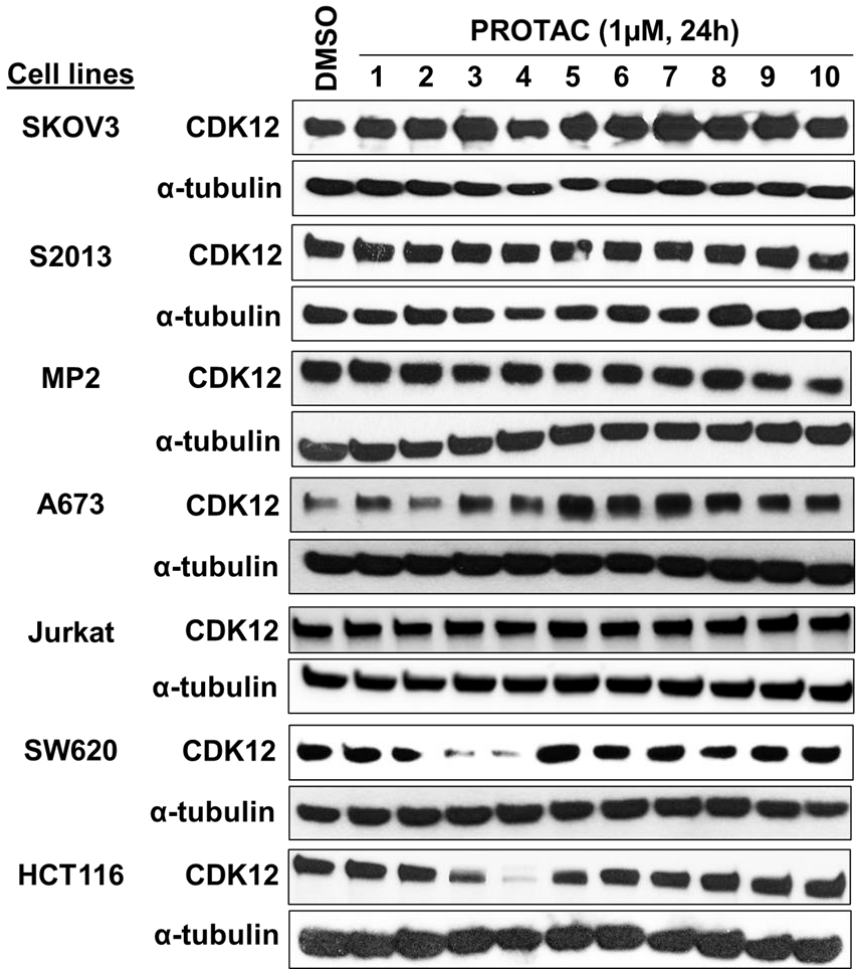

Figure 15. CDK12 degradation across a panel of cancer cell lines. Western blot analysis of the PROTAC panel in seven different cancer cell lines.

Evaluation and characterization of PROTAC 4 in HCT116:

To better determine the degradation profile of PROTAC **4** on CDK12, we performed dose-response and time-course studies. We subjected HCT116 cells to increasing concentrations (0.001 – 10 μM) of PROTAC **4** for 24 hours for the dose-response analysis (**Figure 16A**). We observed CDK12 degradation with as low of a dose as 0.01 μM treatment with PROTAC **4**. For the time-course study, we subjected HCT116 cells with 1 μM of PROTAC **4** for 0, 1, 3, 8, 24, and 48 hours (**Figure 16B**). We see the degradation of CKD12 starting at the 3-hour time point.

Lastly, we verified that PROTAC **4** is causing CDK12 to undergo PROTAC-mediated ubiquitination, which results in its proteasomal-mediated degradation. We also subjected HCT116 cells to increasing concentrations of the proteasome inhibitor MG132 with 1 μM of PROTAC **4** for 24 hours to validate this mechanism. In the presence of MG132, we observed a blockade in the degradation of CDK12 (**Figure 16C**). Membranes were also probed for CDK13 as a control, where no degradation was observed in the PROTAC **4** only treated cells.

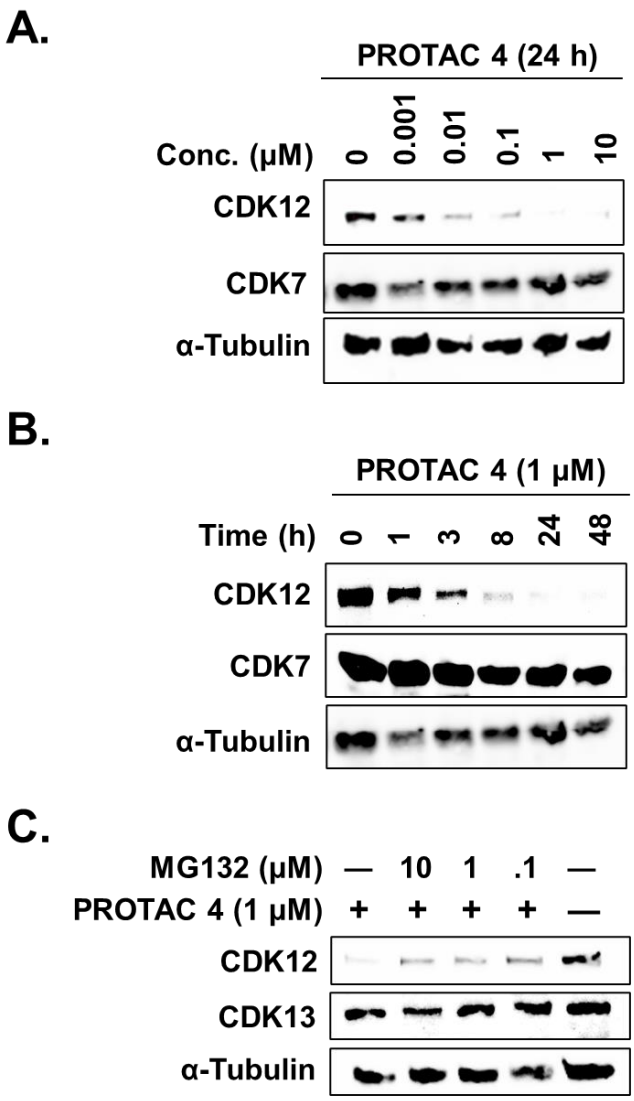

Figure 16. CDK12 degradation is time and dose proteasomal mediated. **A)** Dose-response studies examined after 24-hour treatment with the PROTACs in HCT116 cells. **B)** Time-course studies examined with 1 μM treatment with the PROTAC 4 in HCT116 cells. **C)** Western blot analysis showing **MG132** induced inhibition of CDK12 degradaion.

Exploring potential synergisms with DNA damaging agents:

CDK12 is known to regulate the transcription of genes involved in homologous recombination (HR) driven DDR, mostly genes centered around the BRCA1 locus [17]. Also, loss of function mutations in CDK12 leads to genomic instability and PARP inhibitor susceptibility. Based on these studies, we hypothesized that PROTAC **4** would sensitize colorectal cancer cells to DNA damaging agents.

To test this hypothesis, we selected six known DNA damaging agents. Cisplatin, gemcitabine, mitomycin-C, olaparib, veliparib, and rucaparib. We performed a 72-hour growth inhibition assay to determine if PROTAC **4** sensitizes HCT116 cells to the above DNA damaging agents. HCT116 cells were treated individually with cisplatin, gemcitabine, mitomycin-C, olaparib, veliparib, rucaparib, PROTAC **4**, and the combination with each inhibitor and PROTAC **4**, respectively. Of the tested combination, only gemcitabine and PROTAC **4** showed synergism (**Figure 17**).

When we examine the live-cell images, which demonstrates cell confluence, we can see that both gemcitabine and PROTAC **4** alone inhibited cell growth. However, when used in combination, we see a robust inhibition of growth (**Figure 17A**). This was further validated by quantifying observed cell proliferation, where we see potent inhibition of cell growth in the gemcitabine and PROTAC **4** combination-treated cells (**Figure 17B**).

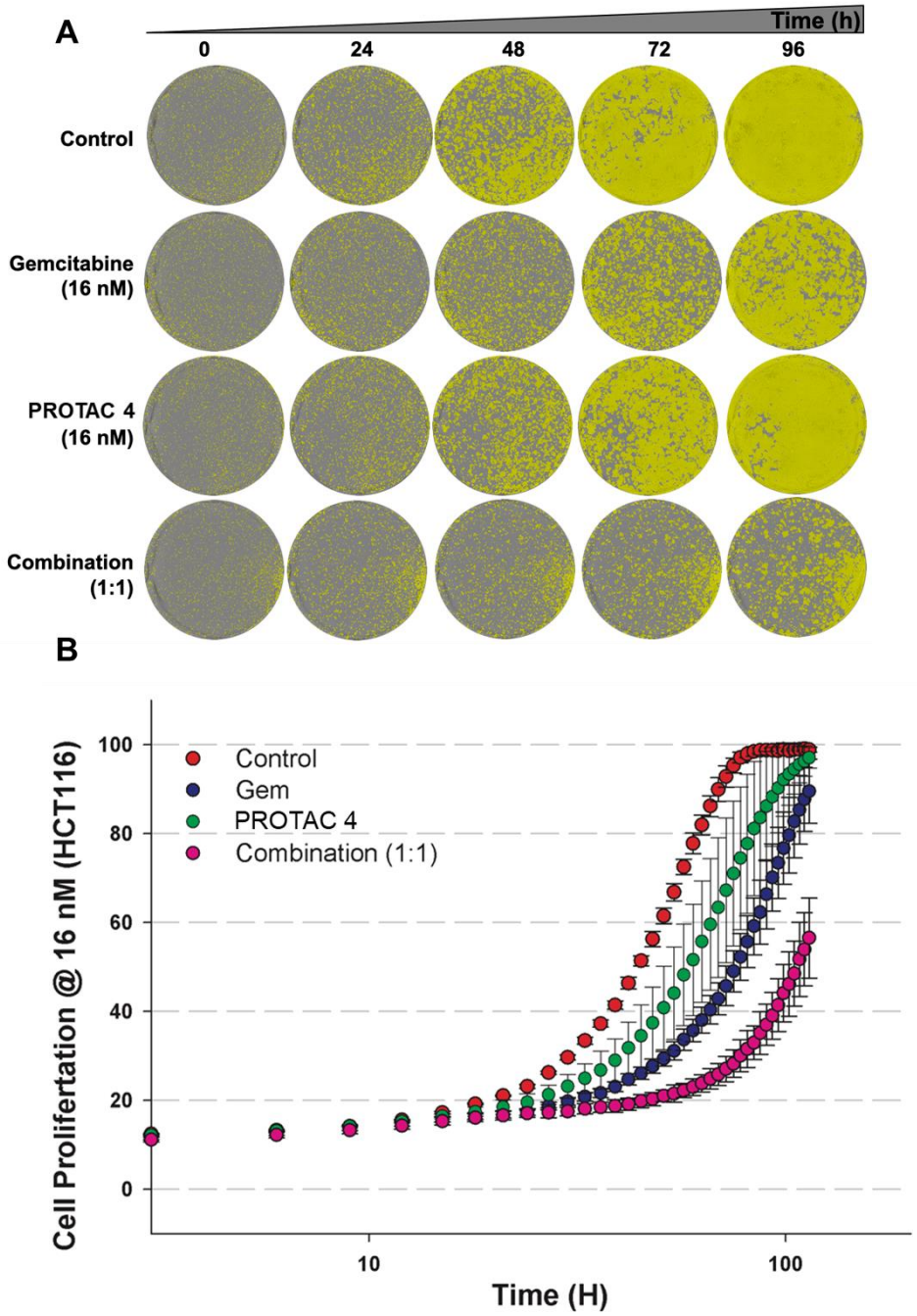

Figure 17. Synergism studies using DNA damaging agents. **A)** Live cell imaging illustarating confluence for DMSO, gemcitabine, PROTAC **4,** and the combination. **B)** Growth inhibition curve of HCT116 treated (16 nM) with gemcitabine and PROTAC **4**, alone and in combination. .

Determining the reason behind the loss of activity of PROTAC 4:

In the summer of 2019, in the middle of characterizing the mechanism of action of PROTAC **4**, we saw a loss in CDK12 activity (data not shown). We were able to determine through literature search that the presence of FBS can cause non-specific binding [188]. After close examination of dates, we decided the change in activity was after we had obtained a new batch of media and FBS. We tried to determine the effects of FBS concentration on PROTAC **4** (**Figure 18A**). While we were initially successful at obtaining activity in PROTAC **4**, this was short-lived. About seven weeks later, even in 1% FBS, we saw no degradation of CDK12 when treated with PROTAC **4** (**Figure 18B**).

Next, we wondered what other molecules in our system could be affecting the activity PROTAC **4**. We determined that different solvents (including DMSO) can affect protein and inhibitor confirmation [189]. To test this theory, we dissolved PROTAC **4** in ethanol instead of DMSO and tested for CDK12 degradation (**Figure 18C**). This also proved to be unsuccessful at returning the degradation profile.

Lastly, it is well known that compounds can become unstable, so we reanalyzed PROTAC **4** using mass spectrometry to determine its current molecular weight. Mass spectrometry analysis determined molecular weight matched the predicted molecular weight, which tells us the compound remained stable (**Figure 19**).

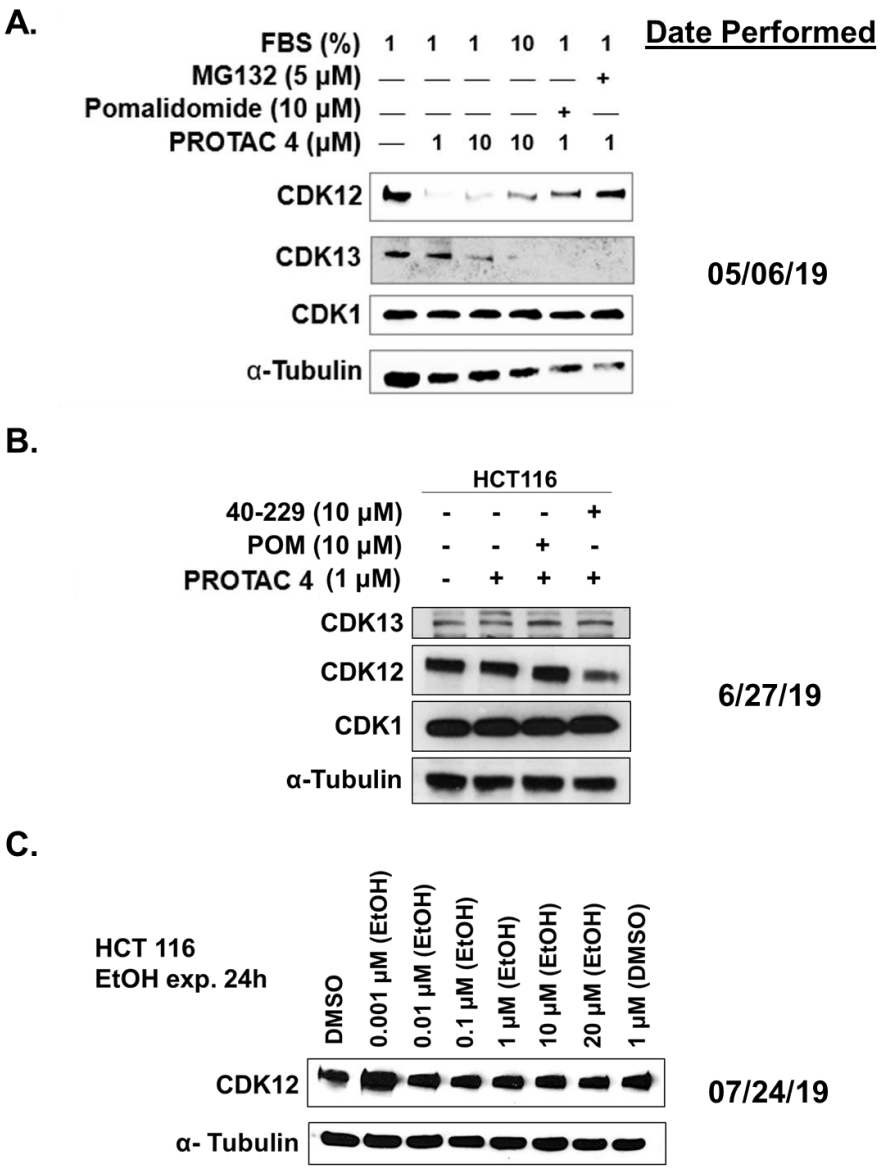

Figure 18. Determine the reason of in the activity of PROTAC 4. **A)** Western blot analysis showing CDK12 degradation in the presence of 1 and 10% FBS. **B)** Western blot analysis for competition experiment performed in 1% FBS. **C)** Western blot analysis of ethanol dissolved PROTAC **4**.

A.

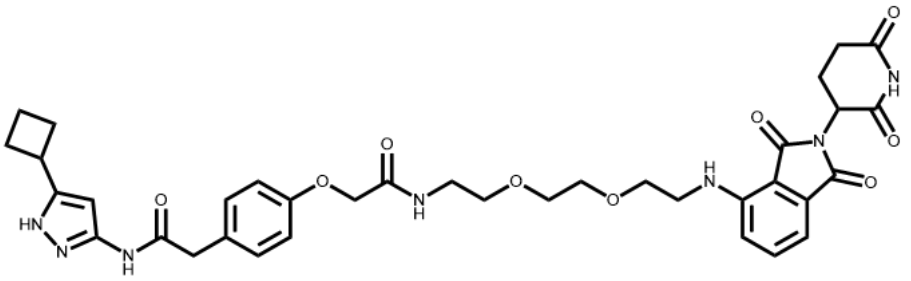

PROTAC 4
Chemical Formula: $C_{36}H_{41}N_7O_9$
Exact Mass: 715.2966
Molecular Weight: 715.7640

B.

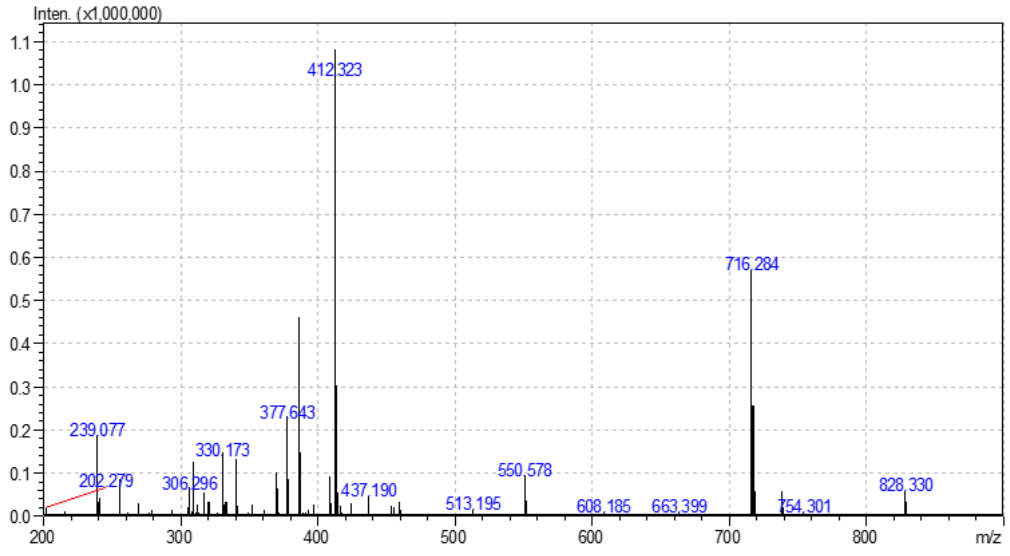

Figure 19. MS analysis of PROTAC 4. **A)** Structure of PROTAC4 with chemical formula and molecular weight. **B)** Mass spectrometry spectra of PROTAC **4** used to determine stability.

CHAPTER 5: DISCUSSION

In the studies outlined above, we set out to synthesize and characterize a potent CDK9 degrader. Our laboratory previously reported the development of compound **3**, an aminopyrazole based proteolysis targeting chimera (PROTAC), as the first selective CDK9 degrader (DC_{50} = 7.8 μM) capable of reducing Ser2 phosphorylation of the CTD of RNA pol II and Mcl-1 expression [149]. This compound showed excellent selectivity but had relatively low potency. Linker length has been determined to be a variable in PROTAC potency [174], so we hypothesized that modulating compound **3** linker could result in higher potency. To achieve this, we synthesized ten aminopyrazole based PROTACs analogs of compound **3.** Contrary to our original intent, one of the heterobifunctional molecules facilitated a ternary complex that consisted of a non-covalent linkage between CDK12 and cereblon. Our studies resulted in the selective degradation of CDK9 with PROTAC **2** and selective degradation of CDK12 with PROTAC **4**.

PROTAC 2

In this study, we identified a selective and potent CDK9 degrader. Initially, we screened the ten aminopyrazole-based PROTACs in time and dose-dependent studies where we studied CDK9 degradation. This initial screen identified four PROTACs (**1-4**) capable of degrading CDK9. If we examine the difference in linker length and composition, several differences exist between the four PROTACs. PROTAC **1**, PROTAC **2**, and PROTAC **3** all have 1 oxygen atom, PROTAC **4** has three oxygen atoms. PROTAC **1**, PROTAC **3**, and PROTAC **4** have an amide at position 3, while PROTAC **2** has an amide at position 5. And PROTAC **3** and PROTAC **4** have the same linker length. These observations demonstrate that linker lengths and composition play an important role in determining PROTAC potency. From this study, we identified PROTAC **1** and PROTAC **2** as the most potent. We next chose our lead compound by quantifying the degradation

profiles of PROTAC **1** (DC_{50} ~ 1000 nM) and PROTAC **2** (DC_{50} = 158 nM) in the dose-response study, where PROTAC **2** demonstrate the higher potency.

PROTAC **2** selectively degraded CDK9 in a time and dose-dependent manner, resulting in a DC_{50} value of ~150 nM. PROTAC **2** mediated degradation of CDK9 was observed as early as 4 hours and was maintained through the 24-hour time point when treated at 1 μM in HEK293 cells. Interestingly, we did not observe the characteristic "hook-effect" even at 10 μM, meaning we had not saturated the system. The "hook-effect" occurs when the PROTAC no longer forms a productive ternary complex (E3-PROTAC-Target) but forms binary complexes (E3-PROTAC & PROTAC-Target) at high concentrations [190]. Additionally, treatment with PROTAC **2** did not affect other members of the CDK family.

Next, we evaluated PROTAC **2** in *in vitro* cell-free kinase assays. Aminopyrazole analogs robustly inhibit CDK2 and CDK5 [111, 177, 181]. However, compound 11, the CDK9 aminopyrazole-based inhibitor used as the POI ligand, only showed inhibitory activity against CDK5 and CDK9 when evaluated by western blot analysis [149]. When we evaluated PROTAC **2** in a cell-free system, we observed similar potency and binding affinities towards CDK2, CDK5, and CDK9. When the PROTAC was compared against its parent inhibitor, we observed a reduction in CDK2 potency and increased CDK5 and CDK9 potency. The binding affinity towards the three kinases tested did not change because of the inhibitor to PROTAC conversion. We concluded that the kinase activity and binding profile of the two compounds were similar, so the selective degradation of CDK9 cannot be attributed to the selective binding. However, we believe it can be attributed to the differential distribution of surface-exposed lysine residues among CDK2, CDK5, and CDK9, previously reported [149].

We were able to establish the mechanism of degradation through three competition studies. First, we confirmed the recruitment of cereblon by our E3 ligand thalidomide. When cells were treated with PROTAC **2** in combination with pomalidomide, CDK9 degradation was inhibited. Pomalidomide and thalidomide are both immunomodulatory drugs that recruit cereblon to our target by binding to the same moiety, resulting in competition for that binding site, ultimately inhibiting the PROTAC from working. Next, we utilized flavopiridol to confirm PROTAC **2**'s engagement with CDK. Both compound **11** (the CDK9 ligand of PROTAC **2)** and flavopiridol are classified as ATP-competitive inhibitors of CDK9; they should engage the same binding moiety within the ATP-binding pocket of CDK9. Lastly, we verified the proteasome's role in the degradation of CDK9 through the use of MG132, a potent 26S proteasome inhibitor. We were also able to determine that PROTAC **2** mediated effects on CDK9 were not due to cyclin K, one of the binding partners of CDK9. Together, establishing PROTAC **2** forms a ternary complex with CDK9 and CRBN to induce ubiquitination mediated proteasomal degradation of CDK9.

Since CDK9 has been demonstrated to be a driver of Mcl-1 expression in pancreatic cancer, thus contributing to its tumorigenicity [61], we wanted to evaluate the ability of PROTAC **2** to degrade CDK9 in pancreatic cancer cell lines. We observed a dose-dependent degradation of CDK9 in both pancreatic cancer cell lines tested, MiaPaCa2 and Suit-2. However, the degree to which PROTAC **2** induced degradation was less in the pancreatic cancer cell lines than the HEK293 cells.

Next, we wanted to determine the kinome and proteome-wide profile of PROTAC **2** since we limited ourselves to CDK family members in earlier experimentation. We employed two different methods to perform quantitative mass spectrometry, label-free proteomics for the MiaPaCa-2 treated samples and TMT labeled proteomics for the HEK293 cells. We were able to quantify 229 unique kinases, including 13 CDKs in the

HEK293 lysate. We determined CDK9 was the only kinase identified as a hit with a 1.5-fold change and a significance threshold of $P < 0.001$. In the MiaPaCa2 lysate, we were able to quantify 3433 proteins, and three kinases, CDK9, CDK2, and RPS6KA1, were identified as hits with a 1.5-fold change and a significance threshold of $P < 0.001$. Further evaluation of the proteomics data is essential to understanding the proteome-wide effects of PROTAC **2** fully.

Several studies have illustrated that the concurrent inactivation of Mcl-1 and Bcl-xL results in robust activation of apoptosis [67, 180, 181, 187]. Also, CDK9 has been recognized in the transcription and stabilization of Mcl-1 in pancreatic cancer, where it has been established as a potential therapeutic target. Furthermore, compound **3**, the precursor molecule to PROTAC **2**, reduced Mcl-1 expression. We tested three Bcl2 inhibitors in combination with PROTAC **2**. We used ABT-263 (Navitoclax), a Bcl2/Bcl-xL/Bcl-w inhibitor that underwent a phase II trial, ABT-199 (Venetoclax), an FDA-approved Bcl2 inhibitor. And WEHI-539, an experimental Bcl-xL inhibitor. We determine that when MiaPaCa2 cells were treated individually with ABT-263 (Bcl2/BclxL/Bcl-w), ABT-199 (Bcl2), WEHI-537 (Bcl-xL), PROTAC **2**, they showed minimal growth inhibitory effects at equimolar concentration. However, we determined that PROTAC **2** sensitizes pancreatic cancer cells to the Bcl2 selective FDA-approved inhibitor ABT-199, known as Venetoclax.

Future Directions

As discussed earlier, aminopyrazole inhibitors have generally been classified as CDK2/5 inhibitors, consistent with the cell-free analysis we received for PROTAC **2.** However, we never analyzed for inhibition of other CDK family members. We want to expand our studies to understand the inhibitory abilities of PROTAC **2**. This can be easily pursued by treating HEK293 cells with PROTAC **2** and probe for the downstream substrates of CDKs. For example, we can evaluate the inhibition of CDK2 by looking for

decrease phosphorylation of RB. We can determine the inhibition of CDK5 by probing for p-FAK, a known downstream substrate of CDK5. It is essential to understand what our PROTAC can degrade and inhibit since it binds through the ATP-binding pocket. Also, since the CDK family has been extensively studied for its regulation of all cell cycle phases, we would like to know if PROTAC **2** affects the cell cycle. CDK2 is essential for progression from the G1 and S phases of the cell cycle, and CDK5 controls the cell cycle through mitotic control and dysregulation of cell cycle inhibitors, p21CIP1 and p27 [4, 191]. Given that PROTAC **2** showed inhibition of CDK2 and CDK5, we would like to determine if PROTAC **2** can alter cell cycle progression.

Additionally, we able to show a loss in the protein abundance of CDK9 via proteomic-wide mass spectrometry analysis. From our studies, we identified a combined total of ~3700 proteins. Of which only a handful were members of the CDK family. We want to determine if the protein changes we identified in either sample (HEK293 or MiaPaCa2) can be attributed to the CDK9 degradation. CDK9 modulates protein expression through gene transcription or protein phosphorylation. We can determine the role of CDK9 on these changes utilizing two experiments. We need to perform RNA-sequencing analysis with PROTAC **2** and CDK9 shRNA knockdown to determine the global effects of CDK9-mediated transcription. The data obtained from this experiment should tell us what proteins are affected by CDK9 degradation at the gene transcription level are. Second, after we have determined which proteins are affected via `transcription, we can use various methods to determine if the remaining proteins are effect by a loss of CDK9-mediated phosphorylation. This can initially be done via western blot analysis of HEK293 PROTAC **2** treated cells.

Last, we demonstrated robust synergism between the FDA-approved Bcl2 inhibitor venetoclax and PROTAC **2** in pancreatic cancer cells. We, however, did not validate the

concurrent inhibition of Bcl2 and Mcl-1 in pancreatic cancer. We want to perform the synergism study again and subject the samples to western blot analysis. This will enable us to determine if the synergism we saw was caused by inhibition of the anti-apoptotic proteins Bcl2 and reduced expression of Mcl-1. Furthermore, due to the potent reduction of cell growth, we want to evaluate this combination in animal studies for pre-clinical development.

PROTAC 4

We initially saw differences in the potency of PROTAC **2** between HEK293 and MiaPaCa2 cells, determined via western blot. This led us to believe the PROTAC panel might have cellular-dependent potencies. The original degrader, compound **3**, was first discovered as a selective CDK9 degrader in HCT116 cells. Consequently, we wanted to test the new panel of aminopyrazole-based PROTACs in HCT116 (1 μM for 24 hours). This screen identified PROTAC **4** as a novel CDK12 degrader. PROTAC **4** did not degrade any other CDK family member, CDK2, CDK4, CDK5, CDK6, CDK9. We also observed no degradation in the non- CDK kinases, IKKβ, RB, ERK, and AKT. Surprisingly, no PROTAC was identified as a CDK9 degrader. However, we see a reduction in the higher molecular weight variant of CDK9, $CDK9_{55}$, when treated with PROTAC **7**. Further experimentation is necessary to validate this observation. Additionally, with the treatment of PROTAC **4**, we potentially see the degradation of Fak, which would require further cellular experimentation to validate.

We observed a reduction in PROTAC **2** mediated CDK9 degradation from the pancreatic cancer cell lines from the HEK293 cells. Therefore, we hypothesized, PROTAC **4** mediated degradation is cell-type dependent. We treated seven cell lines from five different cancer types with the ten-degrader panel. We used two colorectal cancer cell lines, SW620 and HCT116, and two pancreatic cancer cell lines, S2013 and Mia PaCa-2

(MP2). We used one ovarian cancer cell line (SKOV3), an Ewing Sarcoma cell line (A673), and an acute myeloid leukemia cell line (Jurkat). The only observed robust PROTAC **4** mediated degradation was in the colorectal cancer cell lines. Even among those cell lines, from the naked eye, there seemed to be a variable effect. Besides, there might also be some slight degradation of CDK12 in A673 cell lines in the presence of PROTAC **2**. In summary, we only saw potent CDK12 degradation in colorectal cancer cell lines when treated with PROTAC **4**.

PROTAC **4** selectively degraded CDK12 in a time and dose-dependent manner, resulting in a DC50 value of ~1.1 μM, where we observed CDK12 degradation with as low of a dose as 0.01 μM treatment with PROTAC **4**. PROTAC **4** mediated degradation of CDK12 was observed as early as 3 hours and was maintained through the 48-hour time point when treated at 1 μM in HCT116 cells. Again, we did not see the characteristic “hook-effect” even at 20 μM in this experiment.

Lastly, we verified the proteasome's role in the degradation of CDK12 through the use of MG132, a well-known 26S proteasome inhibitor. We used three concentrations of MG132 in combination with PROTAC **4** to show the dose-dependent inhibition of degradation. Interestingly, the ability of MG132 to inhibit degradation was greatly diminished if we compare it to our CDK9 experiment (**Figure 10C**). We think this finding can be explained in two ways: (1) these experiments were done at different times, which could have contributed to the difference of potency, or (2) PROTAC **4** has a much more potent binding affinity for CDK12 than PROTAC **2** does for CDK9. Furthermore, we used CDK13 to control the MG132 experiment because it shares a high amount of homology to CDK12. CDK12 and CDK13 share a broadly conserved kinase domain, which has been pharmacological inhibition of either kinase extremely difficult [192]. However, no degradation of CDK13 was observed in the PROTAC **4** treated cells. We demonstrated

one of the advantages of the PROTAC approach to targeting CDK, selective degradation profile even among high homolog family members.

CDK12 has been shown to regulate gene transcription of crucial DNA replication and repair proteins. Also, several different cancer types have shown CDK12 mutations result in its loss of function. This was found to lead to susceptibility to DNA damaging agents such as PARP inhibitors. As a result, we decided to tests PROTAC **4** in combination with an array of DNA damaging agents, including several PARP inhibitors. We used the PARP inhibitors olaparib, rucaparib, and veliparib. We also used the alkylating agent cisplatin, the antitumor antibiotic mitomycin-C, and the antimetabolite gemcitabine. Out of the six combinations, only gemcitabine in combination with PROTAC **4** proved to be synergistic. When we compare the growth rates of DMSO treated cells versus gemcitabine, and PROTAC **4** observe early-onset inhibition of cellular growth. However, at later time points, gemcitabine and PROTAC **4** treated cells seem to overcome the early growth inhibition because they end at similar proliferation rates. However, we see robust inhibition of growth in the combination-treated cells.

Further development of PROTAC **4** was abruptly stopped due to an unknown loss of activity. We initially reduced the percentage of FBS in our cell culture media because components within FBS can cause non-specific binding. We treated HCT116 cells with PROTAC **4** in the presence of 10% and 1% FBS, which we say, a return in the degradation profile in 1% FBS. However, this success was short-lived. The first experiment where we modulated FBS concentration was performed on May 6, 2019. By June 27th, reducing FBS concentration was unable to return PROTAC activity. We next explored the possibility of solvent saturation, where we dissolved PROTAC **4** in ethanol instead of DMSO. We treated HCT116 with increasing concentrations of PROTAC **4** in ethanol, which was also proved to be unsuccessful at returning the degradation profile. Next, we utilized in-house mass spectrometry to determine the current molecular weight of PROCTAC **4** to ensure it

remained stable. Mass spectrometry established PROTAC **4** had a molecular weight of 716.264, extremely close to the predicted molecular weight 715.764 of based on structure. Thus, proving the stability of PROTAC **4**.

Future Directions

First and foremost, we need to determine how and why the activity of PROTAC **4** changed. So far, we have demonstrated that this change was not due to structural changes within PROTAC **4**, not due to cross-reactivity to FBS in cell culture media, and not due to solvent saturation of DMSO. Based on these observations, it seems the loss is not due to any experimental condition. Instead, we believe this may be due to mutations within the HCT116 cell line. HCT116 are heavily genomic instable cell lines, predisposed to mutations. At any point throughout characterization, we could have switched sub strains of HCT116, one that contained a mutation within any part necessary for productive degradation. To determine if we are working with a sub-strain, we plan to send our HCT116 cell lines out for short-tandem repeat profiling to verify its molecular identity.

Furthermore, we plan to use immunoprecipitation assays to examine whether PROTAC **4** still binds to CDK12 or CRBN in HCT116 cells. Fusion affinity tags such as biotin have been established to modify compounds for further characterization by immunoprecipitation or pull down. We can add a biotin tag on PROTAC **4**. However, special attention must be made to the modification position. The binding affinity of p-PROTAC to POI and E3 ligase and the ternary complex's stability should not be affected [193]. The POI ligand of PROTAC **4** should bind within the active site of CDK12. If given at the correct dose, we should be able to immunoprecipitate biotin-tagged PROTAC **4** and probe for the presence of CDK12. Conversely, the E3 ligand should bind to CRBN, which we should determine using immunoprecipitation probing for CRBN.

Lastly, when we treated a panel of cell lines with PROTAC **4,** we saw differential degradation. We only saw productive CDK12 degradation in colorectal cancer cell lines. As we have discussed, degradation is mediated through the E3 ubiquitin-mediated polyubiquitination of the target protein. Cells also contain deubiquitinating enzymes called deubiquitinases or DUBs. These enzymes are responsible for removing ubiquitin chains from post-translationally modified proteins or trimming ubiquitin chains [194]. Based on the role in ubiquitin control, we believe the cell type-specific profile we observed is due to (1) a mutation in a particular DUB within colorectal cancer, thus allowing CDK12 to be polyubiquitinated or (2) CDK12 is found in complex with a DUB excluding colorectal cancer cells which is prohibiting the polyubiquitination of CDK12 (**Figure 20**) [195]. We plan to investigate each of these theories extensively if we can return the ability of PROTAC **4** to degrade CDK12.

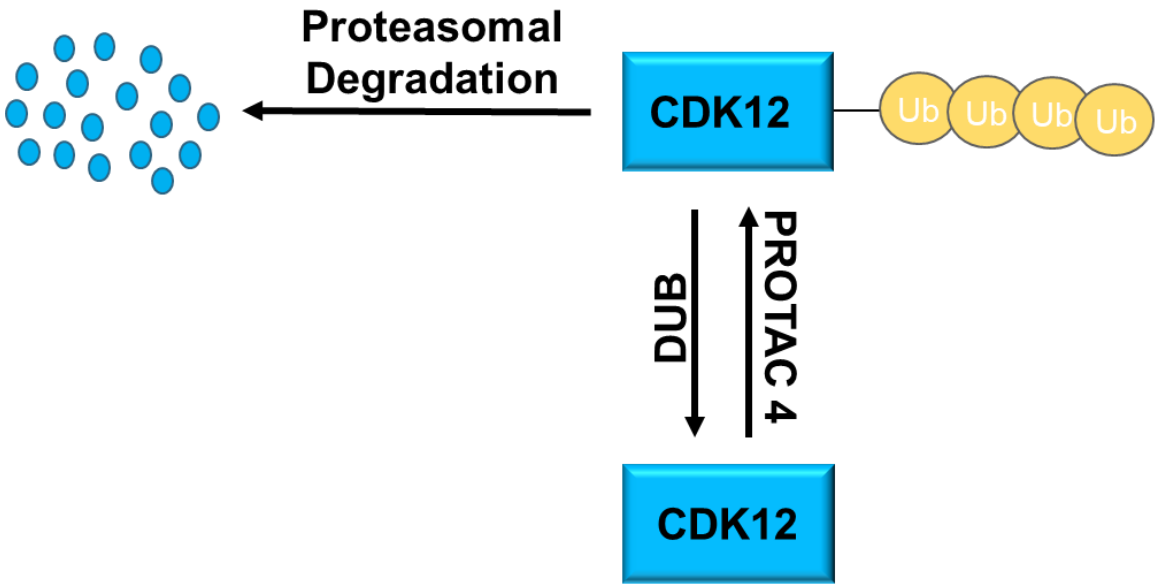

Figure 20. Model of proposed mechanism of cell-type specificity.

BIBLIOGRAPHY

1. Malumbres M, Barbacid M: **Mammalian cyclin-dependent kinases**. *Trends Biochem Sci* 2005, **30**(11):630-641.
2. Malumbres M, Harlow E, Hunt T, Hunter T, Lahti JM, Manning G, Morgan DO, Tsai LH, Wolgemuth DJ: **Cyclin-dependent kinases: a family portrait**. *Nat Cell Biol* 2009, **11**(11):1275-1276.
3. Ferguson FM, Doctor ZM, Ficarro SB, Marto JA, Kim ND, Sim T, Gray NS: **Synthesis and structure activity relationships of a series of 4-amino-1H-pyrazoles as covalent inhibitors of CDK14**. *Bioorg Med Chem Lett* 2019, **29**(15):1985-1993.
4. Malumbres M: **Cyclin-dependent kinases**. *Genome Biol* 2014, **15**(6):122.
5. Mikolcevic P, Rainer J, Geley S: **Orphan kinases turn eccentric: a new class of cyclin Y-activated, membrane-targeted CDKs**. *Cell Cycle* 2012, **11**(20):3758-3768.
6. Cox S, Radzio-Andzelm E, Taylor SS: **Domain movements in protein kinases**. *Curr Opin Struct Biol* 1994, **4**(6):893-901.
7. Li Y, Zhang J, Gao W, Zhang L, Pan Y, Zhang S, Wang Y: **Insights on Structural Characteristics and Ligand Binding Mechanisms of CDK2**. *Int J Mol Sci* 2015, **16**(5):9314-9340.
8. Jeffrey PD, Russo AA, Polyak K, Gibbs E, Hurwitz J, Massague J, Pavletich NP: **Mechanism of CDK activation revealed by the structure of a cyclinA-CDK2 complex**. *Nature* 1995, **376**(6538):313-320.
9. Wood DJ, Endicott JA: **Structural insights into the functional diversity of the CDK-cyclin family**. *Open Biol* 2018, **8**(9).

10. Yang J, Kornbluth S: **All aboard the cyclin train: subcellular trafficking of cyclins and their CDK partners**. *Trends Cell Biol* 1999, **9**(6):207-210.

11. Lolli G, Johnson LN: **CAK-Cyclin-dependent Activating Kinase: a key kinase in cell cycle control and a target for drugs?** *Cell Cycle* 2005, **4**(4):572-577.

12. Russo AA, Jeffrey PD, Pavletich NP: **Structural basis of cyclin-dependent kinase activation by phosphorylation**. *Nat Struct Biol* 1996, **3**(8):696-700.

13. Klein T, Vajpai N, Phillips JJ, Davies G, Holdgate GA, Phillips C, Tucker JA, Norman RA, Scott AD, Higazi DR *et al*: **Structural and dynamic insights into the energetics of activation loop rearrangement in FGFR1 kinase**. *Nat Commun* 2015, **6**:7877.

14. Treiber DK, Shah NP: **Ins and outs of kinase DFG motifs**. *Chem Biol* 2013, **20**(6):745-746.

15. Deshpande A, Sicinski P, Hinds PW: **Cyclins and cdks in development and cancer: a perspective**. *Oncogene* 2005, **24**(17):2909-2915.

16. Endicott JA, Noble ME, Tucker JA: **Cyclin-dependent kinases: inhibition and substrate recognition**. *Curr Opin Struct Biol* 1999, **9**(6):738-744.

17. Blazek D, Kohoutek J, Bartholomeeusen K, Johansen E, Hulinkova P, Luo Z, Cimermancic P, Ule J, Peterlin BM: **The Cyclin K/Cdk12 complex maintains genomic stability via regulation of expression of DNA damage response genes**. *Genes Dev* 2011, **25**(20):2158-2172.

18. Cassandri M, Fioravanti R, Pomella S, Valente S, Rotili D, Del Baldo G, De Angelis B, Rota R, Mai A: **CDK9 as a Valuable Target in Cancer: From Natural Compounds Inhibitors to Current Treatment in Pediatric Soft Tissue Sarcomas**. *Front Pharmacol* 2020, **11**:1230.

19. Hydbring P, Malumbres M, Sicinski P: **Non-canonical functions of cell cycle cyclins and cyclin-dependent kinases**. *Nat Rev Mol Cell Biol* 2016, **17**(5):280-292.

20. Asghar U, Witkiewicz AK, Turner NC, Knudsen ES: **The history and future of targeting cyclin-dependent kinases in cancer therapy**. *Nat Rev Drug Discov* 2015, **14**(2):130-146.

21. Sainsbury S, Bernecky C, Cramer P: **Structural basis of transcription initiation by RNA polymerase II**. *Nat Rev Mol Cell Biol* 2015, **16**(3):129-143.

22. Goodfellow SJ, Zomerdijk JC: **Basic mechanisms in RNA polymerase I transcription of the ribosomal RNA genes**. *Subcell Biochem* 2013, **61**:211-236.

23. Liu X, Bushnell DA, Kornberg RD: **RNA polymerase II transcription: structure and mechanism**. *Biochim Biophys Acta* 2013, **1829**(1):2-8.

24. Venkatesh S, Workman JL: **Histone exchange, chromatin structure and the regulation of transcription**. *Nat Rev Mol Cell Biol* 2015, **16**(3):178-189.

25. Greber BJ, Nogales E: **The Structures of Eukaryotic Transcription Pre-initiation Complexes and Their Functional Implications**. *Subcell Biochem* 2019, **93**:143-192.

26. Bushnell DA, Kornberg RD: **Complete, 12-subunit RNA polymerase II at 4.1-A resolution: implications for the initiation of transcription**. *Proc Natl Acad Sci U S A* 2003, **100**(12):6969-6973.

27. Rimel JK, Poss ZC, Erickson B, Maas ZL, Ebmeier CC, Johnson JL, Decker TM, Yaron TM, Bradley MJ, Hamman KB *et al*: **Selective inhibition of CDK7 reveals high-confidence targets and new models for TFIIH function in transcription**. *Genes Dev* 2020.

28. Allen BL, Taatjes DJ: **The Mediator complex: a central integrator of transcription**. *Nat Rev Mol Cell Biol* 2015, **16**(3):155-166.

29. Naar AM, Taatjes DJ, Zhai W, Nogales E, Tjian R: **Human CRSP interacts with RNA polymerase II CTD and adopts a specific CTD-bound conformation**. *Genes Dev* 2002, **16**(11):1339-1344.

30. Knuesel MT, Meyer KD, Bernecky C, Taatjes DJ: **The human CDK8 subcomplex is a molecular switch that controls Mediator coactivator function**. *Genes Dev* 2009, **23**(4):439-451.

31. Elmlund H, Baraznenok V, Lindahl M, Samuelsen CO, Koeck PJ, Holmberg S, Hebert H, Gustafsson CM: **The cyclin-dependent kinase 8 module sterically blocks Mediator interactions with RNA polymerase II**. *Proc Natl Acad Sci U S A* 2006, **103**(43):15788-15793.

32. Dahmus ME: **The role of multisite phosphorylation in the regulation of RNA polymerase II activity**. *Prog Nucleic Acid Res Mol Biol* 1994, **48**:143-179.

33. Akhtar MS, Heidemann M, Tietjen JR, Zhang DW, Chapman RD, Eick D, Ansari AZ: **TFIIH kinase places bivalent marks on the carboxy-terminal domain of RNA polymerase II**. *Mol Cell* 2009, **34**(3):387-393.

34. Dahmus ME: **Reversible phosphorylation of the C-terminal domain of RNA polymerase II**. *J Biol Chem* 1996, **271**(32):19009-19012.

35. Peng J, Marshall NF, Price DH: **Identification of a cyclin subunit required for the function of Drosophila P-TEFb**. *J Biol Chem* 1998, **273**(22):13855-13860.

36. Gilchrist DA, Dos Santos G, Fargo DC, Xie B, Gao Y, Li L, Adelman K: **Pausing of RNA polymerase II disrupts DNA-specified nucleosome organization to enable precise gene regulation**. *Cell* 2010, **143**(4):540-551.

37. Narita T, Yamaguchi Y, Yano K, Sugimoto S, Chanarat S, Wada T, Kim DK, Hasegawa J, Omori M, Inukai N *et al*: **Human transcription elongation factor**

NELF: identification of novel subunits and reconstitution of the functionally active complex. *Mol Cell Biol* 2003, **23**(6):1863-1873.

38. Wada T, Takagi T, Yamaguchi Y, Ferdous A, Imai T, Hirose S, Sugimoto S, Yano K, Hartzog GA, Winston F *et al*: **DSIF, a novel transcription elongation factor that regulates RNA polymerase II processivity, is composed of human Spt4 and Spt5 homologs**. *Genes Dev* 1998, **12**(3):343-356.
39. Vos SM, Farnung L, Urlaub H, Cramer P: **Structure of paused transcription complex Pol II-DSIF-NELF**. *Nature* 2018, **560**(7720):601-606.
40. Marshall NF, Price DH: **Purification of P-TEFb, a transcription factor required for the transition into productive elongation**. *J Biol Chem* 1995, **270**(21):12335-12338.
41. Mbonye U, Wang B, Gokulrangan G, Shi W, Yang S, Karn J: **Cyclin-dependent kinase 7 (CDK7)-mediated phosphorylation of the CDK9 activation loop promotes P-TEFb assembly with Tat and proviral HIV reactivation**. *J Biol Chem* 2018, **293**(26):10009-10025.
42. Bacon CW, D'Orso I: **CDK9: a signaling hub for transcriptional control**. *Transcription* 2019, **10**(2):57-75.
43. Sanso M, Fisher RP: **Pause, play, repeat: CDKs push RNAP II's buttons**. *Transcription* 2013, **4**(4):146-152.
44. Yamada T, Yamaguchi Y, Inukai N, Okamoto S, Mura T, Handa H: **P-TEFb-mediated phosphorylation of hSpt5 C-terminal repeats is critical for processive transcription elongation**. *Mol Cell* 2006, **21**(2):227-237.
45. Vos SM, Farnung L, Boehning M, Wigge C, Linden A, Urlaub H, Cramer P: **Structure of activated transcription complex Pol II-DSIF-PAF-SPT6**. *Nature* 2018, **560**(7720):607-612.

46. Gromak N, West S, Proudfoot NJ: **Pause sites promote transcriptional termination of mammalian RNA polymerase II**. *Mol Cell Biol* 2006, **26**(10):3986-3996.

47. Laitem C, Zaborowska J, Isa NF, Kufs J, Dienstbier M, Murphy S: **CDK9 inhibitors define elongation checkpoints at both ends of RNA polymerase II-transcribed genes**. *Nat Struct Mol Biol* 2015, **22**(5):396-403.

48. Fan Z, Devlin JR, Hogg SJ, Doyle MA, Harrison PF, Todorovski I, Cluse LA, Knight DA, Sandow JJ, Gregory G *et al*: **CDK13 cooperates with CDK12 to control global RNA polymerase II processivity**. *Sci Adv* 2020, **6**(18).

49. Kuehner JN, Pearson EL, Moore C: **Unravelling the means to an end: RNA polymerase II transcription termination**. *Nat Rev Mol Cell Biol* 2011, **12**(5):283-294.

50. Sanso M, Levin RS, Lipp JJ, Wang VY, Greifenberg AK, Quezada EM, Ali A, Ghosh A, Larochelle S, Rana TM *et al*: **P-TEFb regulation of transcription termination factor Xrn2 revealed by a chemical genetic screen for Cdk9 substrates**. *Genes Dev* 2016, **30**(1):117-131.

51. Grana X, De Luca A, Sang N, Fu Y, Claudio PP, Rosenblatt J, Morgan DO, Giordano A: **PITALRE, a nuclear CDC2-related protein kinase that phosphorylates the retinoblastoma protein in vitro**. *Proc Natl Acad Sci U S A* 1994, **91**(9):3834-3838.

52. Garriga J, Segura E, Mayol X, Grubmeyer C, Grana X: **Phosphorylation site specificity of the CDC2-related kinase PITALRE**. *Biochem J* 1996, **320 (Pt 3)**:983-989.

53. Garriga J, Mayol X, Grana X: **The CDC2-related kinase PITALRE is the catalytic subunit of active multimeric protein complexes**. *Biochem J* 1996, **319 (Pt 1)**:293-298.

54. Peng J, Zhu Y, Milton JT, Price DH: **Identification of multiple cyclin subunits of human P-TEFb**. *Genes Dev* 1998, **12**(5):755-762.

55. Romano G: **Deregulations in the cyclin-dependent kinase-9-related pathway in cancer: implications for drug discovery and development**. *ISRN Oncol* 2013, **2013**:305371.

56. Bullrich F, MacLachlan TK, Sang N, Druck T, Veronese ML, Allen SL, Chiorazzi N, Koff A, Heubner K, Croce CM *et al*: **Chromosomal mapping of members of the cdc2 family of protein kinases, cdk3, cdk6, PISSLRE, and PITALRE, and a cdk inhibitor, p27Kip1, to regions involved in human cancer**. *Cancer Res* 1995, **55**(6):1199-1205.

57. Shore SM, Byers SA, Maury W, Price DH: **Identification of a novel isoform of Cdk9**. *Gene* 2003, **307**:175-182.

58. Baumli S, Lolli G, Lowe ED, Troiani S, Rusconi L, Bullock AN, Debreczeni JE, Knapp S, Johnson LN: **The structure of P-TEFb (CDK9/cyclin T1), its complex with flavopiridol and regulation by phosphorylation**. *EMBO J* 2008, **27**(13):1907-1918.

59. Lin X, Taube R, Fujinaga K, Peterlin BM: **P-TEFb containing cyclin K and Cdk9 can activate transcription via RNA**. *J Biol Chem* 2002, **277**(19):16873-16878.

60. Yu DS, Zhao R, Hsu EL, Cayer J, Ye F, Guo Y, Shyr Y, Cortez D: **Cyclin-dependent kinase 9-cyclin K functions in the replication stress response**. *EMBO Rep* 2010, **11**(11):876-882.

61. Blake DR, Vaseva AV, Hodge RG, Kline MP, Gilbert TSK, Tyagi V, Huang D, Whiten GC, Larson JE, Wang X *et al*: **Application of a MYC degradation screen identifies sensitivity to CDK9 inhibitors in KRAS-mutant pancreatic cancer**. *Sci Signal* 2019, **12**(590).

62. Richters A, Doyle SK, Freeman DB, Lee C, Leifer BS, Jagannathan S, Kabinger F, Koren JV, Struntz NB, Urgiles J *et al*: **Modulating Androgen Receptor-Driven Transcription in Prostate Cancer with Selective CDK9 Inhibitors**. *Cell Chem Biol* 2021, **28**(2):134-147 e114.

63. Tibes R, Bogenberger JM: **Transcriptional Silencing of MCL-1 Through Cyclin-Dependent Kinase Inhibition in Acute Myeloid Leukemia**. *Front Oncol* 2019, **9**:1205.

64. Huang CH, Lujambio A, Zuber J, Tschaharganeh DF, Doran MG, Evans MJ, Kitzing T, Zhu N, de Stanchina E, Sawyers CL *et al*: **CDK9-mediated transcription elongation is required for MYC addiction in hepatocellular carcinoma**. *Genes Dev* 2014, **28**(16):1800-1814.

65. Gordon V, Bhadel S, Wunderlich W, Zhang J, Ficarro SB, Mollah SA, Shabanowitz J, Hunt DF, Xenarios I, Hahn WC *et al*: **CDK9 regulates AR promoter selectivity and cell growth through serine 81 phosphorylation**. *Mol Endocrinol* 2010, **24**(12):2267-2280.

66. Fujita K, Nonomura N: **Role of Androgen Receptor in Prostate Cancer: A Review**. *World J Mens Health* 2019, **37**(3):288-295.

67. Glaser SP, Lee EF, Trounson E, Bouillet P, Wei A, Fairlie WD, Izon DJ, Zuber J, Rappaport AR, Herold MJ *et al*: **Anti-apoptotic Mcl-1 is essential for the development and sustained growth of acute myeloid leukemia**. *Genes Dev* 2012, **26**(2):120-125.

68. Wei G, Margolin AA, Haery L, Brown E, Cucolo L, Julian B, Shehata S, Kung AL, Beroukhim R, Golub TR: **Chemical genomics identifies small-molecule MCL1 repressors and BCL-xL as a predictor of MCL1 dependency**. *Cancer Cell* 2012, **21**(4):547-562.

69. Ko TK, Kelly E, Pines J: **CrkRS: a novel conserved Cdc2-related protein kinase that colocalises with SC35 speckles**. *J Cell Sci* 2001, **114**(Pt 14):2591-2603.

70. Chen HH, Wang YC, Fann MJ: **Identification and characterization of the CDK12/cyclin L1 complex involved in alternative splicing regulation**. *Mol Cell Biol* 2006, **26**(7):2736-2745.

71. Bartkowiak B, Liu P, Phatnani HP, Fuda NJ, Cooper JJ, Price DH, Adelman K, Lis JT, Greenleaf AL: **CDK12 is a transcription elongation-associated CTD kinase, the metazoan ortholog of yeast Ctk1**. *Genes Dev* 2010, **24**(20):2303-2316.

72. Bosken CA, Farnung L, Hintermair C, Merzel Schachter M, Vogel-Bachmayr K, Blazek D, Anand K, Fisher RP, Eick D, Geyer M: **The structure and substrate specificity of human Cdk12/Cyclin K**. *Nat Commun* 2014, **5**:3505.

73. Dixon-Clarke SE, Elkins JM, Cheng SW, Morin GB, Bullock AN: **Structures of the CDK12/CycK complex with AMP-PNP reveal a flexible C-terminal kinase extension important for ATP binding**. *Sci Rep* 2015, **5**:17122.

74. Liang S, Hu L, Wu Z, Chen Z, Liu S, Xu X, Qian A: **CDK12: A Potent Target and Biomarker for Human Cancer Therapy**. *Cells* 2020, **9**(6).

75. Tellier M, Zaborowska J, Caizzi L, Mohammad E, Velychko T, Schwalb B, Ferrer-Vicens I, Blears D, Nojima T, Cramer P *et al*: **CDK12 globally stimulates RNA polymerase II transcription elongation and carboxyl-terminal domain phosphorylation**. *Nucleic Acids Res* 2020, **48**(14):7712-7727.

76. Davidson L, Muniz L, West S: **3' end formation of pre-mRNA and phosphorylation of Ser2 on the RNA polymerase II CTD are reciprocally coupled in human cells**. *Genes Dev* 2014, **28**(4):342-356.

77. Eifler TT, Shao W, Bartholomeeusen K, Fujinaga K, Jager S, Johnson JR, Luo Z, Krogan NJ, Peterlin BM: **Cyclin-dependent kinase 12 increases 3' end processing of growth factor-induced c-FOS transcripts**. *Mol Cell Biol* 2015, **35**(2):468-478.

78. Galganski L, Urbanek MO, Krzyzosiak WJ: **Nuclear speckles: molecular organization, biological function and role in disease**. *Nucleic Acids Res* 2017, **45**(18):10350-10368.

79. Tien JF, Mazloomian A, Cheng SG, Hughes CS, Chow CCT, Canapi LT, Oloumi A, Trigo-Gonzalez G, Bashashati A, Xu J *et al*: **CDK12 regulates alternative last exon mRNA splicing and promotes breast cancer cell invasion**. *Nucleic Acids Res* 2017, **45**(11):6698-6716.

80. Johnson SF, Cruz C, Greifenberg AK, Dust S, Stover DG, Chi D, Primack B, Cao S, Bernhardy AJ, Coulson R *et al*: **CDK12 Inhibition Reverses De Novo and Acquired PARP Inhibitor Resistance in BRCA Wild-Type and Mutated Models of Triple-Negative Breast Cancer**. *Cell Rep* 2016, **17**(9):2367-2381.

81. Cancer Genome Atlas Research N: **Integrated genomic analyses of ovarian carcinoma**. *Nature* 2011, **474**(7353):609-615.

82. Paculova H, Kohoutek J: **The emerging roles of CDK12 in tumorigenesis**. *Cell Div* 2017, **12**:7.

83. Robinson D, Van Allen EM, Wu YM, Schultz N, Lonigro RJ, Mosquera JM, Montgomery B, Taplin ME, Pritchard CC, Attard G *et al*: **Integrative clinical genomics of advanced prostate cancer**. *Cell* 2015, **161**(5):1215-1228.

84. Ji J, Zhou C, Wu J, Cai Q, Shi M, Zhang H, Yu Y, Zhu Z, Zhang J: **Expression pattern of CDK12 protein in gastric cancer and its positive correlation with CD8(+) cell density and CCL12 expression**. *Int J Med Sci* 2019, **16**(8):1142-1148.

85. Ekumi KM, Paculova H, Lenasi T, Pospichalova V, Bosken CA, Rybarikova J, Bryja V, Geyer M, Blazek D, Barboric M: **Ovarian carcinoma CDK12 mutations misregulate expression of DNA repair genes via deficient formation and function of the Cdk12/CycK complex**. *Nucleic Acids Res* 2015, **43**(5):2575-2589.

86. Joshi PM, Sutor SL, Huntoon CJ, Karnitz LM: **Ovarian cancer-associated mutations disable catalytic activity of CDK12, a kinase that promotes homologous recombination repair and resistance to cisplatin and poly(ADP-ribose) polymerase inhibitors**. *J Biol Chem* 2014, **289**(13):9247-9253.

87. Cancer Genome Atlas N: **Comprehensive molecular portraits of human breast tumours**. *Nature* 2012, **490**(7418):61-70.

88. Iorns E, Martens-de Kemp SR, Lord CJ, Ashworth A: **CRK7 modifies the MAPK pathway and influences the response to endocrine therapy**. *Carcinogenesis* 2009, **30**(10):1696-1701.

89. Sircoulomb F, Bekhouche I, Finetti P, Adelaide J, Ben Hamida A, Bonansea J, Raynaud S, Innocenti C, Charafe-Jauffret E, Tarpin C *et al*: **Genome profiling of ERBB2-amplified breast cancers**. *BMC Cancer* 2010, **10**:539.

90. Capra M, Nuciforo PG, Confalonieri S, Quarto M, Bianchi M, Nebuloni M, Boldorini R, Pallotti F, Viale G, Gishizky ML *et al*: **Frequent alterations in the expression of serine/threonine kinases in human cancers**. *Cancer Res* 2006, **66**(16):8147-8154.

91. Natrajan R, Wilkerson PM, Marchio C, Piscuoglio S, Ng CK, Wai P, Lambros MB, Samartzis EP, Dedes KJ, Frankum J *et al*: **Characterization of the genomic features and expressed fusion genes in micropapillary carcinomas of the breast**. *J Pathol* 2014, **232**(5):553-565.

92. Wu YM, Cieslik M, Lonigro RJ, Vats P, Reimers MA, Cao X, Ning Y, Wang L, Kunju LP, de Sarkar N *et al*: **Inactivation of CDK12 Delineates a Distinct Immunogenic Class of Advanced Prostate Cancer**. *Cell* 2018, **173**(7):1770-1782 e1714.

93. Zhou C, Feng X, Yuan F, Ji J, Shi M, Yu Y, Zhu Z, Zhang J: **Difference of molecular alterations in HER2-positive and HER2-negative gastric cancers by whole-genome sequencing analysis**. *Cancer Manag Res* 2018, **10**:3945-3954.

94. Cermelli S, Jang IS, Bernard B, Grandori C: **Synthetic lethal screens as a means to understand and treat MYC-driven cancers**. *Cold Spring Harb Perspect Med* 2014, **4**(3).

95. Toyoshima M, Howie HL, Imakura M, Walsh RM, Annis JE, Chang AN, Frazier J, Chau BN, Loboda A, Linsley PS *et al*: **Functional genomics identifies therapeutic targets for MYC-driven cancer**. *Proc Natl Acad Sci U S A* 2012, **109**(24):9545-9550.

96. Schaub FX, Dhankani V, Berger AC, Trivedi M, Richardson AB, Shaw R, Zhao W, Zhang X, Ventura A, Liu Y *et al*: **Pan-cancer Alterations of the MYC Oncogene and Its Proximal Network across the Cancer Genome Atlas**. *Cell Syst* 2018, **6**(3):282-300 e282.

97. Dominguez-Sola D, Ying CY, Grandori C, Ruggiero L, Chen B, Li M, Galloway DA, Gu W, Gautier J, Dalla-Favera R: **Non-transcriptional control of DNA replication by c-Myc**. *Nature* 2007, **448**(7152):445-451.

98. May WA, Lessnick SL, Braun BS, Klemsz M, Lewis BC, Lunsford LB, Hromas R, Denny CT: **The Ewing's sarcoma EWS/FLI-1 fusion gene encodes a more potent transcriptional activator and is a more powerful transforming gene than FLI-1**. *Mol Cell Biol* 1993, **13**(12):7393-7398.

99. Chahrour O, Cairns D, Omran Z: **Small molecule kinase inhibitors as anti-cancer therapeutics**. *Mini Rev Med Chem* 2012, **12**(5):399-411.

100. Malumbres M, Barbacid M: **Cell cycle, CDKs and cancer: a changing paradigm**. *Nat Rev Cancer* 2009, **9**(3):153-166.

101. Hardcastle IR, Golding BT, Griffin RJ: **Designing inhibitors of cyclin-dependent kinases**. *Annu Rev Pharmacol Toxicol* 2002, **42**:325-348.

102. Zhang J, Yang PL, Gray NS: **Targeting cancer with small molecule kinase inhibitors**. *Nat Rev Cancer* 2009, **9**(1):28-39.

103. Wells CI, Vasta JD, Corona CR, Wilkinson J, Zimprich CA, Ingold MR, Pickett JE, Drewry DH, Pugh KM, Schwinn MK *et al*: **Quantifying CDK inhibitor selectivity in live cells**. *Nat Commun* 2020, **11**(1):2743.

104. Sutanto F, Konstantinidou M, Domling A: **Covalent inhibitors: a rational approach to drug discovery**. *RSC Med Chem* 2020, **11**(8):876-884.

105. Wu P, Nielsen TE, Clausen MH: **FDA-approved small-molecule kinase inhibitors**. *Trends Pharmacol Sci* 2015, **36**(7):422-439.

106. Bhullar KS, Lagaron NO, McGowan EM, Parmar I, Jha A, Hubbard BP, Rupasinghe HPV: **Kinase-targeted cancer therapies: progress, challenges and future directions**. *Mol Cancer* 2018, **17**(1):48.

107. Sedlacek H, Czech J, Naik R, Kaur G, Worland P, Losiewicz M, Parker B, Carlson B, Smith A, Senderowicz A *et al*: **Flavopiridol (L86 8275; NSC 649890), a new kinase inhibitor for tumor therapy**. *Int J Oncol* 1996, **9**(6):1143-1168.

108. Le Tourneau C, Faivre S, Laurence V, Delbaldo C, Vera K, Girre V, Chiao J, Armour S, Frame S, Green SR *et al*: **Phase I evaluation of seliciclib (R-roscovitine), a novel oral cyclin-dependent kinase inhibitor, in patients with advanced malignancies**. *Eur J Cancer* 2010, **46**(18):3243-3250.

109. Meijer L, Kim SH: **Chemical inhibitors of cyclin-dependent kinases**. *Methods Enzymol* 1997, **283**:113-128.

110. Planchais S, Glab N, Inze D, Bergounioux C: **Chemical inhibitors: a tool for plant cell cycle studies**. *FEBS Lett* 2000, **476**(1-2):78-83.

111. Pevarello P, Brasca MG, Amici R, Orsini P, Traquandi G, Corti L, Piutti C, Sansonna P, Villa M, Pierce BS *et al*: **3-Aminopyrazole inhibitors of CDK2/cyclin A as antitumor agents. 1. Lead finding**. *J Med Chem* 2004, **47**(13):3367-3380.

112. Sobhani N, D'Angelo A, Pittacolo M, Roviello G, Miccoli A, Corona SP, Bernocchi O, Generali D, Otto T: **Updates on the CDK4/6 Inhibitory Strategy and Combinations in Breast Cancer**. *Cells* 2019, **8**(4).

113. Finn RS, Crown JP, Lang I, Boer K, Bondarenko IM, Kulyk SO, Ettl J, Patel R, Pinter T, Schmidt M *et al*: **The cyclin-dependent kinase 4/6 inhibitor palbociclib in combination with letrozole versus letrozole alone as first-line treatment of oestrogen receptor-positive, HER2-negative, advanced breast cancer (PALOMA-1/TRIO-18): a randomised phase 2 study**. *Lancet Oncol* 2015, **16**(1):25-35.

114. Hortobagyi GN, Stemmer SM, Burris HA, Yap YS, Sonke GS, Paluch-Shimon S, Campone M, Blackwell KL, Andre F, Winer EP *et al*: **Ribociclib as First-Line Therapy for HR-Positive, Advanced Breast Cancer**. *N Engl J Med* 2016, **375**(18):1738-1748.

115. Roskoski R, Jr.: **Properties of FDA-approved small molecule protein kinase inhibitors**. *Pharmacol Res* 2019, **144**:19-50.

116. Goel S, DeCristo MJ, McAllister SS, Zhao JJ: **CDK4/6 Inhibition in Cancer: Beyond Cell Cycle Arrest**. *Trends Cell Biol* 2018, **28**(11):911-925.

117. Strelow JM: **A Perspective on the Kinetics of Covalent and Irreversible Inhibition**. *SLAS Discov* 2017, **22**(1):3-20.

118. Fitzpatrick FA: **Cyclooxygenase enzymes: regulation and function**. *Curr Pharm Des* 2004, **10**(6):577-588.

119. Kwiatkowski N, Zhang T, Rahl PB, Abraham BJ, Reddy J, Ficarro SB, Dastur A, Amzallag A, Ramaswamy S, Tesar B *et al*: **Targeting transcription regulation in cancer with a covalent CDK7 inhibitor**. *Nature* 2014, **511**(7511):616-620.

120. Hu S, Marineau JJ, Rajagopal N, Hamman KB, Choi YJ, Schmidt DR, Ke N, Johannessen L, Bradley MJ, Orlando DA *et al*: **Discovery and Characterization of SY-1365, a Selective, Covalent Inhibitor of CDK7**. *Cancer Res* 2019, **79**(13):3479-3491.

121. Zhang T, Kwiatkowski N, Olson CM, Dixon-Clarke SE, Abraham BJ, Greifenberg AK, Ficarro SB, Elkins JM, Liang Y, Hannett NM *et al*: **Covalent targeting of remote cysteine residues to develop CDK12 and CDK13 inhibitors**. *Nat Chem Biol* 2016, **12**(10):876-884.

122. Toure M, Crews CM: **Small-Molecule PROTACS: New Approaches to Protein Degradation**. *Angew Chem Int Ed Engl* 2016, **55**(6):1966-1973.

123. Kana O, Brylinski M: **Elucidating the druggability of the human proteome with eFindSite**. *J Comput Aided Mol Des* 2019, **33**(5):509-519.

124. Bett JS: **Proteostasis regulation by the ubiquitin system**. *Essays Biochem* 2016, **60**(2):143-151.

125. Nandi D, Tahiliani P, Kumar A, Chandu D: **The ubiquitin-proteasome system**. *J Biosci* 2006, **31**(1):137-155.

126. Sakamoto KM, Kim KB, Kumagai A, Mercurio F, Crews CM, Deshaies RJ: **Protacs: chimeric molecules that target proteins to the Skp1-Cullin-F box**

complex for ubiquitination and degradation. *Proc Natl Acad Sci U S A* 2001, **98**(15):8554-8559.

127. Lee H, Puppala D, Choi EY, Swanson H, Kim KB: **Targeted degradation of the aryl hydrocarbon receptor by the PROTAC approach: a useful chemical genetic tool**. *Chembiochem* 2007, **8**(17):2058-2062.

128. Schneekloth AR, Pucheault M, Tae HS, Crews CM: **Targeted intracellular protein degradation induced by a small molecule: En route to chemical proteomics**. *Bioorg Med Chem Lett* 2008, **18**(22):5904-5908.

129. Itoh Y, Ishikawa M, Naito M, Hashimoto Y: **Protein knockdown using methyl bestatin-ligand hybrid molecules: design and synthesis of inducers of ubiquitination-mediated degradation of cellular retinoic acid-binding proteins**. *J Am Chem Soc* 2010, **132**(16):5820-5826.

130. Ito T, Ando H, Suzuki T, Ogura T, Hotta K, Imamura Y, Yamaguchi Y, Handa H: **Identification of a primary target of thalidomide teratogenicity**. *Science* 2010, **327**(5971):1345-1350.

131. Lu J, Qian Y, Altieri M, Dong H, Wang J, Raina K, Hines J, Winkler JD, Crew AP, Coleman K *et al*: **Hijacking the E3 Ubiquitin Ligase Cereblon to Efficiently Target BRD4**. *Chem Biol* 2015, **22**(6):755-763.

132. Buckley DL, Van Molle I, Gareiss PC, Tae HS, Michel J, Noblin DJ, Jorgensen WL, Ciulli A, Crews CM: **Targeting the von Hippel-Lindau E3 ubiquitin ligase using small molecules to disrupt the VHL/HIF-1alpha interaction**. *J Am Chem Soc* 2012, **134**(10):4465-4468.

133. Bondeson DP, Mares A, Smith IE, Ko E, Campos S, Miah AH, Mulholland KE, Routly N, Buckley DL, Gustafson JL *et al*: **Catalytic in vivo protein knockdown by small-molecule PROTACs**. *Nat Chem Biol* 2015, **11**(8):611-617.

134. Han T, Goralski M, Gaskill N, Capota E, Kim J, Ting TC, Xie Y, Williams NS, Nijhawan D: **Anticancer sulfonamides target splicing by inducing RBM39 degradation via recruitment to DCAF15**. *Science* 2017, **356**(6336).

135. Zoppi V, Hughes SJ, Maniaci C, Testa A, Gmaschitz T, Wieshofer C, Koegl M, Riching KM, Daniels DL, Spallarossa A *et al*: **Iterative Design and Optimization of Initially Inactive Proteolysis Targeting Chimeras (PROTACs) Identify VZ185 as a Potent, Fast, and Selective von Hippel-Lindau (VHL) Based Dual Degrader Probe of BRD9 and BRD7**. *J Med Chem* 2019, **62**(2):699-726.

136. Li L, Mi D, Pei H, Duan Q, Wang X, Zhou W, Jin J, Li D, Liu M, Chen Y: **In vivo target protein degradation induced by PROTACs based on E3 ligase DCAF15**. *Signal Transduct Target Ther* 2020, **5**(1):129.

137. Sun X, Gao H, Yang Y, He M, Wu Y, Song Y, Tong Y, Rao Y: **PROTACs: great opportunities for academia and industry**. *Signal Transduct Target Ther* 2019, **4**:64.

138. Shimokawa K, Shibata N, Sameshima T, Miyamoto N, Ujikawa O, Nara H, Ohoka N, Hattori T, Cho N, Naito M: **Targeting the Allosteric Site of Oncoprotein BCR-ABL as an Alternative Strategy for Effective Target Protein Degradation**. *ACS Med Chem Lett* 2017, **8**(10):1042-1047.

139. Powell CE, Gao Y, Tan L, Donovan KA, Nowak RP, Loehr A, Bahcall M, Fischer ES, Janne PA, George RE *et al*: **Chemically Induced Degradation of Anaplastic Lymphoma Kinase (ALK)**. *J Med Chem* 2018, **61**(9):4249-4255.

140. Wang Z, He N, Guo Z, Niu C, Song T, Guo Y, Cao K, Wang A, Zhu J, Zhang X *et al*: **Proteolysis Targeting Chimeras for the Selective Degradation of Mcl-1/Bcl-2 Derived from Nonselective Target Binding Ligands**. *J Med Chem* 2019, **62**(17):8152-8163.

141. McCoull W, Cheung T, Anderson E, Barton P, Burgess J, Byth K, Cao Q, Castaldi MP, Chen H, Chiarparin E *et al*: **Development of a Novel B-Cell Lymphoma 6 (BCL6) PROTAC To Provide Insight into Small Molecule Targeting of BCL6**. *ACS Chem Biol* 2018, **13**(11):3131-3141.

142. Lai AC, Toure M, Hellerschmied D, Salami J, Jaime-Figueroa S, Ko E, Hines J, Crews CM: **Modular PROTAC Design for the Degradation of Oncogenic BCR-ABL**. *Angew Chem Int Ed Engl* 2016, **55**(2):807-810.

143. Winter GE, Buckley DL, Paulk J, Roberts JM, Souza A, Dhe-Paganon S, Bradner JE: **DRUG DEVELOPMENT. Phthalimide conjugation as a strategy for in vivo target protein degradation**. *Science* 2015, **348**(6241):1376-1381.

144. Remillard D, Buckley DL, Paulk J, Brien GL, Sonnett M, Seo HS, Dastjerdi S, Wuhr M, Dhe-Paganon S, Armstrong SA *et al*: **Degradation of the BAF Complex Factor BRD9 by Heterobifunctional Ligands**. *Angew Chem Int Ed Engl* 2017, **56**(21):5738-5743.

145. Sun Y, Zhao X, Ding N, Gao H, Wu Y, Yang Y, Zhao M, Hwang J, Song Y, Liu W *et al*: **PROTAC-induced BTK degradation as a novel therapy for mutated BTK C481S induced ibrutinib-resistant B-cell malignancies**. *Cell Res* 2018, **28**(7):779-781.

146. Jiang B, Wang ES, Donovan KA, Liang Y, Fischer ES, Zhang T, Gray NS: **Development of Dual and Selective Degraders of Cyclin-Dependent Kinases 4 and 6**. *Angew Chem Int Ed Engl* 2019, **58**(19):6321-6326.

147. Rana S, Bendjennat M, Kour S, King HM, Kizhake S, Zahid M, Natarajan A: **Selective degradation of CDK6 by a palbociclib based PROTAC**. *Bioorg Med Chem Lett* 2019, **29**(11):1375-1379.

148. Hatcher JM, Wang ES, Johannessen L, Kwiatkowski N, Sim T, Gray NS: **Development of Highly Potent and Selective Steroidal Inhibitors and Degraders of CDK8**. *ACS Med Chem Lett* 2018, **9**(6):540-545.

149. Robb CM, Contreras JI, Kour S, Taylor MA, Abid M, Sonawane YA, Zahid M, Murry DJ, Natarajan A, Rana S: **Chemically induced degradation of CDK9 by a proteolysis targeting chimera (PROTAC)**. *Chem Commun (Camb)* 2017, **53**(54):7577-7580.

150. Huang HT, Dobrovolsky D, Paulk J, Yang G, Weisberg EL, Doctor ZM, Buckley DL, Cho JH, Ko E, Jang J *et al*: **A Chemoproteomic Approach to Query the Degradable Kinome Using a Multi-kinase Degrader**. *Cell Chem Biol* 2018, **25**(1):88-99 e86.

151. Papatzimas JW, Gorobets E, Maity R, Muniyat MI, MacCallum JL, Neri P, Bahlis NJ, Derksen DJ: **From Inhibition to Degradation: Targeting the Antiapoptotic Protein Myeloid Cell Leukemia 1 (MCL1)**. *J Med Chem* 2019, **62**(11):5522-5540.

152. Li W, Gao C, Zhao L, Yuan Z, Chen Y, Jiang Y: **Phthalimide conjugations for the degradation of oncogenic PI3K**. *Eur J Med Chem* 2018, **151**:237-247.

153. Bai L, Zhou H, Xu R, Zhao Y, Chinnaswamy K, McEachern D, Chen J, Yang CY, Liu Z, Wang M *et al*: **A Potent and Selective Small-Molecule Degrader of STAT3 Achieves Complete Tumor Regression In Vivo**. *Cancer Cell* 2019, **36**(5):498-511 e417.

154. Zhao Q, Lan T, Su S, Rao Y: **Induction of apoptosis in MDA-MB-231 breast cancer cells by a PARP1-targeting PROTAC small molecule**. *Chem Commun (Camb)* 2019, **55**(3):369-372.

155. Salami J, Alabi S, Willard RR, Vitale NJ, Wang J, Dong H, Jin M, McDonnell DP, Crew AP, Neklesa TK *et al*: **Androgen receptor degradation by the**

proteolysis-targeting chimera ARCC-4 outperforms enzalutamide in cellular models of prostate cancer drug resistance. *Commun Biol* 2018, **1**:100.

156. Raina K, Lu J, Qian Y, Altieri M, Gordon D, Rossi AM, Wang J, Chen X, Dong H, Siu K *et al*: **PROTAC-induced BET protein degradation as a therapy for castration-resistant prostate cancer**. *Proc Natl Acad Sci U S A* 2016, **113**(26):7124-7129.

157. Madak JT, Cuthbertson CR, Chen W, Showalter HD, Neamati N: **Design, Synthesis, and Characterization of Brequinar Conjugates as Probes to Study DHODH Inhibition**. *Chemistry* 2017, **23**(56):13875-13878.

158. Hu J, Hu B, Wang M, Xu F, Miao B, Yang CY, Wang M, Liu Z, Hayes DF, Chinnaswamy K *et al*: **Discovery of ERD-308 as a Highly Potent Proteolysis Targeting Chimera (PROTAC) Degrader of Estrogen Receptor (ER)**. *J Med Chem* 2019, **62**(3):1420-1442.

159. Cromm PM, Samarasinghe KTG, Hines J, Crews CM: **Addressing Kinase-Independent Functions of Fak via PROTAC-Mediated Degradation**. *J Am Chem Soc* 2018, **140**(49):17019-17026.

160. Potjewyd F, Turner AW, Beri J, Rectenwald JM, Norris-Drouin JL, Cholensky SH, Margolis DM, Pearce KH, Herring LE, James LI: **Degradation of Polycomb Repressive Complex 2 with an EED-Targeted Bivalent Chemical Degrader**. *Cell Chem Biol* 2020, **27**(1):47-56 e15.

161. Tovell H, Testa A, Zhou H, Shpiro N, Crafter C, Ciulli A, Alessi DR: **Design and Characterization of SGK3-PROTAC1, an Isoform Specific SGK3 Kinase PROTAC Degrader**. *ACS Chem Biol* 2019, **14**(9):2024-2034.

162. Wang X, Feng S, Fan J, Li X, Wen Q, Luo N: **New strategy for renal fibrosis: Targeting Smad3 proteins for ubiquitination and degradation**. *Biochem Pharmacol* 2016, **116**:200-209.

163. Crew AP, Raina K, Dong H, Qian Y, Wang J, Vigil D, Serebrenik YV, Hamman BD, Morgan A, Ferraro C *et al*: **Identification and Characterization of Von Hippel-Lindau-Recruiting Proteolysis Targeting Chimeras (PROTACs) of TANK-Binding Kinase 1**. *J Med Chem* 2018, **61**(2):583-598.

164. Gechijian LN, Buckley DL, Lawlor MA, Reyes JM, Paulk J, Ott CJ, Winter GE, Erb MA, Scott TG, Xu M *et al*: **Functional TRIM24 degrader via conjugation of ineffectual bromodomain and VHL ligands**. *Nat Chem Biol* 2018, **14**(4):405-412.

165. Olson CM, Jiang B, Erb MA, Liang Y, Doctor ZM, Zhang Z, Zhang T, Kwiatkowski N, Boukhali M, Green JL *et al*: **Pharmacological perturbation of CDK9 using selective CDK9 inhibition or degradation**. *Nat Chem Biol* 2018, **14**(2):163-170.

166. Neklesa T SL, Willard RR, Vitale N, Pizzano J, Gordon DA, Bookbinder M, Macaluso J, Dong H, Ferraro C, Wang G, Wang J, Crews CM, Houston J, Crew AP, Taylor I **ARV-110: An oral androgen receptor PROTAC degrader for prostate cancer.** In: *ASCO-GU: 2019; San Fransisco, California, USA*.

167. JJ Flanagan YQ, SM Gough, M Andreoli, M Bookbinder, G Cadelina, J Bradley, E Rousseau, R Willard, J Pizzano, CM Crews, AP Crew, I Taylor and J Houston: **ARV-471, an oral estrogen receptor PROTAC degrader for breast cancer**. In: *2018 San Antonio Breast Cancer Symposium 2018*.

168. Yang J, Li Y, Aguilar A, Liu Z, Yang CY, Wang S: **Simple Structural Modifications Converting a Bona fide MDM2 PROTAC Degrader into a Molecular Glue Molecule: A Cautionary Tale in the Design of PROTAC Degraders**. *J Med Chem* 2019, **62**(21):9471-9487.

169. Brümmer OH, T. Z.; Chen, D.-W.; Janda, K. D.,: **Antibody-catalyzed hydrolysis of oligomeric esters: a model for the degradation of polymeric materials.** . *Chemical Communications* 2001, **1**:19-20.

170. Zhang X, Du X, Huang X, Lv Z: **Creating protein-imprinted self-assembled monolayers with multiple binding sites and biocompatible imprinted cavities**. *J Am Chem Soc* 2013, **135**(25):9248-9251.

171. Yang F, Shen Y, Camp DG, 2nd, Smith RD: **High-pH reversed-phase chromatography with fraction concatenation for 2D proteomic analysis**. *Expert Rev Proteomics* 2012, **9**(2):129-134.

172. Rana S, Sonawane YA, Taylor MA, Kizhake S, Zahid M, Natarajan A: **Synthesis of aminopyrazole analogs and their evaluation as CDK inhibitors for cancer therapy**. *Bioorg Med Chem Lett* 2018, **28**(23-24):3736-3740.

173. Bian J, Ren J, Li Y, Wang J, Xu X, Feng Y, Tang H, Wang Y, Li Z: **Discovery of Wogonin-based PROTACs against CDK9 and capable of achieving antitumor activity**. *Bioorg Chem* 2018, **81**:373-381.

174. Donoghue C, Cubillos-Rojas M, Gutierrez-Prat N, Sanchez-Zarzalejo C, Verdaguer X, Riera A, Nebreda AR: **Optimal linker length for small molecule PROTACs that selectively target p38alpha and p38beta for degradation**. *Eur J Med Chem* 2020, **201**:112451.

175. Han YH, Moon HJ, You BR, Park WH: **The effect of MG132, a proteasome inhibitor on HeLa cells in relation to cell growth, reactive oxygen species and GSH**. *Oncol Rep* 2009, **22**(1):215-221.

176. Klaeger S, Heinzlmeir S, Wilhelm M, Polzer H, Vick B, Koenig PA, Reinecke M, Ruprecht B, Petzoldt S, Meng C *et al*: **The target landscape of clinical kinase drugs**. *Science* 2017, **358**(6367).

177. Robb CM, Kour S, Contreras JI, Agarwal E, Barger CJ, Rana S, Sonawane Y, Neilsen BK, Taylor M, Kizhake S *et al*: **Characterization of CDK(5) inhibitor, 20-223 (aka CP668863) for colorectal cancer therapy**. *Oncotarget* 2018, **9**(4):5216-5232.

178. Lopez H, Zhang L, George NM, Liu X, Pang X, Evans JJD, Targy NM, Luo X: **Perturbation of the Bcl-2 network and an induced Noxa/Bcl-xL interaction trigger mitochondrial dysfunction after DNA damage**. *J Biol Chem* 2010, **285**(20):15016-15026.

179. Rajule R, Bryant VC, Lopez H, Luo X, Natarajan A: **Perturbing pro-survival proteins using quinoxaline derivatives: a structure-activity relationship study**. *Bioorg Med Chem* 2012, **20**(7):2227-2234.

180. Contreras JI, Robb CM, King HM, Baxter J, Crawford AJ, Kour S, Kizhake S, Sonawane YA, Rana S, Hollingsworth MA *et al*: **Chemical Genetic Screens Identify Kinase Inhibitor Combinations that Target Anti-Apoptotic Proteins for Cancer Therapy**. *ACS Chem Biol* 2018, **13**(5):1148-1152.

181. Kour S, Rana S, Contreras JI, King HM, Robb CM, Sonawane YA, Bendjennat M, Crawford AJ, Barger CJ, Kizhake S *et al*: **CDK5 Inhibitor Downregulates Mcl-1 and Sensitizes Pancreatic Cancer Cell Lines to Navitoclax**. *Mol Pharmacol* 2019, **96**(4):419-429.

182. Rana S, Kour S, Sonawane YA, Robb CM, Contreras JI, Kizhake S, Zahid M, Karpf AR, Natarajan A: **Symbiotic prodrugs (SymProDs) dual targeting of NFkappaB and CDK**. *Chem Biol Drug Des* 2020, **96**(2):773-784.

183. O'Neill KL, Huang K, Zhang J, Chen Y, Luo X: **Inactivation of prosurvival Bcl-2 proteins activates Bax/Bak through the outer mitochondrial membrane**. *Genes Dev* 2016, **30**(8):973-988.

184. Takahashi H, Chen MC, Pham H, Matsuo Y, Ishiguro H, Reber HA, Takeyama H, Hines OJ, Eibl G: **Simultaneous knock-down of Bcl-xL and Mcl-1 induces apoptosis through Bax activation in pancreatic cancer cells**. *Biochim Biophys Acta* 2013, **1833**(12):2980-2987.

185. Konopleva M, Contractor R, Tsao T, Samudio I, Ruvolo PP, Kitada S, Deng X, Zhai D, Shi YX, Sneed T *et al*: **Mechanisms of apoptosis sensitivity and resistance to the BH3 mimetic ABT-737 in acute myeloid leukemia**. *Cancer Cell* 2006, **10**(5):375-388.

186. Abid M, Sonawane YA, Contreras JI, Rana S, Natarajan A: **Recent Advances in Cancer Drug Development: Targeting Induced Myeloid Cell Leukemia-1 (Mcl-1) Differentiation Protein**. *Curr Med Chem* 2017, **24**(40):4488-4514.

187. Peddaboina C, Jupiter D, Fletcher S, Yap JL, Rai A, Tobin RP, Jiang W, Rascoe P, Rogers MK, Smythe WR *et al*: **The downregulation of Mcl-1 via USP9X inhibition sensitizes solid tumors to Bcl-xl inhibition**. *BMC Cancer* 2012, **12**:541.

188. Teuscher KB, Zhang M, Ji H: **A Versatile Method to Determine the Cellular Bioavailability of Small-Molecule Inhibitors**. *J Med Chem* 2017, **60**(1):157-169.

189. Andreasen PA, Egelund R, Jensen S, Rodenburg KW: **Solvent effects on activity and conformation of plasminogen activator inhibitor-1**. *Thromb Haemost* 1999, **81**(3):407-414.

190. Moreau K, Coen M, Zhang AX, Pachl F, Castaldi MP, Dahl G, Boyd H, Scott C, Newham P: **Proteolysis-targeting chimeras in drug development: A safety perspective**. *Br J Pharmacol* 2020, **177**(8):1709-1718.

191. Huang PH, Chen MC, Peng YT, Kao WH, Chang CH, Wang YC, Lai CH, Hsieh JT, Wang JH, Lee YT *et al*: **Cdk5 Directly Targets Nuclear p21ClP1 and Promotes Cancer Cell Growth**. *Cancer Res* 2016, **76**(23):6888-6900.

192. Krajewska M, Dries R, Grassetti AV, Dust S, Gao Y, Huang H, Sharma B, Day DS, Kwiatkowski N, Pomaville M *et al*: **CDK12 loss in cancer cells affects DNA**

damage response genes through premature cleavage and polyadenylation. *Nat Commun* 2019, **10**(1):1757.

193. Jin J, Wu Y, Chen J, Shen Y, Zhang L, Zhang H, Chen L, Yuan H, Chen H, Zhang W *et al*: **The peptide PROTAC modality: a novel strategy for targeted protein ubiquitination**. *Theranostics* 2020, **10**(22):10141-10153.

194. Komander D, Clague MJ, Urbe S: **Breaking the chains: structure and function of the deubiquitinases**. *Nat Rev Mol Cell Biol* 2009, **10**(8):550-563.

195. Moon S, Lee BH: **Chemically Induced Cellular Proteolysis: An Emerging Therapeutic Strategy for Undruggable Targets**. *Mol Cells* 2018, **41**(11):933-942.

APPENDIX: CHAPTER 2 RAW DATA

FIGURE 6 & 7

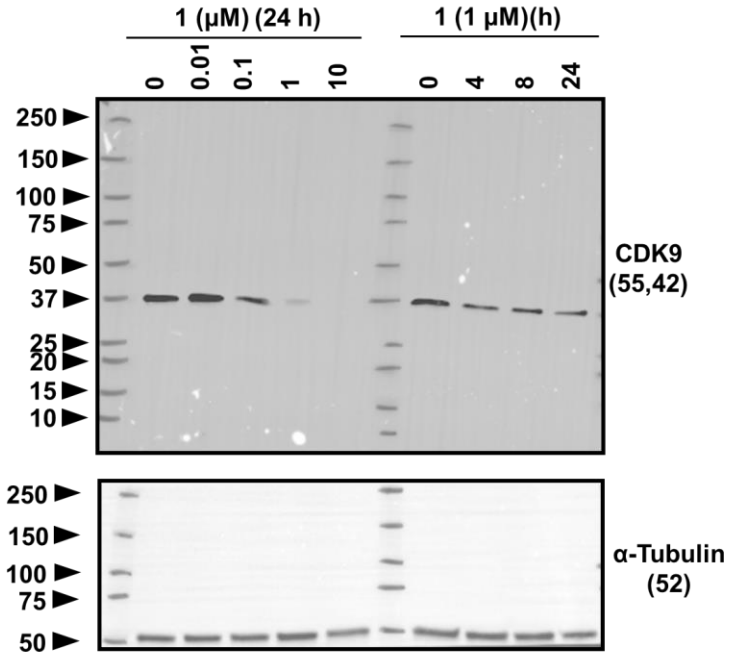

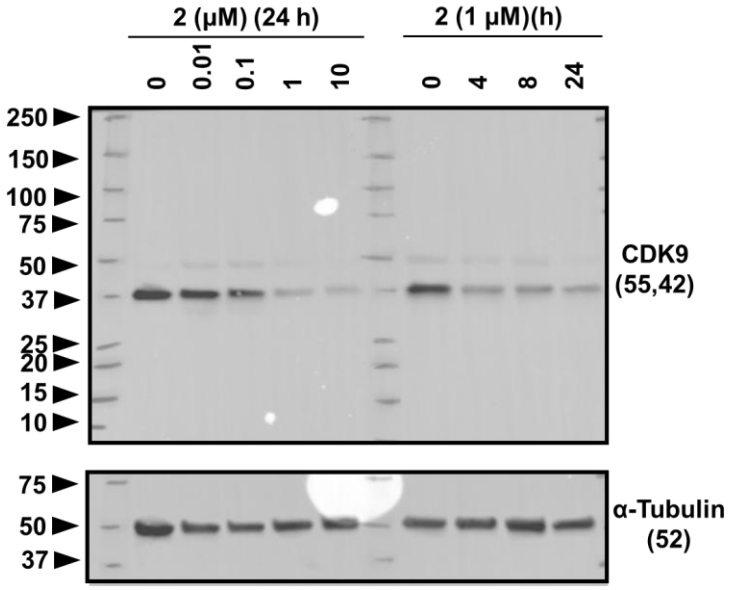

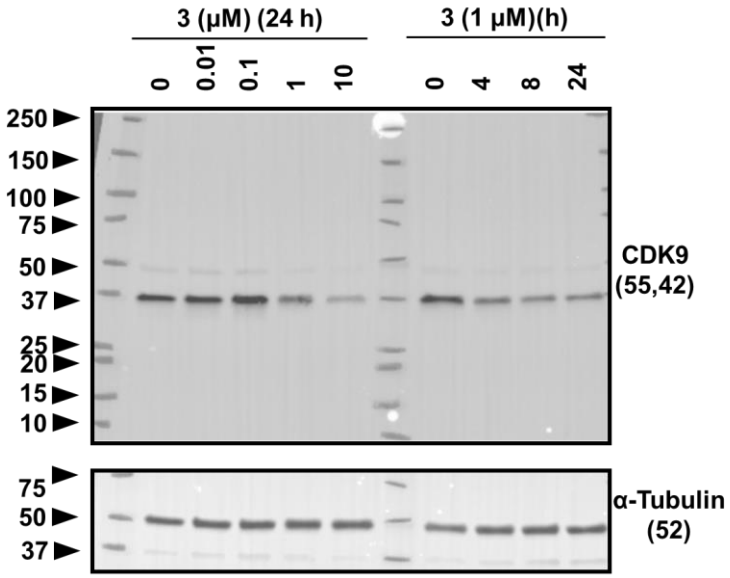
3 (μM) (24 h)
3 (1 μM)(h)
0
0.01
0.1
1
10
0
4
8
24
250
150
100
75
50
37
25
20
15
10
CDK9
(55,42)
75
50
37
α-Tubulin
(52)

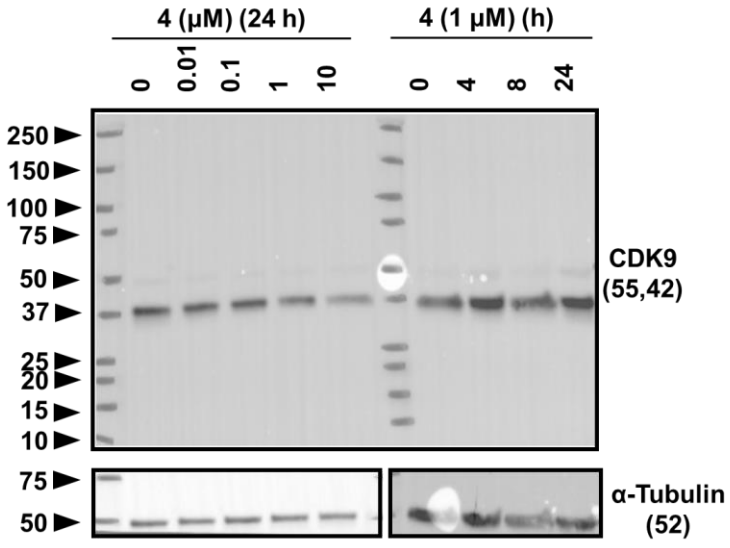
4 (μM) (24 h)
4 (1 μM) (h)
0
0.01
0.1
1
10
0
4
8
24
250
150
100
75
50
37
25
20
15
10
CDK9
(55,42)
75
50
α-Tubulin
(52)

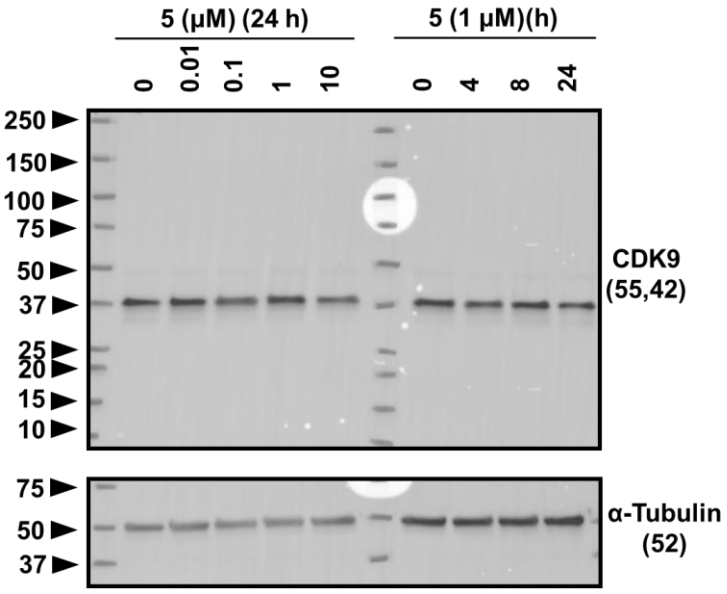
5 (μM) (24 h)
5 (1 μM)(h)
0
0.01
0.1
1
10
0
4
8
24
250
150
100
75
50
37
25
20
15
10
CDK9
(55,42)
75
50
37
α-Tubulin
(52)

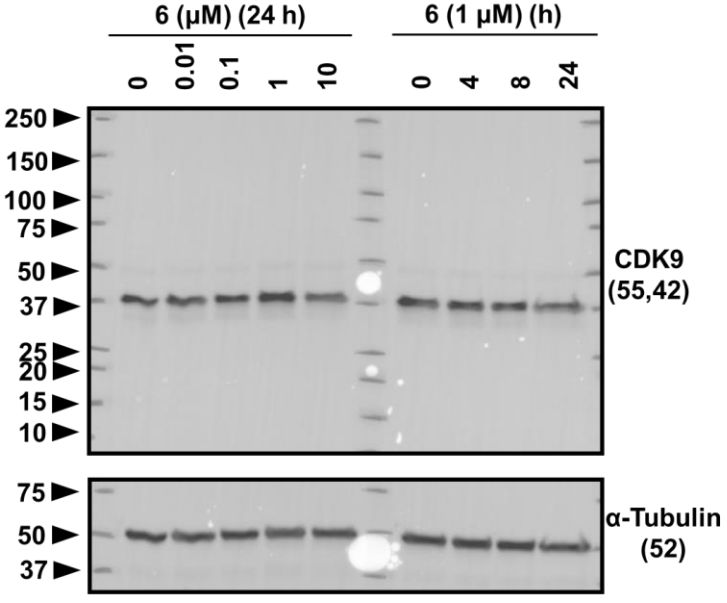
6 (μM) (24 h)
6 (1 μM) (h)
0
0.01
0.1
1
10
0
4
8
24
250
150
100
75
50
37
25
20
15
10
CDK9
(55,42)
75
50
37
α-Tubulin
(52)

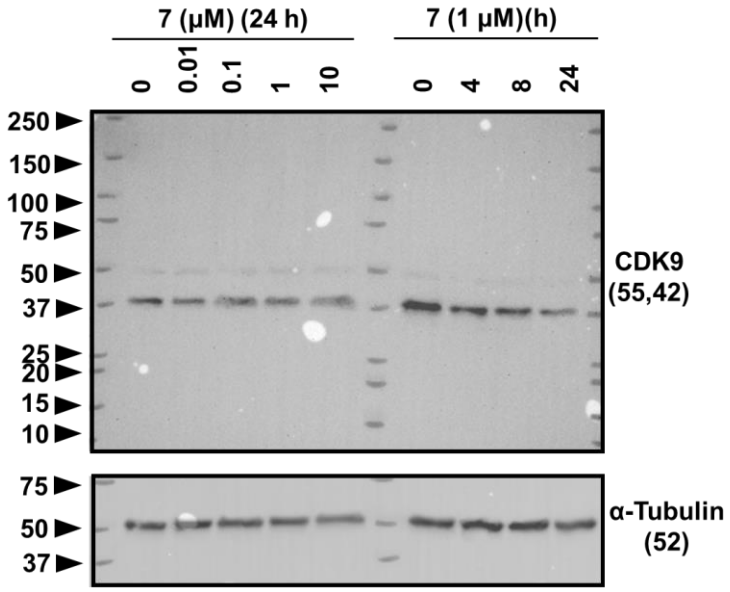
7 (μM) (24 h)
7 (1 μM)(h)
0
0.01
0.1
1
10
0
4
8
24
250
150
100
75
50
37
25
20
15
10
CDK9
(55,42)
75
50
37
α-Tubulin
(52)

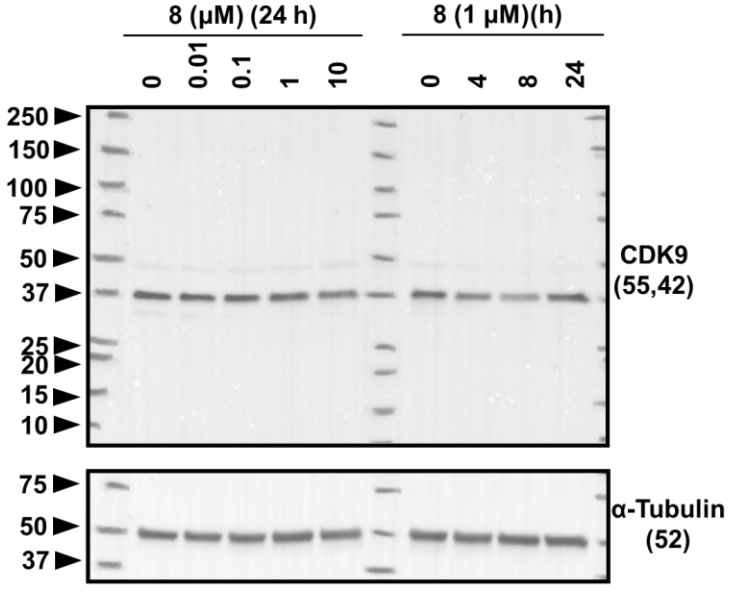
8 (μM) (24 h)
8 (1 μM)(h)
0
0.01
0.1
1
10
0
4
8
24
250
150
100
75
50
37
25
20
15
10
CDK9
(55,42)
75
50
37
α-Tubulin
(52)

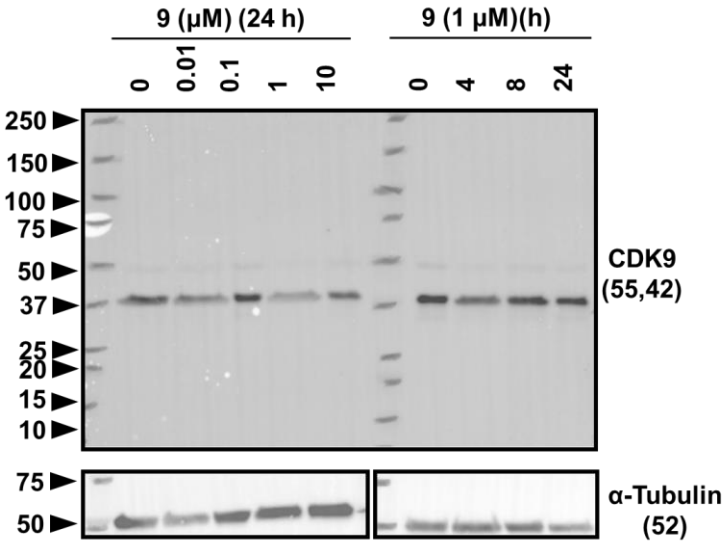
9 (μM) (24 h)
9 (1 μM)(h)
0
0.01
0.1
1
10
0
4
8
24
250
150
100
75
50
37
25
20
15
10
CDK9
(55,42)
75
50
α-Tubulin
(52)

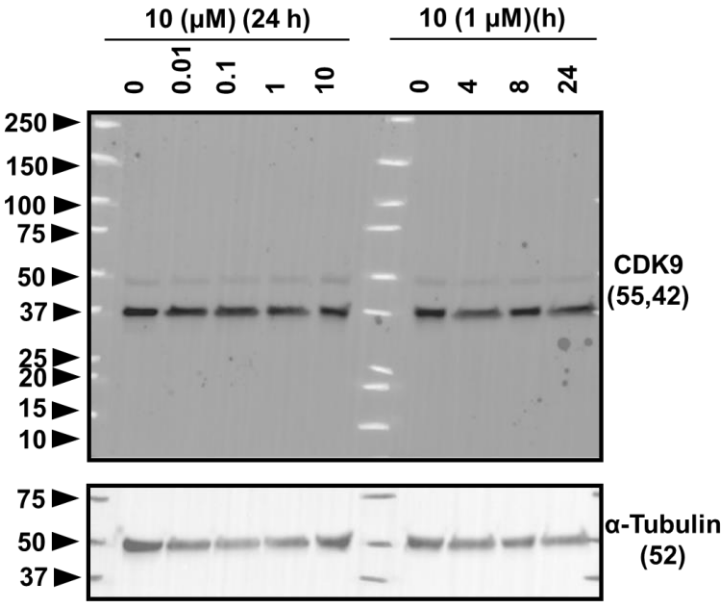
10 (μM) (24 h)
10 (1 μM)(h)
0
0.01
0.1
1
10
0
4
8
24
250
150
100
75
50
37
25
20
15
10
CDK9
(55,42)
75
50
37
α-Tubulin
(52)

FIGURE 9

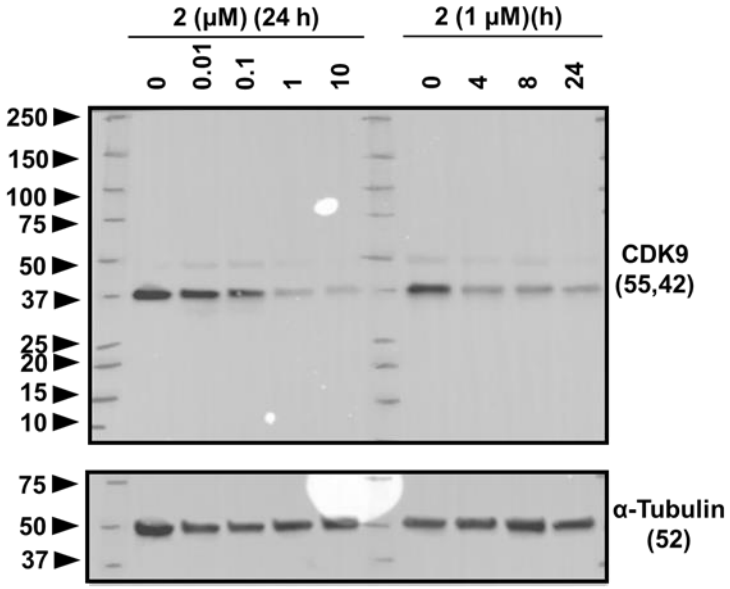
2 (μM) (24 h)
2 (1 μM)(h)
0
0.01
0.1
1
10
0
4
8
24
250
150
100
75
50
37
25
20
15
10
CDK9
(55,42)
75
50
37
α-Tubulin
(52)

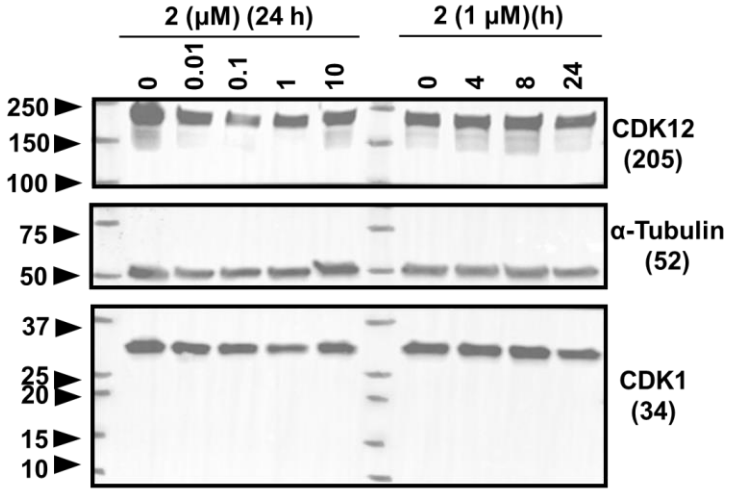
2 (μM) (24 h)
2 (1 μM)(h)
0
0.01
0.1
1
10
0
4
8
24
250
150
100
CDK12
(205)
75
50
α-Tubulin
(52)
37
25
20
15
10
CDK1
(34)

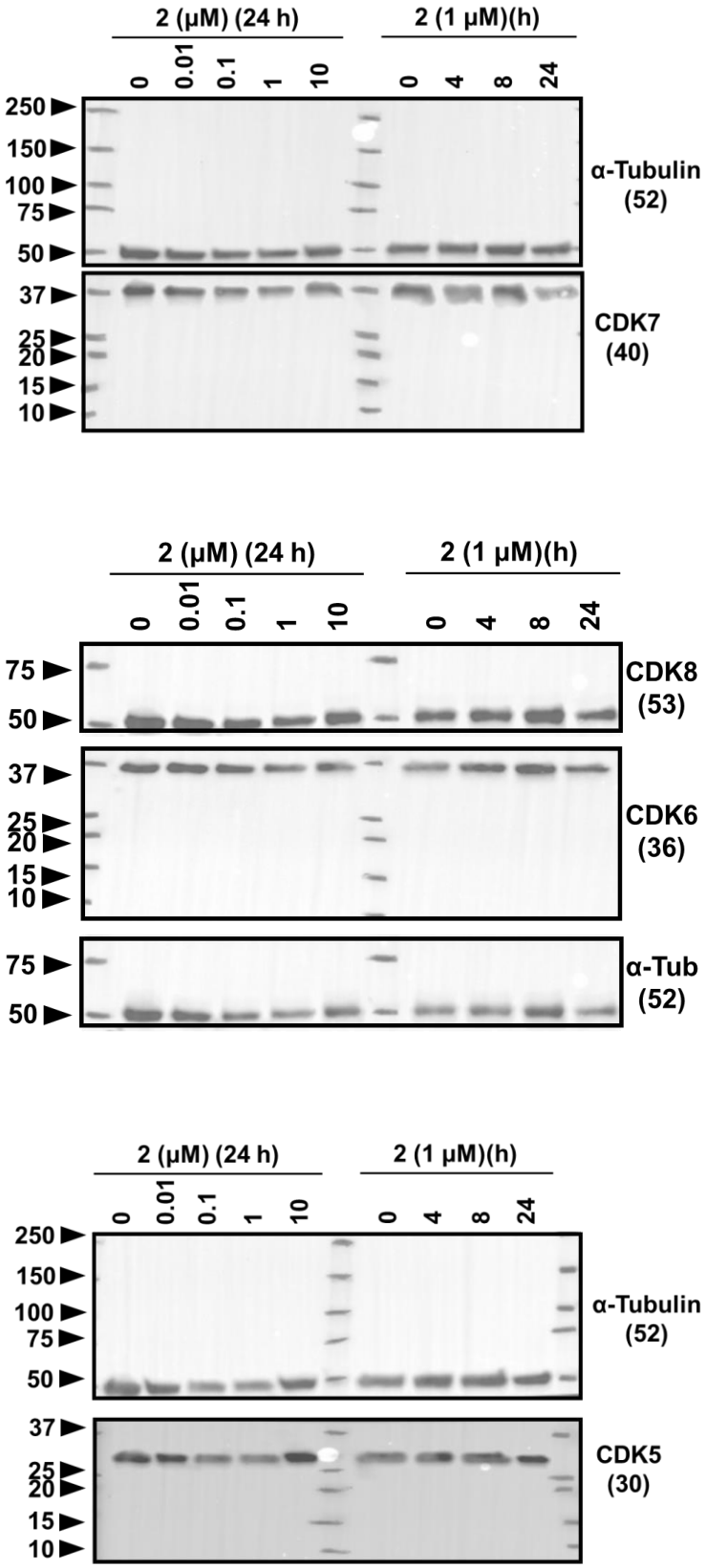
2 (μM) (24 h)
2 (1 μM)(h)
0
0.01
0.1
1
10
0
4
8
24
250
150
100
75
50
37
25
20
15
10
α-Tubulin
(52)
CDK7
(40)
CDK8
(53)
CDK6
(36)
α-Tub
(52)
CDK5
(30)

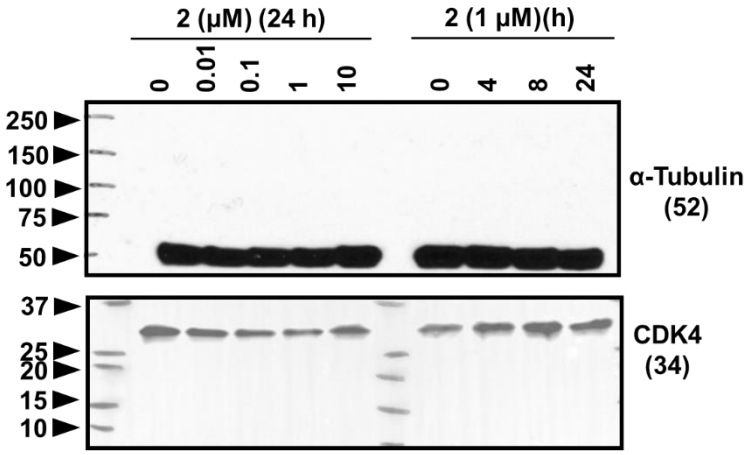
2 (μM) (24 h)
2 (1 μM)(h)
0
0.01
0.1
1
10
0
4
8
24
250
150
100
75
50
α-Tubulin
(52)
37
25
20
15
10
CDK4
(34)

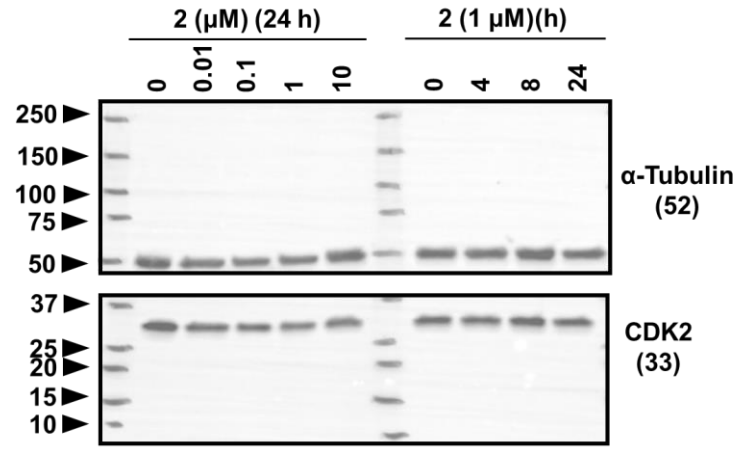
2 (μM) (24 h)
2 (1 μM)(h)
0
0.01
0.1
1
10
0
4
8
24
250
150
100
75
50
α-Tubulin
(52)
37
25
20
15
10
CDK2
(33)

FIGURE 10A & 10B

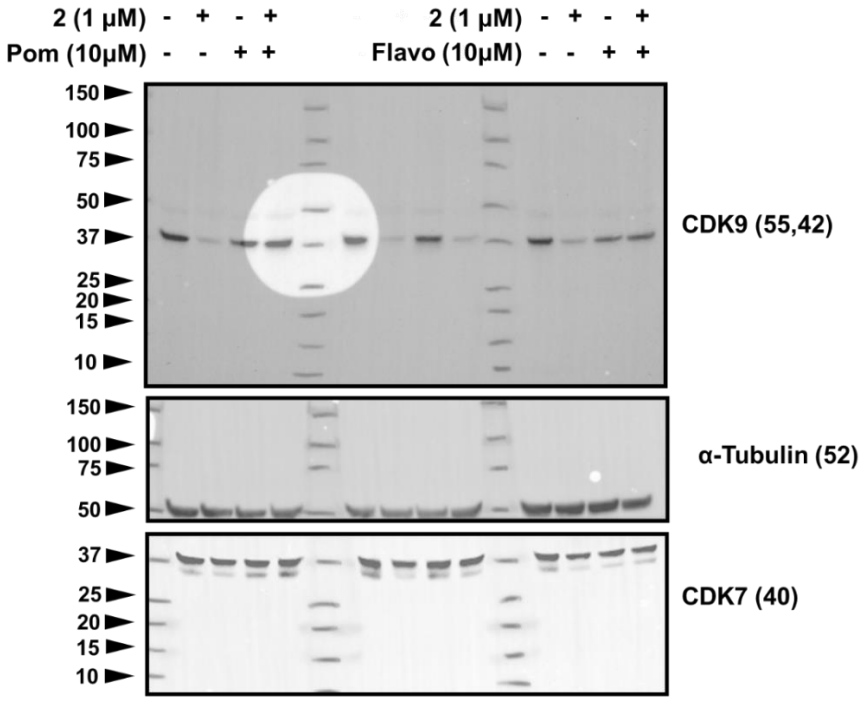

FIGURE 10C

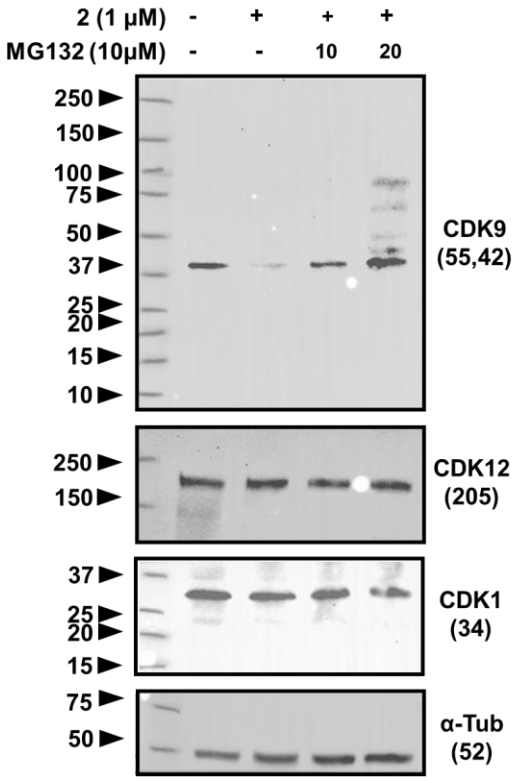

FIGURE 10D

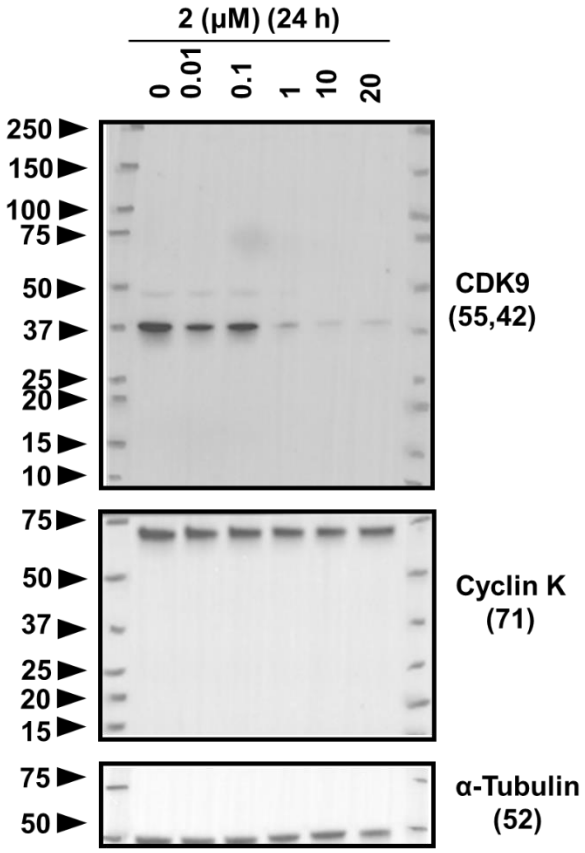

FIGURE 11A

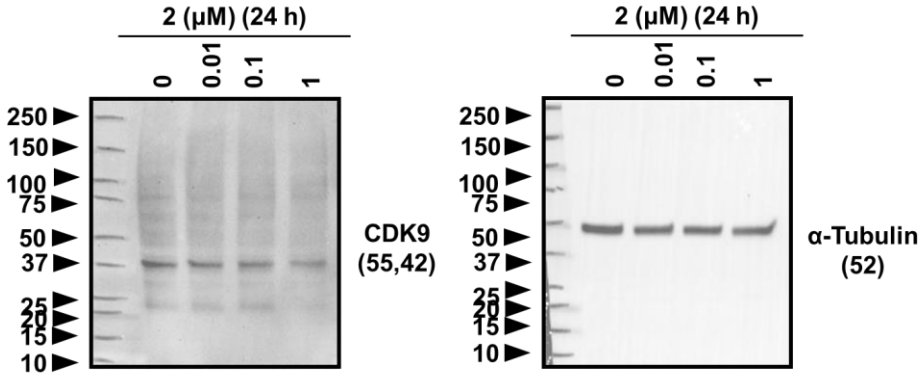

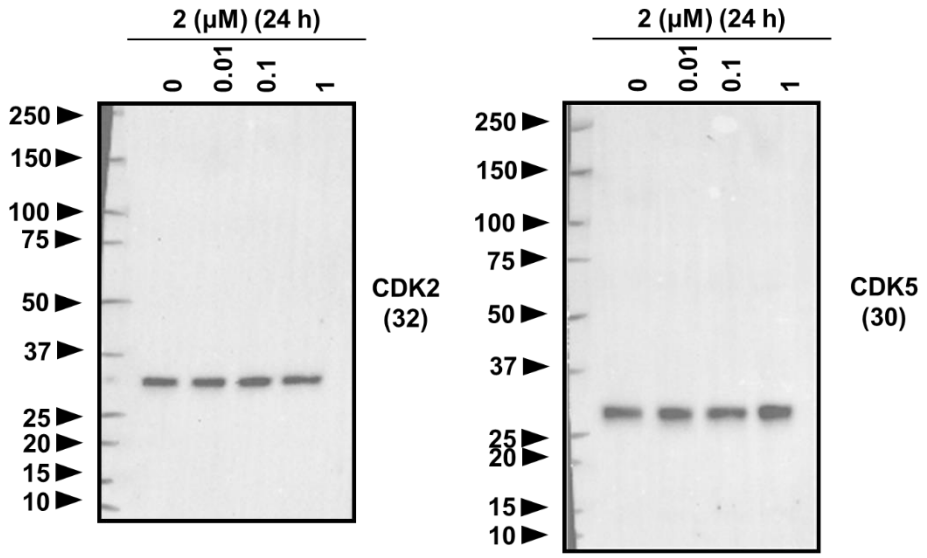

FIGURE 11B & 11C

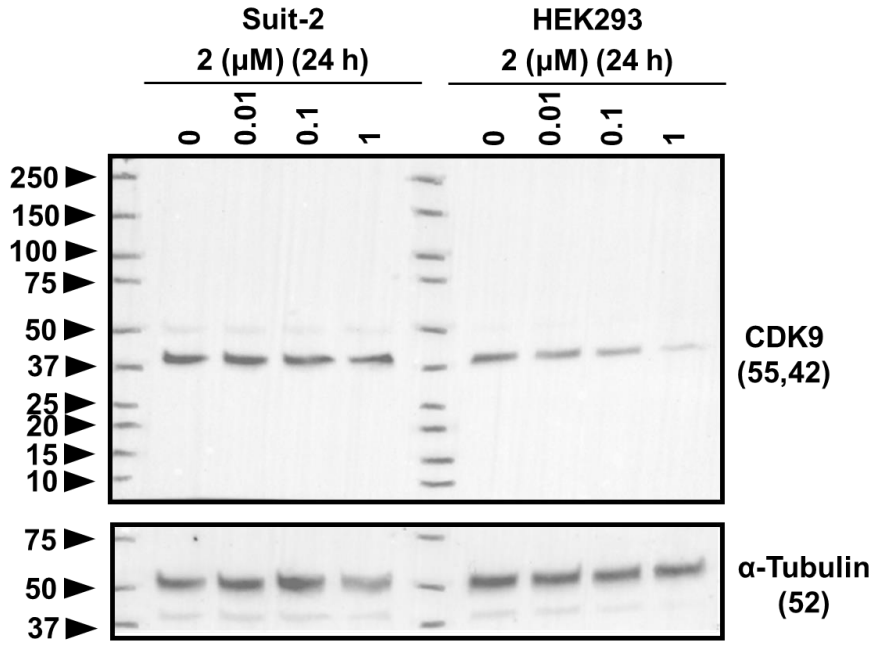

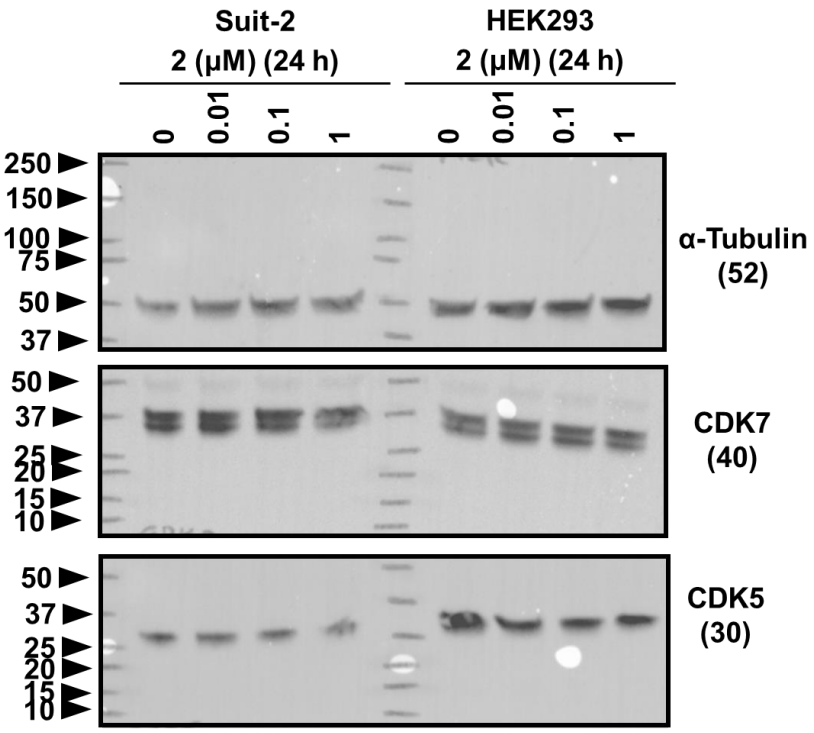
Suit-2
2 (μM) (24 h)
HEK293
2 (μM) (24 h)
0
0.01
0.1
1
0
0.01
0.1
1
250
150
100
75
50
37
α-Tubulin
(52)
50
37
25
20
15
10
CDK7
(40)
50
37
25
20
15
10
CDK5
(30)

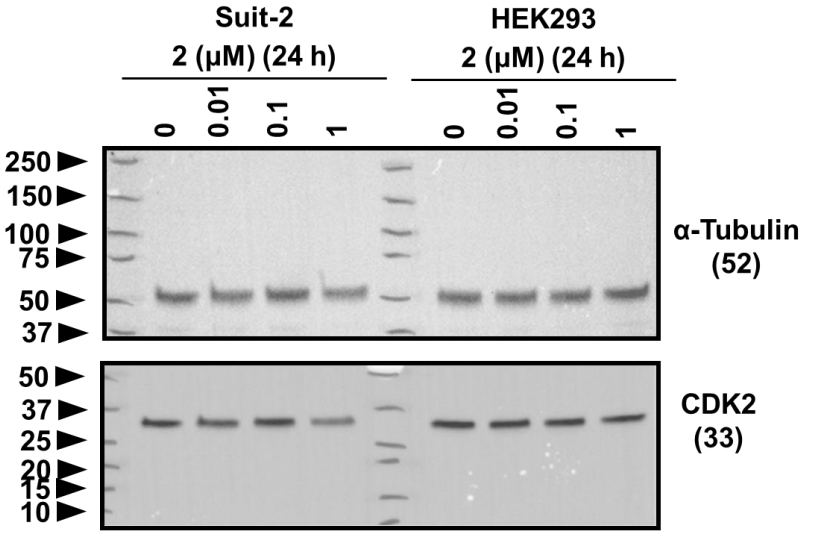
Suit-2
2 (μM) (24 h)
HEK293
2 (μM) (24 h)
0
0.01
0.1
1
0
0.01
0.1
1
250
150
100
75
50
37
α-Tubulin
(52)
50
37
25
20
15
10
CDK2
(33)